to appear in the Astrophysical Journal
Preprint typeset using LaTeX style emulateapj v. 14/09/00

RECURRENT NOVAE AS A PROGENITOR SYSTEM OF TYPE Ia SUPERNOVAE. I. RS OPHIUCHI SUBCLASS — SYSTEMS WITH A RED GIANT COMPANION

Izumi Hachisu
Department of Earth Science and Astronomy, College of Arts and Sciences, University of Tokyo, Komaba, Meguro-ku, Tokyo 153-8902, Japan
hachisu@chianti.c.u-tokyo.ac.jp

AND

Mariko Kato
Department of Astronomy, Keio University, Hiyoshi, Kouhoku-ku, Yokohama 223-8521, Japan
mariko@educ.cc.keio.ac.jp
to appear in the Astrophysical Journal

ABSTRACT

Theoretical light curves of four recurrent novae in outburst are modeled to obtain various physical parameters. The four objects studied here are those with a red giant companion, i.e., T Coronae Borealis, RS Ophiuchi, V745 Scorpii, and V3890 Sagittarii. Our model consists of a very massive white dwarf (WD) with an accretion disk and a red giant companion. Light curve calculation includes reflection effects of the companion star and the accretion disk together with a shadowing effect on the companion by the accretion disk. We also include a radiation-induced warping instability of the accretion disk to reproduce the second peak of T CrB outbursts. The early visual light curves are well reproduced with a thermonuclear runaway model on a very massive white dwarf close to the Chandrasekhar mass limit, i.e., $M_{\rm WD} = 1.37 \pm 0.01\ M_\odot$ for T CrB, $1.35 \pm 0.01\ M_\odot$ for RS Oph with solar metallicity ($Z = 0.02$) but $1.377 \pm 0.01\ M_\odot$ for RS Oph with low metallicity ($Z = 0.004$), $1.35 \pm 0.01\ M_\odot$ for V745 Sco, and $1.35 \pm 0.01\ M_\odot$ for V3890 Sgr. Optically thick winds, which blow from the WDs during the outbursts, play a key role in determining the nova duration and the speed of decline because the wind quickly reduces the envelope mass on the WD. Each envelope mass at the optical maximum is also estimated to be $\Delta M \sim 3 \times 10^{-6} M_\odot$ (T CrB), $2 \times 10^{-6} M_\odot$ (RS Oph), $5 \times 10^{-6} M_\odot$ (V745 Sco), $3 \times 10^{-6} M_\odot$ (V3890 Sgr), indicating an average mass accretion rate $\dot{M}_{\rm acc} \sim 0.4 \times 10^{-7} M_\odot$ yr^{-1} (80 yrs, T CrB), $1.2 \times 10^{-7} M_\odot$ yr^{-1} (18 yrs, RS Oph), $0.9 \times 10^{-7} M_\odot$ yr^{-1} (52 yrs, V745 Sco), $1.1 \times 10^{-7} M_\odot$ yr^{-1} (28 yrs, V3890 Sgr) during the quiescent phase before the last outburst. Although a large part of the envelope mass is blown in the wind, each WD can retain a substantial part of the envelope mass after hydrogen burning ends. Thus, we have obtained net mass-increasing rates of the WDs as $\dot{M}_{\rm He} \sim 0.1 \times 10^{-7} M_\odot$ yr^{-1} (T CrB), $0.12 \times 10^{-7} M_\odot$ yr^{-1} (RS Oph), $0.05 \times 10^{-7} M_\odot$ yr^{-1} (V745 Sco), $0.11 \times 10^{-7} M_\odot$ yr^{-1} (V3890 Sgr). These results strongly indicate that the WDs in the recurrent novae have now grown up to near the Chandrasekhar mass limit and will soon explode as a Type Ia supernova if the WDs consist of carbon and oxygen. We have also clarified the reason why only T CrB shows a secondary maximum but the other three systems do not.

Subject headings: binaries: close — novae, cataclysmic variables — stars: supernovae — stars: symbiotic — stars: individual (RS Oph, T CrB, V3890 Sgr, V745 Sco)

1. INTRODUCTION

Type Ia supernovae (SNe Ia) are one of the most luminous explosive events of stars. Recently, SNe Ia have been used as good distance indicators that provide a promising tool for determining cosmological parameters (Perlmutter et al. 1999; Riess et al. 1998) because of their almost uniform maximum luminosities. These both groups derive the maximum luminosities, $L_{\rm max}$, of SNe Ia completely empirically from the light curve shape (LCS) of nearby SNe Ia, and assume that the same $L_{\rm max}$-LCS relation holds in high red-shift (z) SNe Ia. In order that this method works, the nature of SNe Ia and their progenitors should be the same between high-z and low-z SNe Ia. Therefore, it is necessary to identify the progenitor binary systems, thus confirming whether or not SNe Ia "evolve" from high red-shift to low red-shift galaxies (e.g., Umeda et al. 1999a).

It is widely accepted that the exploding star itself is an accreting white dwarf (WD) in a binary (e.g., Nomoto 1982; Nomoto, Thielemann, & Yokoi 1984). However, the companion star (and thus the observed binary system) is not known. Several types of objects have ever been considered, which include merging double white dwarfs (e.g., Iben & Tutukov 1984; Webbink 1984), recurrent novae (e.g., Starrfield, Sparks, & Truran 1985), symbiotic stars (e.g., Munari & Renzini 1992) etc (see, e.g., Livio 2000, for recent summary).

One of the candidates, the recurrent nova U Scorpii underwent sixth recorded outburst in February 25, 1999 (Schmeer 1999). For the first time, a complete light curve of the outburst has been obtained from the rising phase to the final decline phase through the mid-plateau phase including eclipses (e.g., Hachisu et al. 2000a; Matsumoto, Kato, & Hachisu 2000; Munari et al. 1999). By analyzing these new data on a basis of the theoretical light-curve model of outbursts, Hachisu et al. (2000a) have elucidated

the outburst nature of U Sco much more accurately than the previous estimates (e.g., Starrfield, Sparks, & Shaviv 1988; Kato 1990). We summarize some critically important values they have obtained. (1) The white dwarf mass in U Sco is $1.37 \pm 0.01 M_\odot$. (2) The companion is a slightly evolved main-sequence star of 1.4—1.6 $M_\odot$ that expands to fill the Roche lobe after a large part of the central hydrogen has been consumed and is now transferring mass to the white dwarf in a thermally unstable manner. (3) The white dwarf is now growing in mass at an average rate of $\sim 1 \times 10^{-7} M_\odot$ yr^{-1}. Therefore, the white dwarf will reach the critical mass ($M_{\rm Ia} = 1.378 M_\odot$, in W7 model of Nomoto et al. 1984) for the SN Ia explosion in the quite near future. They concluded that U Sco is a very strong candidate for the immediate progenitor of SNe Ia. Other recurrent novae are also expected to be a strong candidate for SNe Ia.

Thus, we have started our light curve analysis of recurrent novae in which the mass and the growth rate of white dwarfs are determined as accurately as possible and examine the possibility of an SN Ia explosion in the quite near future. In this series of papers, details of our results on recurrent novae are presented, although a part of our results has already been published in several short papers (Hachisu & Kato 1999 for T CrB; Hachisu et al. 2000a,b for U Sco; Hachisu & Kato 2000a for RS Oph; Hachisu & Kato 2000b for V394 CrA).

Here, in the first paper of this series, we have examined four recurrent novae which have a red giant companion, T CrB, RS Oph, V745 Sco, V3890 Sgr. Two of them (T CrB and RS Oph) are reexamined with new observational knowledge. We first summarize the nature of recurrent novae and explain the physical reason why they become so massive as near the Chandrasekhar mass limit in §2. Then, we show details of our numerical methods for calculating evolution of bloated white dwarf envelopes in §3 and for obtaining theoretical light curves in §4, because details of our numerical method have not been fully described yet. New numerical results on determination of white dwarf masses for four recurrent novae are shown and discussed in §5 for T CrB, in §6 for RS Oph, in §7 for V745 Sco, and in §8 for V3890 Sgr. Conclusions follow in §9.

2. RECURRENT NOVAE AS A PROGENITOR OF TYPE IA SUPERNOVAE

Recurrent novae are characterized by nova eruptions with its recurrence time scale from a decade to a century, its brightness amplitude larger than 6 magnitudes, and its expansion velocity faster than 300 km s^{-1} (e.g., Webbink et al. 1987). They are considered to be binary systems in which the secondary companion star overflows the inner critical Roche lobe and transfers matter onto the primary white dwarf (WD) component. When the hydrogen-rich envelope on the WD reaches a critical mass, hydrogen ignites to trigger a nova eruption (hydrogen shell-flash). We call this a *thermonuclear runaway (TNR) event*.

Recurrent novae are morphologically divided into three groups depending on its companion star: dwarf companions, only one member, T Pyxidis with $P = 0.076$ days, (Schaefer 1990, 1992; Patterson et al. 1998); slightly evolved main-sequence (MS) companions, U Scorpii with $P = 1.23$ days (Schaefer 1990; Schaefer & Ringwald 1995), V394 Coronae Austrinae with $P = 0.757$ days (Schaefer 1990), Large Magellanic Cloud Nova 1990 No.2, hereafter LMC RN, with P =unknown but $P \sim 1.3$ days was suggested (Sekiguchi 1992), CI Aquilae with $P = 0.618$ days (Mennickent & Honeycutt 1995), and red giant (RG) companions, T Coronae Borealis with $P = 227.6$ days (Lines, Lines, & McFaul 1988), RS Ophiuchi with $P = 460$ days, (Dobrzycka & Kenyon 1994), recently revised to be $P = 457$ days (Fekel et al. 2000), V745 Scorpii with P =unknown, V3890 Sagittarii with P =unknown, where P is the orbital period of the binary in units of day. These are sometimes called T Pyx subclass, U Sco subclass, and T CrB (or RS Oph) subclass, respectively (e.g., Warner 1995). We have summarized these features in Table 1.

Classical novae, sharing many aspects with the recurrent novae, are also binary systems consisting of a white dwarf and a less massive main-sequence star that fills the Roche lobe and transfers its mass to the white dwarf. The white dwarf accumulates hydrogen-rich matter and ignites hydrogen atop the white dwarf when the hydrogen-rich envelope on the white dwarf reaches a critical mass. A part of the hydrogen diffuses into the white dwarf before the ignition so that a very surface layer of the white dwarf is dredged up into the hydrogen-rich envelope and blown off in the outburst wind (e.g., Prialnik 1986; Kovetz & Prialnik 1994). As a result, nova ejecta contain white dwarf matter, i.e., carbon and oxygen for carbon-oxygen white dwarfs or oxygen, neon, and magnesium for O-Ne-Mg white dwarfs (see, e.g., Prialnik 1986; Kovetz & Prialnik 1994; Warner 1995, and references therein). Thus, the white dwarf is eroded gradually after many cycles of nova outbursts, recurrence periods of which are usually longer than thousands of years.

Recurrent novae show some characteristic differences: (1) heavy elements such as carbon, oxygen and neon are not enriched in ejecta but similar to the solar values (e.g., Livio & Truran 1992; Warner 1995, for summary), indicating that the white dwarf is not eroded; (2) very short recurrence periods from a decade to a century theoretically require very massive white dwarfs close to the Chandrasekhar mass limit (e.g., Fig. 9 of Nomoto 1982). These two arguments indicate that the mass of the white dwarfs in recurrent novae increases toward the Chandrasekhar mass limit (e.g., Starrfield, Sparks, & Truran 1985; Starrfield, Sparks, & Shaviv 1988; Livio & Truran 1992; Della Valle & Livio 1996). We expect that, if the white dwarf is made of carbon and oxygen, the white dwarf ignites carbon at the center and explodes as a Type Ia supernova when it reaches the critical mass of $M_{\rm Ia} = 1.378 M_\odot$ (Nomoto 1982; Nomoto et al. 1984). However, the evolutionary path to recurrent novae has not long been elucidated as well as the reason why so massive white dwarfs can exist in recurrent novae.

2.1. *Accretion Wind Evolution vs. Common Envelope Evolution*

In this subsection, we briefly explain how white dwarfs in recurrent novae have grown its mass toward the Chandrasekhar mass limit. The reason why the standard binary evolution theory (will be cited below) has failed to explain the evolutionary path to recurrent novae is mainly in the

theoretical prediction of a common envelope formation and the ensuing spiral-in process, because these processes inhibit the growth of white dwarfs in binary systems. As discussed in many previous papers on binary evolutions, it had been widely accepted that hydrogen-rich envelopes on mass-accreting white dwarfs expand to a red giant size when its mass accretion rate, $\dot{M}_{\rm acc}$, exceeds a critical limit, $\dot{M}_{\rm cr}$, i.e., $\dot{M}_{\rm acc} > \dot{M}_{\rm cr} \sim 1 \times 10^{-6} M_\odot$ yr^{-1} (see, e.g., Fig. 9 of Nomoto 1982), and easily forms a common envelope (e.g., Nomoto, Nariai, & Sugimoto 1979). Once a common envelope is formed, two stars begin to spiral-in each other due to viscous drag; thus, producing a double degenerate system (e.g., Iben & Tutukov 1984; Webbink 1984).

However, Hachisu, Kato, & Nomoto (1996) found that white dwarfs begin to blow strong winds ($v_{\rm wind} \sim 1000$ km s^{-1} and $\dot{M}_{\rm wind} \gtrsim 1 \times 10^{-6} M_\odot$ yr^{-1}) when the mass accretion rate exceeds the critical rate, i.e., $\dot{M}_{\rm acc} > \dot{M}_{\rm cr}$, as illustrated in Figure 1; thus, preventing the binary from collapsing. The binary does not spiral-in but keeps its separation. Hydrogen burns steadily and therefore the helium layer of the white dwarf can grow at a rate of $\dot{M}_{\rm He} \approx \dot{M}_{\rm cr}$. The other transferred matter is blown in the wind ($\dot{M}_{\rm wind} \approx \dot{M}_{\rm acc} - \dot{M}_{\rm cr}$), where $\dot{M}_{\rm wind}$ is the wind mass loss rate. We call this *accretion wind* because it begins to blow when the accretion rate exceeds the critical rate.

Therefore, as shown in Figure 2, we have to revise Figure 9 of Nomoto (1982), which has been widely used in binary evolution scenarios as basic processes of mass-accreting white dwarfs (e.g., Kahabka & van den Heuvel 1997). The most important difference of Figure 2 from old Nomoto's (1982) is that white dwarfs grow its mass in a much wider parameter region. In our new diagram, the status of a mass-accreting white dwarf is specified by the following three phases: (1) accretion wind phase ($\dot{M}_{\rm acc} > \dot{M}_{\rm cr}$); (2) steady shell-burning phase ($\dot{M}_{\rm std} < \dot{M}_{\rm acc} < \dot{M}_{\rm cr}$); and (3) intermittent shell-flash phase ($\dot{M}_{\rm acc} < \dot{M}_{\rm std}$), where $\dot{M}_{\rm std}$ means the lowest limit of mass accretion rate for steady hydrogen shell burning. The new growing region of white dwarfs, $\dot{M}_{\rm acc} > \dot{M}_{\rm std}$, is much wider than old Nomoto's (1982) narrow strip, $\dot{M}_{\rm std} < \dot{M}_{\rm acc} < \dot{M}_{\rm cr}$.

2.2. *Evolutionary Paths to Recurrent Novae and Type Ia Supernovae*

Based on the new mechanism of Figures 1 and 2, Hachisu et al. (1999a,b) have found two paths to SNe Ia (see also, Li & van den Heuvel 1997). In these two paths, white dwarfs can accrete mass continuously from the companion and grow at a rate of $\dot{M}_{\rm cr} \sim 1 \times 10^{-6} M_\odot$ yr^{-1}. Therefore, candidates of SN Ia progenitors are systems at the final stages on these paths; i.e., one is a supersoft X-ray source (SSS) consisting of a white dwarf and a lobe-filling more massive main-sequence star (WD+MS system, e.g., Li & van den Heuvel 1997) and the other is a symbiotic star consisting of a white dwarf and a mass-losing red giant (WD+RG system, e.g., Hachisu et al. 1996). Both the systems contribute to main parts of the SN Ia birth rate (Hachisu et al. 1999a,b) (see also Livio 2000, for a recent review).

Hachisu et al. (1999a,b) have followed many evolutionary paths and obtained the initial parameter regions of binaries that finally produce an SN Ia. Figure 3 shows such two regions of the WD+MS systems (SSS channel) and the WD+RG systems (symbiotic channel). We have added in this figure the final parameter regions just before an SN Ia explosion occurs. Starting from the initial region encircled by the thin solid lines, binary systems evolve and can explode as an SN Ia in the regions enclosed by the thick solid lines. Hachisu et al. (1999a,b) showed that some recurrent novae lie on the boarder of their parameter region that can produce an SN Ia. Among six recurrent novae with known orbital periods, five fall in the final regions of SN Ia progenitors just before the explosion. Only T Pyx is far out of the regions of SNe Ia.

3. OPTICALLY THICK WINDS IN DECAY PHASE OF NOVAE

In the thermonuclear runaway (TNR) model of nova explosions, WD envelopes expand greatly as large as $\sim 100\ R_\odot$ or more and then the photospheric radius gradually shrinks to the original size of the white dwarfs (e.g., $R_{\rm WD} = 0.0032\ R_\odot$ for $M_{\rm WD} = 1.37\ M_\odot$). Here, we call this *decay phase*, i.e., the phase after the maximum expansion of the photosphere. In the decay phase of novae, the photospheric temperature increases from $T_{\rm ph} \sim 10^4$ K to $\sim 10^6$ K with the bolometric luminosity being almost constant (near the Eddington limit). Therefore, the main emitting region moves from optical to soft X-ray through UV. Correspondingly, the optical luminosity reaches its maximum at the maximum expansion of the photosphere and then decays toward the level in quiescent phase. Since the WD envelope reaches a steady-state in the decay phase of novae (e.g., Prialnik 1986; Kato & Hachisu 1994), we are able to approximate the development of the envelope structure with a unique sequence of steady-state wind solutions having a different envelope mass (ΔM) as shown by Kato & Hachisu (1994).

Optically thick winds, blowing from WDs in the decay phase of novae, play a key role in determining the nova duration, because the winds eject a large part of the envelope mass and drastically reduce the fuel. The winds blow when the WD photosphere is larger than $\sim 0.05 - 0.1 R_\odot$, i.e., when the photospheric temperature is lower than $\log T_{\rm ph} \lesssim 5.5$, because the wind is driven by a strong peak at $\log T \sim 5.2$ in OPAL opacity (e.g., Iglesias & Rogers 1996), and $\log T_{\rm ph} \sim 5.5$ corresponds to the shoulder of the peak on the high temperature side. This opacity peak strongly blocks photons and, as a reaction, matter is effectively accelerated to blow a wind deep inside the photosphere (see, e.g., Figs. 2, 3, and 4 in Kato & Hachisu 1994).

Assuming the solar abundance of heavy elements ($Z = 0.02$), we have calculated the steady-state envelope solutions and obtained sequences for WDs with various masses of $M_{\rm WD} = 0.6$, 0.7, 0.8, 0.9, 1.0, 1.1, 1.2, 1.3, 1.34, 1.35, 1.36, 1.37, and $1.377 M_\odot$. Here, we have adopted the updated OPAL opacity (Iglesias & Rogers 1996) with lower hydrogen contents of $X = 0.70$, 0.50, 0.35, 0.15, 0.10, 0.08, 0.07, 0.06, 0.05, and 0.04. The numerical methods and various assumptions are essentially the same as those in Kato & Hachisu (1994) except the opacities. Some of them are plotted in Figure 4.

For RS Oph and LMC RN, we have also obtained the envelope solutions for lower metallicities, i.e., $Z = 0.001$,

0.002, 0.004, and 0.01 with $X = 0.70$, 0.50, 0.35, 0.15, 0.10, 0.08, 0.07, 0.06, 0.05, and 0.04. Some of them are also shown in Figure 5.

3.1. *Evolution of White Dwarf Envelope*

Hydrogen shell-flashes occur when the mass transfer rate is below the lowest limit for the steady hydrogen shell-burning, i.e., $\dot{M}_{\rm acc} < \dot{M}_{\rm std}$. In this subsection, we describe such a rapid development of white dwarf envelopes. As already mentioned above, optically thick winds blow in the decay phase of hydrogen shell-flashes. Since each wind solution is a unique function of the envelope mass ΔM for a given WD mass, we can follow the development of the envelope structure by calculating the envelope mass, which is decreasing due to the wind mass loss at a rate of $\dot{M}_{\rm wind}(\Delta M)$ and hydrogen shell burning at a rate of $\dot{M}_{\rm nuc}(\Delta M)$, i.e.,

$$\frac{d}{dt}\Delta M = \dot{M}_{\rm acc} - \dot{M}_{\rm wind} - \dot{M}_{\rm nuc}, \tag{1}$$

where $\dot{M}_{\rm acc}$ is the mass accretion rate of the WD. Directly integrating equation (1), we obtain the time-development of the envelope, ΔM, and then the evolutionary changes of physical quantities such as the photospheric temperature $T_{\rm ph}(\Delta M)$, photospheric radius $R_{\rm ph}(\Delta M)$, photospheric velocity $v_{\rm ph}(\Delta M)$, wind mass loss rate $\dot{M}_{\rm wind}(\Delta M)$, and nuclear burning rate $\dot{M}_{\rm nuc}(\Delta M)$, all of which are a unique function of the envelope mass, ΔM.

We have shown, in Figures 4 and 5, the envelope mass ΔM, the photospheric radius $R_{\rm ph}$, the photospheric temperature $T_{\rm ph}$, and the photospheric velocity $v_{\rm ph}$ against the mass decreasing rate of the envelope, $\dot{M}_{\rm wind} + \dot{M}_{\rm nuc}$. The wind mass loss rate becomes as large as 10^{-4}—$10^{-3} M_\odot$ yr^{-1} at the maximum expansion of the photosphere $R_{\rm ph} \sim 100 R_\odot$, and then decreases down to $1 \times 10^{-6} M_\odot$ yr^{-1} just before the wind stops, i.e., when $R_{\rm ph} \sim 0.1 R_\odot$. The photospheric temperature increases from 1×10^4 K to 3×10^5 K. The photospheric velocity remains as high as ~ 1000 km s^{-1} during the wind phase.

When the envelope mass decreases to below the critical mass, the wind stops and the photosphere rapidly shrinks towards its original size before the outburst, for example, from $R_{\rm ph} = 0.06 R_\odot$ to $0.005 R_\odot$ within a week for $M_{\rm WD} = 1.37\ M_\odot$. Shortly after the wind stops, steady-state shell burning on the WD ends but hydrogen burning itself is still continuing and supplying a part of the luminosity. In this phase, the envelope mass is decreased only by nuclear burning. The rest of the luminosity comes from the thermal energy of the hydrogen envelope and the hot ash (helium) below the hydrogen layer. The thermal energy amounts to several times 10^{43} ergs for the case of $M_{\rm WD} = 1.37\ M_\odot$, $X = 0.05$, and $Z = 0.02$ (for the 1999 outburst of U Sco). It can supply a bolometric luminosity of 10^{38} ergs s^{-1} for about ten days or so.

The mass lost by the wind, $\Delta M_{\rm wind}$, and the mass added to the helium layer of the WD, $\Delta M_{\rm He}$, are calculated from

$$\Delta M_{\rm wind} = \int \dot{M}_{\rm wind}\ dt, \tag{2}$$

and

$$\Delta M_{\rm He} = \int \dot{M}_{\rm nuc}\ dt, \tag{3}$$

respectively. The efficiency of hydrogen shell-flashes (nova outbursts) is defined by

$$\eta_{\rm H} = \frac{\Delta M_{\rm He}}{\Delta M_{\rm max}} \approx \frac{\Delta M_{\rm He}}{\Delta M_{\rm wind} + \Delta M_{\rm He}}, \tag{4}$$

where $\Delta M_{\rm max}$ is the envelope mass at the optical maximum.

Assuming a high constant rate of $\dot{M}_{\rm acc} \sim 10^{-3} M_\odot$ yr^{-1} in equation (1), we start the calculation. The envelope mass is quickly increased and the optical luminosity soon reaches the observational maximum in a day or so. Then, we drop the rate to $\dot{M}_{\rm acc} \sim 1 \times 10^{-7} M_\odot$ yr^{-1} or zero and further follow the decay phase of nova. Therefore, our rising phase is not a realistic one but just a rough sketch. Once the envelope has reached the optical maximum, our theoretical light curve in the decay phase represents a realistic one because the flow in the envelope is approximately in a steady-state as already mentioned above.

3.2. *White Dwarf Envelope in Steady Mass Accretion*

If the mass accretion rate ($\dot{M}_{\rm acc}$) does not vary, the envelope solution is obtained from $d(\Delta M)/dt = 0$ in equation (1). The mass accretion rate is in a balance with the mass decreasing rate of the envelope,

$$\dot{M}_{\rm acc} = \dot{M}_{\rm wind} + \dot{M}_{\rm nuc}. \tag{5}$$

If the steady mass-accretion rate is given, we can directly (without integration) obtain the corresponding state of the envelope from Figures 4 and 5. The critical envelope-mass decreasing rate, i.e., at the cease point of wind, exactly coincides with the critical mass-accretion rate, i.e., at the beginning point of wind, $\dot{M}_{\rm cr} \equiv (\dot{M}_{\rm acc})_{\rm cr} = (\dot{M}_{\rm nuc})_{\rm cr}$, which can be approximately expressed by

$$\dot{M}_{\rm cr} = 5.3 \times 10^{-7} \frac{1.7 - X}{X} \left(\frac{M_{\rm WD}}{M_\odot} - 0.40 \right) M_\odot\ {\rm yr}^{-1}, \tag{6}$$

for various WD masses ($M_{\rm WD}$) and hydrogen contents (X) with solar metallicity ($Z = 0.02$). This relation is reduced from our wind solutions for $X = 0.70$, $X = 0.50$, $X = 0.35$, $X = 0.15$, and $X = 0.10$ ($Z = 0.02$) and has accuracy within to 3—5%.

In the same steady mass-accretion mentioned above, we also obtain the lower limit of the mass accretion rate for steady hydrogen shell-burning as

$$\begin{aligned} \dot{M}_{\rm std} &= 2.6 \times 10^{-7} \frac{1.7 - X}{X} \left(\frac{M_{\rm WD}}{M_\odot} - 0.40 \right) M_\odot\ {\rm yr}^{-1} \\ &\approx 0.5 \dot{M}_{\rm cr}, \end{aligned} \tag{7}$$

for solar metallicity ($Z = 0.02$). This relation is reduced from our steady-state solutions for $X = 0.70$, $X = 0.50$, $X = 0.35$, $X = 0.15$, and $X = 0.10$ ($Z = 0.02$) and has accuracy better than 10%.

4. THEORETICAL LIGHT CURVES

One of our binary models is graphically shown in Figure 6. A circular orbit is assumed. Our light curves include the contributions of three components: photosphere of WD, red giant (RG) companion, and accretion disk (ACDK or DK).

4.1. *White Dwarf Photosphere*

We assume a black-body photosphere of the WD envelope and calculate the V-magnitude with a window function given by Allen (1973). The photospheric surface is divided into 32 pieces in the latitudinal angle ($\Delta\theta = \pi/32$) and into 64 pieces in the longitudinal angle ($\Delta\phi = 2\pi/64$) as illustrated in Figure 6. The contributions to the V light are summed up from each piece. We do not consider the limb-darkening effect because it is as small as $\Delta V \lesssim 0.2$ mag.

We have assumed the luminosity of the WD given by

$$L_{\rm WD} = L_{\rm WD,0} + \frac{1}{2}\frac{GM_{\rm WD}\dot{M}_{\rm acc}}{R_{\rm WD}}, \tag{8}$$

where the first term is the intrinsic luminosity of the WD calculated by our wind and steady hydrogen shell burning solutions and the second term is the accretion luminosity (e.g., Starrfield, Sparks, & Shaviv 1988); $R_{\rm WD}$ is the radius of the WD (e.g., $R_{\rm WD} = 0.0032 R_\odot$ for $1.37 M_\odot$ WD). The accretion luminosity is as large as 700 $L_\odot$ for a mass accretion rate of $\dot{M}_{\rm acc} \sim 1\times10^{-7} M_\odot$ yr^{-1} onto a $1.37 M_\odot$ WD. Therefore, the accretion luminosity itself is negligibly small during the steady hydrogen shell burning phase ($L_{\rm WD,0} \gtrsim 10^4 L_\odot$) but may be important after the hydrogen burning diminishes. In such a case, we recalculate the surface temperature of the white dwarf, i.e.,

$$\sigma T_{\rm ph}^4 = \frac{L_{\rm WD}}{4\pi R_{\rm WD}^2}, \tag{9}$$

including the accretion luminosity.

4.2. *Companion's Irradiated Photosphere*

We have to include the contribution of the companion star when it is strongly irradiated by the WD photosphere. The companion star is assumed to fill the inner critical Roche lobe as shown in Figure 6 for T CrB, but underfill for RS Oph, V745 Sco, and V3890 Sgr as described later. Dividing the latitudinal angle into 32 pieces ($\Delta\theta = \pi/32$) and the longitudinal angle into 64 pieces ($\Delta\phi = 2\pi/64$), we have also summed up the contribution from each area, but we neglect both the limb-darkening effect and the gravity-darkening effect of the companion star because the both effects are negligibly small ($\Delta V \lesssim 0.2$ mag) for the strongly irradiated companion. Here, we assume that 50% of the absorbed energy is reemitted from the hemisphere of the companion with a black-body spectrum at a local temperature, that is, the efficiency of irradiation is $\eta_{\rm RG} = 0.5$ unless otherwise specified.

The original (non-irradiated) photospheric temperature of the companion star is obtained from the light curve fitting, for example, $T_{\rm RG,org} = 3100$ K for T CrB. The irradiated surface temperature is roughly estimated by

$$\sigma T_{\rm RG}^4 \approx \eta_{\rm RG}\frac{L_{\rm WD}}{4\pi r^2}\cos\theta + \sigma T_{\rm RG,org}^4, \tag{10}$$

where r is the distance from the WD and $\cos\theta$ is the inclination angle of the surface. The irradiated temperature is as high as $T_{\rm RG} \sim 5000$ K for $\cos\theta = 0.5$, $M_{\rm WD} = 1.37\ M_\odot$ ($L_{\rm WD} = 2\times10^{38}$ ergs s^{-1}), and $r \sim 150 R_\odot$ (T CrB). Therefore, the effect of the irradiation becomes very important in the late phase of outbursts when the irradiated hemisphere faces towards the Earth.

If the accretion disk around the WD blocks the light from the WD photosphere, it makes a shadow on the surface of the companion star. Such an effect is also included in our calculation as explained below.

4.3. *Accretion Disk Surface*

We have to include the luminosity coming from the accretion disk when it is irradiated by the WD photosphere. Here, we assume a circular accretion disk, the edge of which is defined by

$$R_{\rm disk} = \alpha R_1^*, \tag{11}$$

where α is a numerical factor indicating a size of the accretion disk, and R_1^* the effective radius of the inner critical Roche lobe given by Eggleton's (1983) formula.

The surface of the accretion disk is strongly irradiated and dragged outward by the strong wind from the WD during the nova outburst. Its thickness may be increasing outward by both the ablation and the Kelvin-Helmholtz instability. We here approximate such a surface by

$$h = \beta R_{\rm disk}\left(\frac{\varpi}{R_{\rm disk}}\right)^\nu, \tag{12}$$

where h is the height of the surface from the equatorial plane, ϖ the distance on the equatorial plane from the center of the WD, and β is a numerical factor showing the degree of thickness. For comparison, we have calculated the three cases of ν, i.e., $\nu = 9/8$ for the case of standard accretion disk model by Shakura & Sunyaev (1973), $\nu = 2$ and $\nu = 3$ for the case of flaring-up disk (Schandl, Meyer-Hofmeister, & Meyer 1997).

The surface of the accretion disk is divided into 32 pieces logarithmically evenly in the radial direction and into 64 pieces evenly in the azimuthal angle as shown in Figure 6. The outer edge of the accretion disk is also divided into 64 pieces in the azimuthal direction and 2 (or 8) pieces in the vertical direction by rectangles. When the photosphere of the WD becomes very small, e.g., $R_{\rm disk}/R_{\rm ph} > 10$, we attribute the first 16 meshes to the outer region (from $\varpi = R_{\rm disk}$ to $\varpi = R_{\rm disk}/\sqrt{10}$) to avoid coarse meshes in the outer part, and then 16 meshes to the inner region (from $\varpi = R_{\rm disk}/\sqrt{10}$ to $\varpi = R_{\rm ph}$), each region of which is divided logarithmically evenly.

The surface of the accretion disk absorbs photons and reemits in the same way as the companion does. Each area of the heated disk surface emits blackbody photons at its local temperature, $T_{\rm disk}$. We assume that 50% of the absorbed energy is emitted from the surface while the other is carried into interior of the accretion disk and eventually brought into the WD, that is, the efficiency of irradiation is $\eta_{\rm DK} = 0.5$.

The non-irradiated temperature of the disk surface is assumed to be determined by the viscous heating of the standard accretion disk model (Shakura & Sunyaev 1973). Then, the original disk surface temperature is given by

$$\sigma T_{\rm disk,org}^4 = \frac{3GM_{\rm WD}\dot{M}_{\rm acc}}{8\pi\varpi^3}. \tag{13}$$

The viscous temperature is estimated to be $T_{\rm disk,org} \sim$ 9,000 K at $\varpi = 1R_\odot$ for $M_{\rm WD} = 1.37 M_\odot$ and $\dot{M}_{\rm acc} = 1\times10^{-7} M_\odot$ yr^{-1}. However, the viscous heating is negligibly small when the disk surface is strongly irradiated because of $T_{\rm disk} \sim$ 40,000—50,000 K at $\varpi = 1R_\odot$ for the

luminosity of the WD, $L_{\rm WD} = 50,000 L_\odot$, and the average inclination of the surface, $\cos\theta = 0.1$, which is estimated from (e.g., Schandl et al. 1997)

$$\sigma T_{\rm disk}^4 \approx \eta_{\rm DK} \frac{L_{\rm WD}}{4\pi\varpi^2}\cos\theta + \frac{3GM_{\rm WD}\dot{M}_{\rm acc}}{8\pi\varpi^3}. \quad (14)$$

The outer rim of the accretion disk is not irradiated by the WD photosphere so that the temperature of the disk rim is simply assumed, for example, to be 2000 K for T CrB.

4.4. *Radiation-induced Warping*

Radiation-induced warping of accretion disks have been suggested by Pringle (1996). Here, we have introduced a warping surface calculated by Maloney, Begelman, & Pringle (1996). In their formulation, when the tilt vector of the accretion disk surface is defined by

$$\boldsymbol{l}(\varpi, t) = (\sin\tilde{\beta}\cos\tilde{\gamma}, \sin\tilde{\beta}\sin\tilde{\gamma}, \cos\tilde{\beta}), \quad (15)$$

one of their stationary solutions,

$$W = \tilde{\beta} e^{i\tilde{\gamma}}, \quad (16)$$

can be analytically solved as

$$M(1,2,2ix) = e^{ix}\frac{\sin(x)}{x}, \quad (17)$$

where $x \propto \sqrt{\varpi}$. So, we have

$$x = c_1\pi\sqrt{\varpi}, \quad (18)$$

and

$$\tilde{\beta} = c_2 \frac{\sin(c_1\pi\sqrt{\varpi})}{c_1\pi\sqrt{\varpi}}, \quad (19)$$

$$\tilde{\gamma} = c_1\pi\sqrt{\varpi}, \quad (20)$$

where c_1 and c_2 are numerical factors indicating a degree of warping. Here, we adopt $c_1 = 0.5$ and $c_2 = -1.0$, unless otherwise specified. Then, we have transformed the coordinates of the disk, i.e., equation (12), by a rotation matrix of

$$\boldsymbol{T} = \begin{pmatrix} \cos\tilde{\beta}\cos\tilde{\gamma} & -\sin\tilde{\gamma} & -\sin\tilde{\beta}\cos\tilde{\gamma} \\ \cos\tilde{\beta}\sin\tilde{\gamma} & \cos\tilde{\gamma} & -\sin\tilde{\beta}\sin\tilde{\gamma} \\ \sin\tilde{\beta} & 0 & \cos\tilde{\beta} \end{pmatrix}. \quad (21)$$

Such an example is shown in Figure 6 for T CrB. As will be discussed later, the condition of warping instability is satisfied only in T CrB.

4.5. *Numerical Method*

Total V light of the system is calculated from the contribution of each patch with a window (response) function of the V-filter (e.g., Allen 1973). Each patch is almost quadrangular but, strictly speaking, not quadrangular for the Roche geometry of the companion star and for the warping surface of the accretion disk, because the four vertices are not on a plane. Therefore, we define approximately the normal unit vector to each patch as follows: the center of gravity of each patch can be defined by

$$\boldsymbol{r}_{\rm G} = \frac{1}{4}\left(\boldsymbol{r}_{\rm A} + \boldsymbol{r}_{\rm B} + \boldsymbol{r}_{\rm C} + \boldsymbol{r}_{\rm D}\right), \quad (22)$$

where G denotes the center of gravity of the patch, and A, B, C, and D are the apexes of each quadrangle as illustrated in Figure 7. Defining $\boldsymbol{n}_1$ as the normal unit vector to $\triangle$ABG, $\boldsymbol{n}_2$ to $\triangle$BCG, $\boldsymbol{n}_3$ to $\triangle$CDG, and $\boldsymbol{n}_4$ to $\triangle$DAG, we obtain an approximate normal unit vector of $\boldsymbol{n}$ to patch $\square$ABCD by

$$\boldsymbol{n} = \frac{S_1\boldsymbol{n}_1 + S_2\boldsymbol{n}_2 + S_3\boldsymbol{n}_3 + S_4\boldsymbol{n}_4}{S_1 + S_2 + S_3 + S_4}, \quad (23)$$

where each area of the triangles is corresponding to

$$S_1 = \triangle{\rm ABG}, \quad S_2 = \triangle{\rm BCG}, \\ S_3 = \triangle{\rm CDG}, \quad S_4 = \triangle{\rm DAG}, \quad (24)$$

as shown in Figure 7, and the total area of this patch $\square$ABCD is given by

$$S = S_1 + S_2 + S_3 + S_4. \quad (25)$$

Then, patch i receives flux from patch j as much as

$$\Delta L_{ij} = \frac{\sigma T_j^4 S_j(\boldsymbol{n}_j\cdot\boldsymbol{r}_{ji}) S_i(\boldsymbol{n}_i\cdot\boldsymbol{r}_{ij})}{2\pi|\boldsymbol{r}_{ji}|^4}, \quad (26)$$

where

$$\boldsymbol{r}_{ij} = \boldsymbol{r}_{{\rm G},j} - \boldsymbol{r}_{{\rm G},i}, \quad (27)$$

$$\boldsymbol{r}_{ji} = \boldsymbol{r}_{{\rm G},i} - \boldsymbol{r}_{{\rm G},j}, \quad (28)$$

as illustrated in Figure 8. We sum up all combinations of pair patches on the condition of

$$(\boldsymbol{n}_j\cdot\boldsymbol{r}_{ji}) \geq 0, \quad \text{and} \quad (\boldsymbol{n}_i\cdot\boldsymbol{r}_{ij}) \geq 0, \quad (29)$$

and obtain the total flux from all patches, i.e.,

$$L_i = \sum_j\sum_k \xi_{i,j,k}\frac{\sigma T_j^4 S_j(\boldsymbol{n}_j\cdot\boldsymbol{r}_{ji}) S_i(\boldsymbol{n}_i\cdot\boldsymbol{r}_{ij})}{2\pi|\boldsymbol{r}_{ji}|^4}. \quad (30)$$

Here, we set

$$\xi_{i,j,k} = \begin{cases} 1, & \text{for not-blocked} \\ 0, & \text{for blocked} \end{cases} \quad (31)$$

depending whether the line connecting the centers of gravity is blocked by patch k as shown in Figure 8.

The surface (patch i) absorbs photon flux and reemits by a black-body spectrum with a local temperature of T_i, which is determined by

$$\sigma T_i^4 S_i = \eta_{\rm BB} L_i + \sigma T_{i,{\rm org}}^4 S_i, \quad (32)$$

where $\eta_{\rm BB}$ is the efficiency of the irradiation, $T_{i,{\rm org}}$ the unheated temperature of the surface. We adopt 50% efficiency, i.e., $\eta_{\rm BB} = 0.5$ unless otherwise specified.

Using the window functions, $W_V(\lambda)$ and $W_B(\lambda)$, for V- and B-filters (Allen 1973), respectively, we have calculated V-, B-, and bolometric magnitudes of the patches, i.e.,

$$\Delta E_i({\rm V}) = (\boldsymbol{n}_i\cdot\boldsymbol{e}) S_i \int_0^\infty W_V(\lambda) B_\lambda(T_i) d\lambda, \quad (33)$$

$$\Delta E_i({\rm B}) = (\boldsymbol{n}_i\cdot\boldsymbol{e}) S_i \int_0^\infty W_B(\lambda) B_\lambda(T_i) d\lambda, \quad (34)$$

$$\Delta E_i({\rm bol}) = (\boldsymbol{n}_i\cdot\boldsymbol{e}) S_i \sigma T_i^4, \quad (35)$$

respectively. Here, the unit vector $\boldsymbol{e}$ denotes the direction from the patch to the Earth, $B_\lambda(T_i)$ the Planck function for the temperature of T_i. We have summed up the patches having $(\boldsymbol{n}_i\cdot\boldsymbol{e}) > 0$, i.e.,

$$E(V) = \sum_i \Delta E_i(V), \quad \text{for} \quad (\boldsymbol{n}_i\cdot\boldsymbol{e}) > 0 \quad (36)$$

$$E(B) = \sum_i \Delta E_i(B), \quad \text{for} \quad (\boldsymbol{n}_i\cdot\boldsymbol{e}) > 0 \quad (37)$$

$$E({\rm bol}) = \sum_i \Delta E_i({\rm bol}), \quad \text{for} \quad (\boldsymbol{n}_i\cdot\boldsymbol{e}) > 0. \quad (38)$$

We have finally calculated the V-magnitude, m_V, B-magnitude, m_B, and the bolometric magnitude, $m_{\rm bol}$, as

$$m_V = \frac{5}{2}\,(-\log E(V) + 33.582) + m_{V,0} + 5\ \log(\frac{d}{10}), \quad (39)$$

$$m_B = \frac{5}{2}\,(-\log E(B) + 33.582) + m_{B,0} + 5\ \log(\frac{d}{10}), \quad (40)$$

$$m_{\rm bol} = \frac{5}{2}\,(-\log E({\rm bol}) + 33.582) + 4.75 + 5\ \log(\frac{d}{10}), \quad (41)$$

where d is the distance to the object in units of pc, $m_{V,0}$ is a constant determined to satisfy

$$m_V = m_{\rm bol}, \quad {\rm at} \quad T = 6500\ {\rm K}, \quad (42)$$

and $m_{B,0}$ is also a constant determined to satisfy

$$m_B = m_V, \quad {\rm at} \quad T = 9600\ {\rm K\ (A0)}, \quad (43)$$

so that we use

$$m_{V,0} = 4.52, \quad (44)$$

and

$$m_{B,0} = 4.91. \quad (45)$$

In addition, in order to compare our brightness with the recent CCD photometry, we also calculate the Cousins $R_{\rm c}$- and $I_{\rm c}$-magnitudes with the window functions given by Bessell (1990) along the same way as those described above for V- and B-magnitudes. Then, we adopt

$$m_{R,0} = 4.91, \quad (46)$$

and

$$m_{I,0} = 4.50. \quad (47)$$

The most time-consuming part of the calculation is proportional to cubic of the patch number N, that is, $\propto N^3$. Therefore, it is hard to increase the patch number substantially more than the present maximum case, i.e.,

$$N = 32\times64 + 32\times64 + (32\times64\times2 + 8\times64) = 8704, \quad (48)$$

because it takes about a half day on the Compaq (old DEC) Alpha 21264 (500 MHz) machine but about two days on the Intel Pentium III (500 MHz) machine to compute one time sequence for the 1999 U Sco outburst, about 3000 steps for the m_V and m_B light curve calculations (Hachisu et al. 2000a).

5. T CORONAE BOREALIS

5.1. *Nature of T CrB Outbursts*

T Coronae Borealis (T CrB) is one of the well observed recurrent novae and characterized by a secondary maximum occurring ~ 150 days after the primary peak. Historically, T CrB bursted twice, in 1866 and 1946, with the light curves very similar each other (e.g., Pettit 1946a, b, c, d). Large ellipsoidal variations of optical and infrared light curves in quiescence suggest that an M3 giant fills its Roche lobe (e.g., Bailey 1975; Lines et al. 1988; Yudin & Munari 1993; Leibowitz et al. 1997; Shahbaz et al. 1997; Belczyński & Mikołajewska 1998). From the ellipsoidal variations, the orbital period and ephemeris were determined to be HJD 2,431,931.05 + 227.67E at the epoch of spectroscopic conjunction with the M-giant in front (Lines et al. 1988).

There have been debates on the nature of the hot component of the binary system. Radial velocity curves of $K_1 \sim 31$ km s^{-1} (*hot* component) and $K_2 \sim 23$ km s^{-1} (*cool* component) indicated the mass ratio of $q = M_2/M_1 \sim 1.4$ (Kraft 1958; Paczynski 1965; Kenyon & Garcia 1986). Adopting the inclination angle of $i = 68°$, the resulting masses were $M_1 = M_{\rm hot} \sim 1.9 M_\odot$ and $M_2 = M_{\rm cool} \sim 2.6 M_\odot$, thus placing the hot component above the Chandrasekhar limit. Therefore, Webbink (1976) and Webbink et al. (1987) proposed an outburst mechanism of T CrB based on their main-sequence accretor model: the outburst was caused by the transfer of a chunk of matter ejected by the giant and, then, by the subsequent shock dissipation of the kinetic energy. This accretion event model was investigated further by 3D numerical simulations (Cannizzo & Kenyon 1992; Ruffert, Cannizzo, & Kenyon 1993).

However, Selvelli, Cassatella, & Gilmozzi (1992) have been opposed to the main-sequence accretor model from their analysis of *IUE* data in quiescence, which indicates the existence of a mass-accreting white dwarf (WD) as follows: (1) the bulk of the luminosity is emitted in the UV with little contribution to the optical; (2) the presence of strong He II and N V emission lines suggests temperatures of the order of 10^5 K; (3) the rotation broadening of the high-excitation lines is larger than 1300 km s^{-1} without inclination correction. Moreover, the detection of X-rays (Cordova, Mason, & Nelson 1981) and the presence of flickering in the optical light curves (e.g., Ianna 1964; Zamanov & Bruch 1998) are also naturally explained in terms of accretion onto a WD.

The mass accretion rate estimated by Selvelli et al. (1992) in quiescence is very high ($\dot{M}_{\rm acc} \sim 2.5\times10^{-8} M_\odot$ yr^{-1}) and is exactly required by the thermonuclear runaway (TNR) theory to produce a TNR event every 80 yr on a massive ($\gtrsim 1.3 M_\odot$) WD. They also pointed out that the measurement of the emission-line radial velocities (Kraft 1958) was intrinsically difficult and uncertain. Thus, the 1866 and 1946 outbursts can be interpreted in terms of a TNR event on a very massive WD (e.g., Starrfield et al. 1985).

5.2. *Very Massive White Dwarf in T CrB*

Rapid decline rates of the light curves indicate a very massive WD close to the Chandrasekhar limit. Assuming the solar metallicity ($Z = 0.02$) of the WD envelope, Kato (1995, 1999) calculated nova light curves for the WD mass of $M_{\rm WD} = 1.2$, 1.3, 1.35 and 1.377 $M_\odot$, and found that the light curve of the $1.377 M_\odot$ model is in better agreement with the observational light curve of T CrB than the other lower mass models.

Recently, other observational supports of a massive WD in T CrB have been reported. Belczyński & Mikołajewska (1998) derived a permitted range of binary parameters, $M_{\rm WD} = 1.2 \pm 0.2 M_\odot$ and $q = M_{\rm RG}/M_{\rm WD} \sim 0.6$, i.e., $M_{\rm RG} \sim 0.6$—$0.8 M_\odot$, from amplitude of the ellipsoidal variability and constraints from the orbital solution of M-giants. In Shahbaz et al. (1997), a massive WD of $M_{\rm WD} = 1.3 - 2.5 M_\odot$ is suggested from the infrared light curve fitting. Moreover, the measurement of the radial velocities (Kraft 1958) has been revised including the effect of gas-streams around the hot component (Hric et al. 1998). Hric et al. (1998) estimated the masses, $M_{\rm WD} = 1.2 \pm 0.2\ M_\odot$ for the hot component and $M_{\rm RG} = 1.38 \pm 0.2\ M_\odot$ for the M-giant, assuming the in-

clination of $i = 68°$. Combining these permitted ranges of the WD mass in T CrB, we may conclude that a mass of the WD is between $M_{\rm WD} = 1.3{-}1.4 M_\odot$, which is very consistent with the light curve analysis $M_{\rm WD} \sim 1.37{-}1.38 M_\odot$ by Kato (1999).

5.3. *Secondary Maximum of Outbursts*

The secondary maximum in outbursts is rarely observed in fast novae and in other recurrent novae. Selvelli et al. (1992) suggested a possibility of an irradiated stationary shell around the binary system, although the presence of such a shell is just speculation. Recently, Hachisu & Kato (1999) proposed another mechanism of the second peak, i.e., radiation-induced tilting disk around a massive WD. The main results of their analysis are: (1) the first peak is naturally reproduced by a fast developing photosphere of the WD envelope based on the TNR model of a very massive WD, $M_{\rm WD} \sim 1.35 M_\odot$; (2) the second peak is not fully reproduced by an irradiated M-giant model as simply estimated by Webbink et al. (1987); (3) instead, the second peak can be well reproduced if an irradiated tilting accretion disk around the WD is introduced together with the partly irradiated M-giant companion.

Such a radiation-induced, tilting instability of an accretion disk has been suggested by Pringle (1996) when a central star is as luminous as the Eddington limit. This radiation-induced instability sets in if the condition

$$\frac{\dot{M}_{\rm acc}}{10^{-7}\ M_\odot\ {\rm yr}^{-1}} \lesssim \left(\frac{R_{\rm disk}}{10\ R_\odot}\right)^{1/2} \left(\frac{L_{\rm bol}}{2\times 10^{38}\ {\rm ergs\ s}^{-1}}\right) \times \left(\frac{R_{\rm WD}}{0.003\ R_\odot}\right)^{1/2} \left(\frac{M_{\rm WD}}{1.37\ M_\odot}\right)^{-1/2} \quad (49)$$

is satisfied (Southwell, Livio, & Pringle 1997), where $R_{\rm disk}$ is the radius at the edge of the optically thick accretion disk. Selvelli et al. (1992) estimated the accretion rate of T CrB as low as $\dot{M}_{\rm acc} \sim 0.25\times 10^{-7} M_\odot\ {\rm yr}^{-1}$, which meets condition (49) above even if the optically thick radius is as small as $R_{\rm disk} \sim 1\ R_\odot$. Therefore, it is likely that the radiation induced instability grows during the outburst in T CrB. The growth timescale of warping is estimated by Pringle (1996) and Livio & Pringle (1996) as

$$\tau_{\rm prec} \simeq 30 \left(\frac{M_{\rm disk}}{10^{-8}\ M_\odot}\right) \left(\frac{M_{\rm WD}}{1.37\ M_\odot}\right) \left(\frac{R_{\rm disk}}{R_\odot}\right)^{-1/2} \times \left(\frac{L_{\rm bol}}{2\times 10^{38}\ {\rm ergs\ s}^{-1}}\right)^{-1}\ {\rm day}\ , \quad (50)$$

where we assume that the α-parameter in the Shakura-Sunyaev (1973) standard accretion disk is $\alpha \sim 0.1$. Thus, the growth timescale is short enough to excite warping of the accretion disk.

5.4. *Revised Model of Warping Accretion Disk*

We have revised Hachisu & Kato (1999) model to be consistent with the observations described below. The main difference is in the accretion disk, which plays an essential role in the mid/late phase of the V light curve. Hachisu & Kato (1999) assumed that the size of the accretion disk is as large as 0.7 times the Roche lobe size, i.e., $R_{\rm disk} \sim 50\ R_\odot$. This is because the mass transfer is not a wind-fed type but a Roche lobe overflow type (e.g., Schandl et al. 1997). However, Selvelli et al. (1992) estimated the optically thick region of the accretion disk in quiescence is as small as $R_{\rm disk} \lesssim 1\ R_\odot$ because the disk luminosity contributes mostly to the satellite UV. Belczyński & Mikołajewska (1998) pointed out that the optical contribution of the accretion disk is clearly visible in the U, B, and V bands in 1981–85 (optically high state) while it is practically absent in 1990–94 (optically low state) as first shown by Payne-Gaposchkin & Wright (1946). Thus, Belczyński & Mikołajewska derived the disk radius (hot spot) of $R_{\rm disk} \sim 0.1a$ ($20\ R_\odot$) in the optically high state.

Therefore, we here adopt a small size of the optically thick disk, i.e., $R_{\rm disk} \sim 1\ R_\odot$ just before the outburst. A large accretion disk of $\sim 50\ R_\odot$ requires that (1) the irradiation efficiency is too small and that (2) the disk is inclined from too early phase of the outburst. If we introduce a small size of the accretion disk, we do not need to assume such unnatural assumptions. This accretion disk satisfies the warping condition (49) so that we adopt an analytic form proposed by Maloney et al. (1996).

5.5. *Light Curve of Early Phase*

The very fast decay during the first 10 days can be well reproduced only by a WD photosphere of a very massive WD, $M_{\rm WD} \sim 1.35$—$1.37\ M_\odot$, as already shown by Kato (1999) and Hachisu & Kato (1999). We have found that the decay rate of the $1.37\ M_\odot$ light curve is in better agreement with the observational points than the others. The difference from Hachisu & Kato (1999) comes from the difference of the disk size which affects the light curve 10—30 days after maximum. Hachisu & Kato (1999) adopted a large accretion disk which in general contributes more to the luminosity. Therefore, they reduced the WD luminosity to be consistent with the observational points by occulting the WD photosphere with the accretion disk. In the present model, on the other hand, the small disk cannot occult a large part of the WD photosphere during the day 10—30. Thus, we need a more massive WD to generate a faster decline. Therefore, we have determined the WD mass of $M_{\rm WD} = 1.37 \pm 0.01\ M_\odot$ in T CrB, giving a much better fit with the observational points even in the day 0—10.

Deutsch (1948) suggested from the observations of Ashbrook (1946), Wright (1946), and Pettit (1946a) that the color index of T CrB was about zero February 12 (4 days after maximum). Our model indicates the photospheric color of $(B{-}V)_0 = -0.2$ ($T_{\rm ph} \sim 18,500$ K, $R_{\rm ph} \sim 18\ R_\odot$), which is consistent with the observational color because the reddening is about $E(B{-}V) = 0.15$.

The mass of the companion is estimated as follows: Adopting $M_{\rm WD} = 1.37\ M_\odot$ and the radial velocity of the cool component $K_2 = 23.32$ km s^{-1} (Kenyon & Garcia 1986), i.e.,

$$f(M) = \frac{M_{\rm WD}^3 \sin^3 i}{(M_{\rm WD}+M_{\rm RG})^2} = 0.30 \pm 0.01 M_\odot, \quad (51)$$

we have $M_{\rm RG} = 1.30$, 1.25, 1.16, and $1.0\ M_\odot$, for the inclination angle of $i = 70°$, 68°, 65°, and 60°, respectively. Following Belczyński & Mikołajewska (1998), $q \equiv M_{\rm RG}/M_{\rm WD} \sim 0.6$ and an inclination angle of $i \sim 60°$, we have assumed the red giant mass of $M_{\rm RG} = 1.0\ M_\odot$ ($i = 60°$). So we show here only the results for $M_{\rm RG} = 1.0 M_\odot$. In this case, the separation is $a = 209.2 R_\odot$, the effective

radius of the inner critical Roche lobe for the WD component is $R_1^* = 85.0 R_\odot$, the effective radius for the red giant companion is $R_2 = R_2^* = 73.6 R_\odot$. We have examined the other two cases of the red giant mass, i.e., $M_{\rm RG} = 1.25\ M_\odot$ ($i = 68°$) and $M_{\rm RG} = 1.16\ M_\odot$ ($i = 65°$), and obtained similar light curves to that of $M_{\rm RG} = 1.0\ M_\odot$ ($i = 60°$).

Figure 9 shows the best fitted model to the 1946 outburst together with the observational points. Here, we assume the solar metallicity ($Z = 0.02$) and hydrogen content of $X = 0.70$ for the WD envelope. We also assume that the V magnitude reached its maximum on HJD 2,431,861. The dotted curve denotes the total V light from the WD photosphere and the non-irradiated red giant at $T_{\rm RG,org} = 3100$ K. Ellipsoidal light variations can be seen in the late stage (dotted). The effective temperature of the M-giant is estimated to be $T_{\rm RG,org} = 3100$ K from our light-curve fitting, which is a little bit lower than $T_{\rm eff} = 3560$ K by Belczyński & Mikołajewska (1998), but roughly consistent with $T_{\rm eff} = 3200$ K by Shahbaz et al. (1999).

If we include irradiation of the companion, the light curve changes to the dash-dotted curve. This irradiation effect can be well seen both 10—40 days after the optical maximum and 120—260 days after the optical maximum. The irradiation effect was once examined and discarded by Webbink et al. (1987) as a main mechanism of the secondary maximum, mainly because its maximum largely deviates from the observational secondary maximum as seen in the figure.

The solid curve includes further the irradiated accretion disk. Here, we have started the calculation by assuming the disk size of $\alpha = 0.007$ in equation (11), i.e., $R_{\rm disk} = 0.6\ R_\odot$.

The photospheric radius expands to $R_{\rm ph} \sim 100\ R_\odot$ in order to fit the peak luminosity of the V light. We have derived the distance modulus of $(m - M)_V = 10.2$. The light curve during the first 10 days of the 1946 outburst can be well reproduced only with the fast-developing WD photosphere of $M_{\rm WD} = 1.37\ M_\odot$ as already shown by Kato (1999). The envelope mass of the WD at the optical maximum is $\Delta M = 3.3 \times 10^{-6} M_\odot$ from our wind solutions. Then, the mass accretion rate was estimated to be $\dot{M}_{\rm acc} = 4 \times 10^{-8} M_\odot$ yr^{-1} during the quiescent phase between 1866 and 1946. This value is roughly consistent with the estimation of $2.5 \times 10^{-8} M_\odot$ yr^{-1} by Selvelli et al. (1992).

After the WD photosphere shrinks to smaller than $R_{\rm disk} \sim 0.6\ R_\odot$, the accretion disk reappears but its contribution to the V light is small as shown in Figure 9, because radiation emits mainly in UV. We assume a flaring-up rim of the accretion disk, i.e., $\beta = 0.30$ in equation (12), during the strong wind phase for the 1946 outburst of T CrB, since Hachisu et al. (2000a) suggested that the rim of the accretion disk is flaring-up during the 1999 outburst of U Sco, Then, the V light is reduced 20—30 days after maximum because the disk rim makes shadow on the red giant component. The warping of the accretion disk does not occur yet, because the strong wind suppresses the warping. The spherically symmetric wind momentum is much larger than the radiation momentum as shown by Kato & Hachisu (1994).

5.6. *Light Curve Model of the Second Peak*

Warping (or wobbling) instability of the accretion disk begins to grow after the strong wind stops ~ 60 days after maximum (on HJD 2,431,920) and, as a result, the V light attains another peak. We expect that the radiation induced warping of the accretion disk grows in a time scale of a few tens of days as derived in equation (50) and further that the mass transfer from the red giant to the WD increases because the red giant surface is strongly irradiated and the Roche lobe overflow is enhanced. Such enhancement of the mass transfer certainly increases the radius of the optically thick region of the accretion disk up to ~ 10—$20\ R_\odot$ as suggested by Belczyński & Mikołajewska (1998). Thus, we conclude that the radius of the optically thick accretion disk increased from $\alpha = 0.007$ ($R_{\rm disk} \sim 0.6\ R_\odot$) to $\alpha = 0.07$ ($R_{\rm disk} \sim 6\ R_\odot$) during the day $\sim$60—150, by fitting with the observational points as shown in Figure 9.

The second peaks of the 1866 and 1946 outbursts are very similar. This is explained as follows: (1) The first peak ends up when the wind stops about 60 days after maximum. This period (~ 60 days), between the optical peak and the termination of the strong wind, is almost uniquely determined by the WD mass. (2) The second peak begins to rise when the warping of the accretion disk grows, which is about 120 days after maximum. The growth time is estimated to be about a few times 30 days as in equation (50). This growth time depends on the mass ($M_{\rm disk}$) and the optically thick radius ($R_{\rm disk}$) of disk, which are determined mainly by the mass transfer rate from the red giant companion. We can naturally expect the similar time scales between the 1866 and 1946 outbursts, because the irradiation of the red giant by the WD photosphere is almost the same. (3) Thus, we are able to obtain quite similar light curves if the orbital phases of the 1866 and 1946 outbursts happen to be the same (see the light curves of the 1866 and 1946 outbursts, Pettit 1946d). Accidentally, the two orbital phases were almost similar to each other.

The precessing period of the warping disk is similar to the growth time of warping (e.g., Livio & Pringle 1996). About 60% faster precessing angular velocity than the orbital motion is required from the phase relation between the rising shoulder of the second peak near HJD 2,431,960, a small dip near HJD 2,432,090, and then a small bump near HJD 2,432,120 as shown in Figure 9. These dips are caused by a large shadow on the companion cast by the accretion disk. In other words, the accretion disk blocks the light from the WD photosphere and makes its shadow on the companion surface. Finally, we have determined $P_{\rm prec} = 145$ days by fitting. This period is similar to the 164 days precessing period of SS 433.

Webbink et al. (1987) summarized the observational development of the 1946 outburst, showing the color index at the second peak of $B-V \sim 0.4$ after correcting the reddening of $E(B-V) = 0.15$. They further pointed out that the reflection by the M-giant is about $B-V \sim 1.35$, therefore, rejected the possibility of reflection by the M-giant. Instead, they suggested that the much bluer color index of ~ 0.4 is typical of the accretion disks seen in outbursting accretion-powered symbiotic stars (e.g., Kenyon & Webbink 1984). In our warping-disk model, the color index is ranging from $B-V = 0.15$ (on HJD 2,432,000)

to $B-V = 0.35$ (on HJD 2,432,050), which is reasonably consistent with the observational color at the second peak because the reflection effect by the warping disk dominates during the second peak rather than the irradiated M-giant.

Ever since the emission lines of O III, N III, He II, [O III], [Ne III], and [Ne V] first appeared, they have been always present until two years after the outburst, except in early June, at the most, from May 15 to July 17, 1946 ($\sim$ 105—135 days after maximum, Sanford 1949). In our modeling, the warping-up disk occulted both the WD and the innermost region of the disk during these period, being consistent with the disappearance of the emission lines.

5.7. *The Distance, Envelope Mass of the White Dwarf, and Possibility of SN Ia Explosion*

The distance to T CrB is estimated to be $d = 0.94$ kpc with the absorption of $A_V = 0.35$ (Harrison, Johnson, & Spyromilio 1993) because the distance modulus is $(m-M)_0 = (m-M)_V - A_V = 10.2 - 0.35 = 9.85$. This is consistent with both Harrison et al.'s estimation of $d = 1100$ pc, Belczyński & Mikołajewska's (1998) estimation of $d = 960 \pm 150$ pc, and Bailey's (1981) estimation of $d = 1180$ pc. Harrison et al. determined the infrared spectral type of the cool companion as M3 III. Assuming the absolute magnitude of $M_K = -5.3$ (M3 III), they obtain the distance modulus of $(m-M)_0 = m_K - M_K - A_K = 4.79 - (-5.3) - 0.04 = 10.05$, where they used a relation between the absorptions of A_K and A_V given by Rieke & Lebofsky (1985), i.e., $A_K/A_V = 0.112$.

The envelope mass of the WD at the first peak is $\Delta M = 3.3 \times 10^{-6} M_\odot$ from our wind solutions. Therefore, the mass accretion rate can be estimated to be $\dot{M}_{\rm acc} = 4 \times 10^{-8} M_\odot$ yr^{-1} if the envelope mass had been accumulated during the quiescent phase between 1866 and 1946. This value is roughly consistent with the estimation of $2.5 \times 10^{-8} M_\odot$ yr^{-1} by Selvelli et al. (1992). The wind mass loss rate at the first peak is $\dot{M}_{\rm wind} = 3.7 \times 10^{-4} M_\odot$ yr^{-1} while the nuclear burning rate is as small as $\dot{M}_{\rm nuc} = 9.3 \times 10^{-7} M_\odot$ yr^{-1}. The wind mass loss rate is quickly decreasing to $\dot{M}_{\rm wind} \sim 1 \times 10^{-6} M_\odot$ yr^{-1} about 30 days after the first peak. Then, 90% of the envelope mass has been blown in the wind. The residual 10% is left on the WD as a part of the helium layer. Therefore, the net growth rate of the WD is $\dot{M}_{\rm He} = 4 \times 10^{-9} M_\odot$ yr^{-1}.

At the end of this section, we discuss whether or not T CrB will explode as a Type Ia supernova in the near future. The conditions for SN Ia explosions are summarized as follows (see, e.g., Nomoto & Kondo 1991): (1) the accretion rate of the C+O WD should be higher than the critical accretion rate under which helium detonation occurs, i.e.,

$$\dot{M}_{\rm acc} > \dot{M}_{\rm He-det} \sim 1 \times 10^{-8} M_\odot \ {\rm yr}^{-1}, \qquad (52)$$

for Population I stars; (2) the initial mass of the C+O WD at the beginning of the mass transfer is less massive than

$$M_{\rm C+O,0} < 1.2 \ M_\odot. \qquad (53)$$

T CrB satisfies the first condition as has already been suggested to be $\dot{M}_{\rm acc} \sim 4 \times 10^{-8} M_\odot$ yr^{-1} (even if $\dot{M}_{\rm acc} \sim 2.5 \times 10^{-8} M_\odot$ yr^{-1} by Selvelli et al. 1992). For the second condition, we cannot estimate the initial WD mass of T CrB. However, evolutionary scenario strongly suggests that the mass of the WD in T CrB has been increased up to the present mass from a much lower initial mass (see e.g., the evolutionary path to SNe Ia proposed by Hachisu et al. 1999a). Moreover, it is theoretically predicted that an upper limit of degenerate carbon-oxygen core is about 1.07 $M_\odot$, i.e., $M_{\rm C+O,0} < 1.07 \ M_\odot$ (Umeda et al. 1999b). Thus, we may conclude that T CrB will explode as a Type Ia supernova in quite a near future if the hot component is a carbon-oxygen white dwarf.

5.8. *Summary of T CrB Outburst*

The main features of the T CrB outbursts can be well understood with a thermonuclear runaway model on a very massive white dwarf having a warping accretion disk. We have summarized the following important points from the fitting of the modeled light curve with observation:
(1) The early phase ($\sim$ 0—10 days) visual light curve of T CrB outbursts can be well reproduced only by a bloated white dwarf photosphere of $M_{\rm WD} = 1.37 \pm 0.01 \ M_\odot$ for solar metallicity of $Z = 0.02$. This is because decline rates of optical light curves depends sensitively on white dwarf mass especially for white dwarf masses near the Chandrasekhar mass limit. Thus, we are able to specify the mass of white dwarf with a great accuracy (three digits).
(2) The ensuing early phase ($\sim$ 10—40 days) visual light curve cannot be reproduced by any combination of a white dwarf photosphere and a non-irradiated red giant. It requires an irradiation effect of the red giant component. This heated-up red giant surface is consistent with the very early appearance of M-type spectrum (TiO bands) shortly after the outburst, indicating the luminosity of M-type giant much brighter than 10th magnitude (Deutsch 1948).
(3) Through the mid and late phase ($\sim$ 40—300 days), the secondary maximum can be well modeled if we introduce the radiation-induced warping instability of the accretion disk, which sets in after the wind stops $\sim$ 60 days after maximum. Introducing an analytic form of warping (Maloney et al. 1996), we obtain the size of the accretion disk as large as $R_{\rm disk} \sim 6 \ R_\odot$ and the precessing period of the warping disk as fast as $\sim$ 140 days to reproduce the late phase light curve.
(4) The envelope mass of the bloated white dwarf is $3.3 \times 10^{-6} M_\odot$, suggesting the mass accretion rate of $0.4 \times 10^{-7} M_\odot$ yr^{-1} between the 1866 and 1946 outbursts.
(5) The wind carries away about 90% of the envelope mass, so that the residual 10% can be accumulated to the helium layer on the white dwarf. As a result, the white dwarf grows at a rate of $0.4 \times 10^{-8} M_\odot$ yr^{-1}.
(6) T CrB will certainly explode as a Type Ia supernova in quite a near future if the white dwarf consists of carbon and oxygen.

6. RS OPHIUCHI

RS Oph is also one of the well-observed recurrent novae. It is characterized by a long orbital period of 460 days (Dobrzycka & Kenyon 1994, but recently 457 days by Fekel et al. 2000), a relatively short recurrence period of $\sim$ 10—20 yrs compared with 80 yrs of T CrB. It has been suggested that a companion (M-giant) star is underfilling the Roche lobe and losing its mass by massive stellar winds (e.g., Dobrzycka et al. 1996). RS Oph underwent five recorded

outbursts (in 1898, 1933, 1958, 1967, and 1985), with the light curves being very similar to each other (e.g., Rosino 1987). The latest (1985) outburst has been observed at all wave lengths from radio to X-rays (see papers in Bode 1987).

Although there had been intense debates on the mechanism of RS Oph outbursts (e.g., Livio, Truran, & Webbink 1986; Webbink et al. 1987), various observational aspects favor TNR models on a very massive WD (see, e.g., Anupama & Mikołajewska 1999, for a recent summary). Rapid decline rates of the V light curves also indicate a very massive WD close to the Chandrasekhar limit. Kato (1991) has first calculated RS Oph outburst light curves for the WD masses of 1.33, 1.35, 1.36 and 1.37 $M_\odot$ and found that the light curve of the $1.36 M_\odot$ model is in better agreement with the observational light curve of RS Oph than the other mass models.

Since Kato (1991) adopted an old opacity in her calculation, Hachisu & Kato (2000a) recalculated the light curves of RS Oph outbursts with the new opacity (e.g., Iglesias & Rogers 1996), including irradiation effects of both an M-giant companion and an accretion disk around the WD. Their main results are summarized as: (1) the first 4 days light curve of the outbursts can be well reproduced with a TNR model based on a $M_{\rm WD} = 1.35 \pm 0.01 M_\odot$ and an apparent distance modulus of $(m - M)_V = 11.09$. (2) To reproduce the V and UV light curves in the late stage ($t \sim 4$—100 days after the optical maximum), the contributions of the irradiated M-giant and the irradiated accretion disk must be introduced. (3) The distance to RS Oph is estimated to be 0.6 kpc both from the V and UV light curve fittings with the absorption of $A_V = 2.3$. (4) About 90% envelope mass of the WD has been blown off in the wind but the residual 10% has been left on the WD. Thus, Hachisu & Kato (2000a) has concluded that RS Oph will explode as an SN Ia in the near future if the hot component is a carbon-oxygen white dwarf.

In Hachisu & Kato's (2000a) calculations, they assumed the solar metallicity ($Z = 0.02$) of the M-giant envelope. However, it has recently been suggested that the cool component of RS Oph is a metal-poor giant. Scott et al. (1994) obtained the carbon abundance of [C/H]$= -3$ for RS Oph 143 days after the 1985 outburst and of [C/H]$= -4$ in 1992. Similar depletions of carbon, oxygen, neon, sulphur, and iron with respect to solar values are suggested by Contini, Orio, & Prialnik (1995). They obtained one or two tenths of the solar values for C, O, Ne, S, and Fe, in order to reproduce the line ratios based on their shock models of nova shells. Smith et al. (1996) estimated metal abundance of AG Dra as [Fe/H]$= -1.3$ and suggested that all yellow symbiotic stars including RS Oph are metal-poor. They attributed K6 I–II to the cool component of RS Oph.

If the envelope of the white dwarf is also metal-poor, the mass determination of the white dwarf from the light curve fitting may not be correct because the optically thick wind is driven by iron lines and the decay timescale is much longer in low metallicity envelopes. Therefore, we must reexamine the light curves of the 1985 outburst by introducing lower metallicities and study the possible range of the metallicity and the WD mass.

6.1. *The Model of the 1985 Outburst*

Assuming an extremely massive white dwarf of $M_{\rm WD} = 1.377\ M_\odot$ just prior to the SN Ia explosion, we have calculated light curves for various metallicities of $Z = 0.001$, 0.004, 0.01, and 0.02 as shown in Figure 10. The V light of the first five days (HJD 2,446,092 – 2,446,096) can be reproduced only by the bloated WD photosphere as already shown in Hachisu & Kato (2000a). The case of $Z = 0.001$ is too slow to be compatible with the observations. Thus, we may conclude that the metallicity is $Z \gtrsim 0.004$. Here, we assume $Z = 0.004$ for RS Oph as a lower limit of metallicity. For the set of $M_{\rm WD} = 1.377\ M_\odot$ and $Z = 0.004$, we have obtained the envelope mass at the optical maximum, $\Delta M = 2.2 \times 10^{-6} M_\odot$, which indicates a mass accretion rate of $1.2 \times 10^{-7} M_\odot$ yr^{-1} during the quiescent phase between the 1968 and the 1985 outbursts.

The irradiation effects of the accretion disk and the red giant (RG) are necessary to reproduce the optical and UV light curves of the outburst as already shown by Hachisu & Kato (2000a). Dobrzycka & Kenyon (1994) obtained the radial velocities of the M-type feature and the A-type feature but concluded that the A-type absorption feature does not associate with any of the components. Thus, RS Oph is a single line binary with

$$\frac{M_{\rm WD}^3 \sin^3 i}{(M_{\rm WD} + M_{\rm RG})^2} \approx 0.1\ M_\odot, \tag{54}$$

from the semiamplitude of the radial velocity $K_{\rm RG} = 12.8 \pm 2.0$ km s^{-1} and the orbital period of $P = 460$ days. They suggested a relatively low inclination angle of $i \sim 30$—$40°$. If $M_{\rm WD} = 1.377\ M_\odot$, then we obtain $M_{\rm RG} = 0.5\ M_\odot$ for $i = 30°$, $M_{\rm RG} = 0.7\ M_\odot$ for $i = 33°$, $M_{\rm RG} = 0.9\ M_\odot$ for $i = 36°$, $M_{\rm RG} = 1.0\ M_\odot$ for $i = 37°$, or $M_{\rm RG} = 1.2\ M_\odot$ for $i = 39°$. We assume $M_{\rm RG} = 1.0\ M_\odot$ and $i = 37°$ in the present paper, although we have already confirmed that the other set of $M_{\rm RG} = 0.7\ M_\odot$ and $i = 33°$ reproduces almost the same light curves.

For the cool component of the RS Oph system, as suggested by Dobrzycka et al. (1996), the RG lies well within the inner critical Roche lobe, i.e.,

$$R_{\rm RG} = \gamma R_2^* \quad (\gamma < 1), \tag{55}$$

where R_2^* is the effective radius of the inner critical Roche lobe for the RG component and γ is a numerical factor. Dobrzycka et al. (1996) adopted $\gamma = 0.4$ for the distance of $d = 1.5$ kpc to RS Oph. On the other hand, Hachisu & Kato (2000a) estimated the distance of $d = 0.6$ kpc to RS Oph much shorter than Dobrzycka et al.'s value, so that we adopt $\gamma = 0.25$ for $d = 0.6$ kpc in this paper. Even if we use $\gamma = 0.4$, the light curve itself is not so different from that for $\gamma = 0.25$ as shown in Hachisu & Kato (2000a). Only the difference is in the irradiation effect of the M-giant, but the irradiation itself is relatively small compared with the case of T CrB ($\gamma = 1$).

Recent studies on the radii of M-giants in symbiotic stars indicate $\gamma \sim 0.5$ for the normal S-type symbiotic stars (e.g., Mürset & Schmid 1999). The cool component of the RS Oph system is not a normal giant. It is suggested to be metal-poor and sometimes classified to K-giant (e.g., Smith et al. 1996) rather than M-giant. Therefore, we may adopt the relatively small radius of $\gamma = 0.25$.

As for the orbit of the binary system, the ephemeris for the inferior conjunction of the red giant in front is

2,444,999.9+460 × E (Dobrzycka & Kenyon 1994). The separation is $a = 325.0R_\odot$, the effective radii of the inner critical Roche lobes for the WD component and the RG component are $R_1^* = 138.6R_\odot$ and $R_2^* = 108.2R_\odot$. For $\gamma = 0.25$, we have $R_{\rm RG} = 0.25R_2^* \sim 27R_\odot$.

We assume 50% efficiency of the irradiation of the red giant (RG) component ($\eta_{\rm RG} = 0.5$). The nonirradiated photospheric temperature of the RG is a parameter which is determined to be fitted with observation. Here, we adopt $T_{\rm RG} = 3400$ K against $\gamma = 0.25$ as shown in Figure 11.

We have also included the contribution of irradiated accretion disk (ACDK) luminosity. Here, we also assume 50% efficiency of the ACDK irradiation ($\eta_{\rm DK} = 0.5$). The viscous heating is neglected because it is much smaller than that of the irradiation effects. The temperature of the unheated surface of the ACDK including the rim is assumed to be $T_{\rm disk} = 2000$ K. We have checked two other cases of $T_{\rm disk} = 1000$ and 0 K and have found no significant differences in the light curves. The power of ν is assumed to be $\nu = 9/8$ from the standard disk model. We have checked the dependency of the light curves on the parameter ν by changing from $\nu = 9/8$ to $\nu = 2$ but cannot find any significant differences as far as the disk rim is small ($\beta = 0.01$—0.05).

The late-phase V light curve ($t \sim 5$—100 days after maximum) indicates strong irradiation of the ACDK. We have examined the case of a lobe-filling RG companion ($\gamma = 1$), but the irradiation of the RG is too luminous to be compatible with the observational light curves. On the other hand, a smaller size of the RG such as $\gamma = 0.25$ ($\sim 27R_\odot$) gives a reasonable fit with the observations as shown in Figures 11 and 12.

To fit the late-phase light curve, we have calculated the two cases of the disk parameters, i.e., $(\alpha, \beta) = (0.1, 0.05)$ and (0.008, 0.05), as shown in Figure 11. Here, two solid lines denote the cases of $\alpha = 0.1$ ($R_{\rm disk} = 14\ R_\odot$) and $\beta = 0.05$ and $\alpha = 0.008$ ($R_{\rm disk} = 1\ R_\odot$) and $\beta = 0.05$, respectively. Something between these two can roughly reproduce the light curve of the 1985 outburst but the gradual transition from $\alpha = 0.1$ to $\alpha = 0.008$ is much better for reproducing the observations as shown in Figure 12. It is very likely that the surface of the accretion disk has been dragged by the strong wind and been gradually blown in the strong wind. As a result, the accretion disk has become smaller during the strong wind phase (~ 70 days after maximum). Thus, we adopt

$$\alpha = \alpha_0 \left(\frac{\alpha_1}{\alpha_0}\right)^{(t-t_0)/72}, \ \text{for } t_0 < t < t_0 + 72 \text{ day} \quad (56)$$

where $\alpha_0 = 0.1$, $\alpha_1 = 0.008$, t is the days after maximum, $t_0 = 7$ days is the reappearance day of the accretion disk, and 72 days is roughly the wind period.

We have also calculated UV light curves with a response function of 911—3250Å to fit the reddening corrected UV data (Snijders 1987a). Figure 11 shows two cases of UV light curves with the parameters of ($\alpha = 0.1$, $\beta = 0.05$) and ($\alpha = 0.008$, $\beta = 0.05$). The calculated UV light curves can reproduce well the UV observations both for $\alpha = 0.1$ and $\alpha = 0.008$ with the distance of $d = 0.57$ kpc because the innermost region ($\lesssim 0.5\ R_\odot$) of the accretion disk radiates strong UV but the outer region of $\gtrsim 1\ R_\odot$ mainly contributes to optical light.

6.2. *Development of the 1985 Outburst*

In this subsection, we summarize the observational developments of the RS Oph 1985 outburst and discuss them in relation to our model calculation.

Rosino (1987) and Rosino & Iijima (1987) divided the outburst into several phases along with the development of the optical spectrum: [[Phase 0—2 days]] after the optical maximum, broad emission lines of H I, He I, and Fe II are observed with narrow absorption component (40—60 km s^{-1}) and broad P Cygni troughs (-2700 to -3700 km s^{-1}). [[Phase 2—14 days]], He II 4686 Å , [N II], [O I], [O III], [Ne III], [S II], and [Fe II] 6374 Å appear. [[Phase 14—29 days]], He II 4686 Å and N III 4640 Å become strong. [[Phase 29—51 days]], coronal lines appear and become strong. [[Phase 51—72 days]], the coronal line phase lasts. [[Phase 72—119 days]], the coronal lines disappear. Most of high excitation lines, including He II 4686 Å, are fading.

Snijders (1987a) presented an overall development of the UV light curve during the 1985 outburst of RS Oph as already shown in Figures 11 and 12.

Since RS Oph exploded in a circumstellar envelope that is formed by the slow wind of the red giant component (Wallerstein 1958), the rapidly expanding ejecta ($\sim$ 3,000—4,000 km s^{-1}, e.g., Rosino 1987; Snijders 1987a) of the outburst is decelerated by the slowly expanding ($\lesssim 20$ km s^{-1}) circumstellar matter to form a strong shock as noticed by Pottasch (1967). The secular variation of coronal lines was interpreted by Gorbatskii (1972) in terms of a decelerating shock wave (see also Wallerstein & Garnavich 1986, for the 1985 outburst). This shock-heated layer is also responsible for soft X-ray (Mason et al. 1987) and radio (Hjellming et al. 1986) emission as will be mentioned below.

In our numerical modeling, the photospheric temperature of the WD envelope has once decreased down to $T_{\rm ph} = 12,200$ K at the optical maximum (HJD 2,446,093). Then, it increases gradually to [[Phase 0—2]] $T_{\rm ph} = 12,200$ — 17,700 K for the WD photospheric radius of $R_{\rm ph} = 45$ — 21 $R_\odot$, [[Phase 2—14]] $T_{\rm ph} = 17,700$ — 67,100 K for $R_{\rm ph} = 21$ — 1.6 $R_\odot$, [[Phase 14—29]] $T_{\rm ph} = 67,100$ — 114,000 K for $R_{\rm ph} = 1.6$ — 0.56 $R_\odot$, [[Phase 29—51]] $T_{\rm ph} = 114,000$ — 181,000 K for $R_{\rm ph} = 0.56$ — 0.23 $R_\odot$, [[Phase 51—72]] $T_{\rm ph} = 181,000$ — 302,000K for $R_{\rm ph} = 0.23$ — 0.083 $R_\odot$, [[Phase 72—119]] $T_{\rm ph} = 302,000$ — 1,020,000 K for $R_{\rm ph} = 0.083$ — 0.0037 $R_\odot$. The accretion disk reappears 4 days after the optical maximum, i.e., the photosphere shrinks to $R_{\rm ph} \sim 8\ R_\odot$, which is smaller than the size of the accretion disk $R_{\rm disk} \sim 10\ R_\odot$ that we assume. The optically thick strong wind, which is blowing from the WD, stops 77 days after the optical maximum (HJD 2,446,170). The photospheric radius shrinks from $R_{\rm ph} = 0.06\ R_\odot$ to $R_{\rm ph} = 0.01\ R_\odot$ within a few days. Correspondingly, the photospheric temperature increases from $T_{\rm ph} = 343,000$ K to $T_{\rm ph} = 1 \times 10^6$ K. This sharp decrease in the photospheric radius causes the sharp drop in the UV light curve in Figures 11 and 12, because the effective angle of $\cos\theta$ in equation (14) against the disk surface drops by a factor of three. The steady hydrogen shell-burning also ends 109 days after maximum (HJD 2,446,202).

The appearance of He II 4686 Å , [N II], [O I], [O III],

[Ne III], [S II], and [Fe II] 6374 Å in [[Phase 2—14]] and [[Phase 14—29]] is consistent with our model because the WD photospheric temperature increases to high enough to excite these elements. The appearance of the coronal lines are related with the appearance of X-rays heated by the blast shock as shown below (Mason et al. 1987) because they need high temperature photons of $T \gtrsim 1\times10^6$ K as in the solar corona. The disappearance of the coronal lines is usually understood by the shock breakout at the day $\sim$ 70. However, the quick disappearance of the coronal lines in [[Phase 72—119]] might be caused by the extinction of the hydrogen shell burning, as suggested by Shore et al. (1996), because it is consistent with the extinction time of the steady hydrogen shell burning in our model.

Evans et al. (1988) presented infrared observation (J, H, K, and L bands) of the RS Oph 1985 outburst. The decline rates of J, H, K, and L are almost the same as $t_2 \sim 30$ days (t_2 is the time taken to drop 2 mag from maximum). At each wave length it is noticeable that the IR flux of RS Oph had returned to its pre-outburst value by the day $\sim$ 85 (after the optical maximum, but Evans et al. took the optical maximum on HJD 2,466,095.5 as a origin of time) and that the decline continued beyond this level. However, the IR fluxes had reverted to their pre-outburst levels until the day $\sim$400. The post-outburst minimum lasted during about 300 days, i.e., from the day $\sim$100 to the day $\sim$400. This post-outburst minimum is discussed below in relation to the super-soft X-ray detection on the day 251 and the distance to RS Oph.

Evans et al. (1988) also estimated the IR flux from the circumstellar material in the RS Oph system by removing the contribution from the M-giant companion. Assuming that the He II 1640 Å line and the IR continuum do in fact arise in the same region, they fitted the IR continuum on HJD 2,466,119 by a nebular continuum having electron temperature $T_{\rm e} \sim 1.6\times10^5$ K. In our model calculation, we have the photospheric temperature of the bloated WD envelope $T_{\rm ph} \sim 1.1\times10^5$ K on the same day, being roughly consistent with Evans et al.'s estimation, though Evans et al. attributed it to the cooled shocked layer. Evans et al. also estimated that the spectral type of RS Oph cool component is K8 III ($\pm$2 sub-divisions) from $[2.35]-[2.2]$ color.

Shore et al. (1996) also divided the outburst into two phases along with the development of the UV spectrum: The first phase, [[Phase 0—60 days]] after the optical maximum, is the broad line phase. The high velocity material dominated the emission. This is roughly consistent with the strong wind phase of our numerical modeling, i.e., until HJD 2,446,170. In the second phase, i.e., [[Phase 60—130 days]], the newly ionized red giant wind dominated the spectrum. This period is also consistent with the steady hydrogen burning phase of our numerical modeling, i.e., until HJD 2,446,202.

Shore et al. also discussed that the line ratio of Si III] 1892Å to C III] 1910 Å, which measures the electron density (Nussbaumer & Stencel 1989), steadily decreased from an initial value of 1.0 on HJD 2,446,106 to a minimum of 0.3 on HJD 2,446,164. Then, the ratio began to rise thereafter, reaching 0.6 by HJD 2,446,202. This trend can be explained by our wind model: (1) The wind mass loss rate is gradually decreasing from $\sim 10^{-4}$ to $\sim 10^{-7} M_\odot$ yr^{-1} and this causes the decrease in the electron density because of $\rho \sim \dot{M}_{\rm wind}/4\pi r^2 v_{\rm wind}$. (2) After the hot wind from the WD stops, the cool red giant wind resumes to expand slowly and the newly ionized red giant wind dominates the spectrum.

RS Oph became a strong X-ray source with characteristic temperature of a few times 10^6 K (Mason et al. 1987). Mason et al. observed X-rays from 55 days after the optical maximum through 251 days with the medium-energy proportional counter array (ME) and the low-energy imaging telescope (LE) onboard *EXOSAT*. They made six separate observations, 55, 62, 74, 83, 93, and 251 days after the optical maximum. The source became very weak in the ME from day 83 and only upper limits were derived. However, there was still some residual X-ray emission detected even more than 250 days after maximum only with the LE band. The authors interpreted the early X-ray emission in terms of emissions by the pre-outburst M-giant's wind that had been shock-heated by the outburst ejecta (see also Bode & Kahn 1985; O'Brien & Kahn 1987; Itoh & Hachisu 1990; O'Brien, Bode, & Kahn 1992). On the other hand, the late X-ray emissions have been interpreted in terms of the continued hydrogen shell burning on top of the white dwarf. This interpretation is not consistent with our model calculation because the steady hydrogen shell-burning ended long before the day 251, i.e., at the day $\sim$ 110. We will discuss this point again in the next subsection in relation to the distance to RS Oph.

6.3. *The Distance to RS Ophiuchi*

The distance to RS Oph is determined to be 0.57 kpc from the dereddened UV flux (Snijders 1987a) as shown in Figures 11 and 12. We assume the accretion disk exists during the outburst. We cannot reproduce the UV light curve if the disk does not exist or its size is smaller than $\alpha < 0.003$, i.e., $\lesssim 0.5 R_\odot$, as already shown in Hachisu & Kato (2000a). The UV light curves depend hardly on the disk parameters of α, β, or ν when $\alpha \gtrsim 0.01$, mainly because the UV light is coming from the innermost part of the accretion disk. The distance depends weakly on the irradiation efficiency ($\eta_{\rm DK}$), for example, $d = 0.70$ kpc for $\eta_{\rm DK} = 1.0$ or $d = 0.50$ kpc for $\eta_{\rm DK} = 0.25$. The red giant does not contribute to the UV because its irradiated temperature is as low as $\sim$ 4000 K. Thus, the distance estimation is rather robust.

We have calculated the absorption of $A_V = 11.09 - 5\log(570/10) = 2.3$ for $d = 0.57$ kpc from our light curve fitting. This absorption of $A_V = 2.3$ is consistent with the color excess of $E(B-V) = 0.73$ (Snijders 1987b) because of $A_V = 3.1\ E(B-V)$. This distance of ~ 0.6 kpc is not consistent with other estimations of $d = 1.6$ kpc from the hydrogen column density (Hjellming et al. 1986), $d = 1290$ pc (Harrison et al. 1993), and $d = 1$ kpc (Sekiguchi et al. 1990), both of which are determined from the K-band luminosity. In the following, therefore, we discuss extensively other distance estimations supporting our short distance of 0.6 kpc to RS Oph.

The VLBI map 77 days after the optical maximum (Taylor et al. 1989) shows an elongated structure with a long axis of $0\farcs22$ and a short axis of $0\farcs08$. If we assume the distance of $d = 1.6$ kpc to RS Oph, this fastest average expansion velocity should be 4,000 km s^{-1}. This is

not consistent with the initial velocity of ejecta $\sim 3,000$—$4,000$ km s^{-1} because the ejecta is strongly decelerated by the circumbinary matter that is formed by the red giant wind in quiescence. If the distance is $d = 0.6$ kpc, on the other hand, the average expansion velocity is much slower ($\sim 1,400$ km s^{-1}), which is consistent with the initial velocity of the ejecta. Then, the slowest average expansion velocity is estimated to be ~ 500 km s^{-1}, which is also consistent with the optical line width (e.g., ~ 490 km s^{-1} 110 days after optical maximum, Snijders 1987a).

The outer edge of the circumbinary matter (CBM) that is formed by the red giant wind is about $R_{\rm CBM} \lesssim 1 \times 10^{15}$ cm, since an upper limit of 20 km s^{-1} to the velocity of the red giant wind has been given by Gorbatskii (1972) based on spectra by Dufay et al. (1964). Here, we assume that the ejecta of the previous 1967 outburst swept up the previously existing CBM far away. The soft X-ray rapidly fell down from 60—70 days after the optical maximum so that the shock had broken out of the circumbinary matter on that day (Mason et al. 1987; Itoh & Hachisu 1990; Lloyd et al. 1993). If the outer edge of the circumbinary matter corresponds to the elongated radius of the VLBI map on the day 77 ($0''.11$ of half axis), we obtain the distance to RS Oph, $d \lesssim R_{\rm CBM}/(\Delta\theta) = 2 \times 10^{21}$ cm $= 0.65$ kpc.

Very soft X-rays were observed 251 days after the optical maximum in the 1985 outburst of RS Oph (Mason et al. 1987). Mason et al. estimated a blackbody temperature of 3.5×10^5 K and a total energy flux of

$$L_{\rm X,obs} = 1 \times 10^{37} \left(\frac{d}{1.6 \text{ kpc}} \right)^2 \text{ ergs s}^{-1}, \qquad (57)$$

for a hydrogen column density of $N_{\rm H} = 3 \times 10^{21}$ cm^{-1}, and concluded that these soft X-rays come from a WD photosphere with steady hydrogen shell burning. However, steady hydrogen shell burning has stopped 109 days after the optical maximum (HJD 2,446,202) in our model of $X = 0.70$, $Z = 0.004$, and $M_{\rm WD} = 1.377 M_\odot$ (Figs. 11 and 12), that is, this soft X-ray detection is indicating accretion luminosity rather than hydrogen shell burning luminosity. Using a blackbody temperature of $T_{\rm BB} \sim 3.5 \times 10^5$ K and a WD radius of 0.003 $R_\odot$ for 1.377 $M_\odot$, we estimate a total luminosity of

$$L_{\rm X,WD} = 4\pi R_{\rm WD}^2 \sigma T_{\rm BB}^4 \sim 120 L_\odot. \qquad (58)$$

Thus, a rather short distance of 0.4 kpc to RS Oph can be derived by equating equation (57) and (58), i.e., $L_{\rm X,obs} = L_{\rm X,WD}$. Thus, our short distance of 0.6 kpc is roughly consistent with the soft X-ray observation by Mason et al. (1987) about eight months after the optical maximum. This low luminosity corresponds to the accretion luminosity of

$$\dot{M}_{\rm acc} = \frac{2 L_{\rm X,WD} R_{\rm WD}}{G M_{\rm WD}} \sim 0.2 \times 10^{-7} M_\odot \text{ yr}^{-1}. \qquad (59)$$

This accretion rate is six times lower than our estimated mass accretion rate of $\dot{M}_{\rm acc} = 1.2 \times 10^{-7} M_\odot$ yr^{-1} averaged between 1967 and 1985.

Dobrzycka et al. (1996) pointed out that the line fluxes in H I and He I before the 1985 outburst are about four times larger than the fluxes after the 1985 outburst, thus indicating a decrease in the mass accretion rate after the outburst (see also the low luminosity during the post-outburst minimum $\sim$100—400 days after maximum pointed by Evans et al. 1988). If our value of $\dot{M}_{\rm acc} = 1.2 \times 10^{-7} M_\odot$ yr^{-1} is adopted as the mass accretion rate before the 1985 outburst, these line fluxes before/after the outburst are roughly consistent with the ratio of the estimated mass accretion rates before and after the outburst (1.2/0.2) if the line fluxes depend proportionally on the gravitational energy release. The day 251 was just in the period of the post-outburst minimum ($m_V \sim 11.5$) of the day $\sim$100—400, after which the visual luminosity increased to $m_V \sim 10.5$, by about one magnitude (e.g., Fig. 1 of Evans et al. 1988).

Bohigas et al. (1989) estimated the Hβ intensity photoionized by X-ray photons from the central hot WD and compared it with the observation 201 days after maximum. Their theoretically estimated value of

$$I(\text{H}\beta) = 1.24 \times 10^{-10} \text{ergs cm}^{-1}\text{s}^{-1} \times \left(\frac{R_{\rm WD}}{1 \times 10^9 \text{ cm}} \right)^2 \left(\frac{d}{1.6 \text{ kpc}} \right)^{-2} \qquad (60)$$

is 3.5 times larger than the observed value of $I(\text{H}\beta) = 3.55 \times 10^{-11}$ ergs cm^{-1} s^{-1} when we adopt $R_{\rm WD} = 10^9$ cm and $d = 1.6$ kpc. However, if we use $R_{\rm WD} = 0.003\ R_\odot$ and $d = 0.6$ kpc, the estimated value is $I(\text{H}\beta) = 3.8 \times 10^{-11}$ ergs cm^{-1} s^{-1}, being consistent with the observed intensity.

X-rays were also observed at the quiescent phase (Orio 1993), but the flux is too low to be compatible with the TNR model. One possible explanation is an absorption by the massive cool wind (e.g., Shore et al. 1996) from the RG component as suggested by Anupama & Mikołajewska (1999). On the other hand, soft X-rays were observable just after the outburst, because the ejecta swept away the cool wind around the RS Oph system. The cool red giant wind fills again its Roche lobe and can cover the hot component in a time scale of $\Delta t = a/v \sim 300 R_\odot/10$ km s^{-1} = 300 days, which is roughly consistent with the recovery of the quiescent V luminosity as shown in Figure 1 of Evans et al. (1988).

Hjellming et al. (1986) estimated the distance to RS Oph of $d = 1.6$ kpc from H I absorption line measurements, using the hydrogen column density of $N_{\rm H} = (2.4 \pm 0.6) \times 10^{21}$ cm^{-2} and the relation of $N_{\rm H}/(T_{\rm s}\ d) = 1.59 \times 10^{19}$ cm^{-2} K^{-1} kpc^{-1} together with $T_{\rm s} = 100$ K. If a large part of this hydrogen column density stems not from the Galactic absorption but from the local one belonging to RS Oph, the distance is overestimated. For example, in the direction of the recurrent nova U Sco, Kahabka et al. (1999) reported a hydrogen column density of (3—4)$\times 10^{21}$ cm^{-2}, which is much higher than the Galactic hydrogen column density of 1.4×10^{21} cm^{-2}. If RS Oph is in the same case as in U Sco, the distance of 1.6 kpc is just an upper limit and we possibly derive a much shorter distance.

6.4. *The Ejected Envelope Mass and Possibility of SN Ia Explosion*

The envelope mass at the optical maximum is estimated to be $\Delta M = 2.2 \times 10^{-6} M_\odot$, which indicates a mass accretion rate of $1.2 \times 10^{-7} M_\odot$ yr^{-1} during the quiescent phase between the 1968 and 1985 outbursts. In our calculation, about 90% of the envelope mass ($2.0 \times 10^{-6} M_\odot$)

has been blown off in the optically thick wind, and the residual 10% ($0.2 \times 10^{-6} M_\odot$) has been left and added to the helium layer of the WD. The residual mass itself depends on both the hydrogen content X and the WD mass. It is roughly ranging from 10% ($X = 0.70$) to 15%($X = 0.50$) including ambiguities of the WD mass ($M_{\rm WD} = 1.377 \pm 0.01 M_\odot$). Therefore, the net mass increasing rate of the WD is $\dot{M}_{\rm He} = 1.2 \times 10^{-8} M_\odot$ yr^{-1}.

Our calculated ejecta (wind) mass seems to be inconsistent with observation. Bohigas et al. (1989) estimated the (fully ionized hydrogen) shell mass from their observation 201 days after maximum. The obtained value is $M_{\rm shell} \sim 1.5 \times 10^{-5} (d/1 \ {\rm kpc})^2 M_\odot$. Then, they obtained the ejecta mass form their equation (8), i.e., $M_{\rm ejecta} \sim 3 (V_{\rm s}/V_{\rm e})^2 M_{\rm shell}$, where $V_{\rm s}$ is the shell velocity after the shock has broken out of the circumstellar envelope and $V_{\rm e}$ is the velocity of the ejecta before it collides with the circumstellar matter. Assuming $V_{\rm s} = 200$ km s^{-1} and $V_{\rm e} = 2000$ km s^{-1}, Bohigas et al. estimated $M_{\rm ejecta} \sim 4.5 \times 10^{-7} (d/1 \ {\rm kpc})^2 M_\odot$. This ejecta mass is not consistent with our numerical model ($\Delta M_{\rm wind} = 2.0 \times 10^{-6} M_\odot$) if we use $d = 0.6$ kpc.

This inconsistency comes from the inappropriate pair of velocities because the estimated mass depends sensitively on the ratio $V_{\rm s}/V_{\rm e}$. If we adopt an appropriate pair of velocities, our wind model is consistent with the observational shell mass. Starting from the set of $d = 0.6$ kpc and $M_{\rm ejecta} \equiv \Delta M_{\rm wind} \sim 2.0 \times 10^{-6} M_\odot$, we obtain $M_{\rm shell} \sim 5.4 \times 10^{-6} M_\odot$ and $V_{\rm s}/V_{\rm e} \sim 0.35$. Adopting $V_{\rm e} \sim 4000$ km s^{-1} from the observation (e.g., Rosino & Iijima 1987; Snijders 1987a,b) gives $V_{\rm s} \sim 1400$ km s^{-1}.

This velocity of 1400 km s^{-1} is consistent with the radio map obtained 77 days after maximum (Taylor et al. 1989). The VLBI map shows an elongated structure of angular dimensions of $\sim 0\farcs22$ (long axis) and $\sim 0\farcs08$ (short axis), which is consistent with the distance of 0.6 kpc and the fastest expansion velocity of 1400 km s^{-1} after shock, i.e., $0\farcs092 \ (d/1 \ {\rm kpc})^{-1} \cdot (V_{\rm s}/1000 \ {\rm km \ s^{-1}}) \sim 0\farcs22$. Thus, we have obtained a consistent set of physical quantities, $M_{\rm shell} \sim 5.4 \times 10^{-6} M_\odot$, $M_{\rm ejecta} \sim 2.0 \times 10^{-6} M_\odot$, and $V_{\rm s} = 1400$ km s^{-1} for the distance of $d = 0.6$ kpc.

Thus, we obtain the cool wind mass loss rate of $4 \times 10^{-7} M_\odot$ yr^{-1} ($= M_{\rm shell}/18$ yr), indicating that one fourth of the cool wind has been captured by the WD. Observationally, a very high mass loss rate of the cool wind, $\sim 10^{-5} M_\odot$ yr^{-1}, was suggested by Shore et al. (1996) based on the UV data. However, Dobrzycka et al. (1996) argued against such a high mass loss rate of the M-giant cool wind. If the wind mass loss rate approaches such a high rate of $10^{-5} M_\odot$ yr^{-1}, a very large 10μm excess should be observed. But, the giant of RS Oph has only a modest 10—20μm excess. They estimated a few times $10^{-7} M_\odot$ yr^{-1} (e.g., Kenyon, Fernandez-Castro, & Stencel 1988). This mass loss rate of the cool wind is very consistent with the present estimation.

Finally, we examine whether or not RS Oph will explode as a Type Ia supernova in quite a near future. One of the conditions for SN Ia explosions is changed as follows:

$$\dot{M}_{\rm acc} > \dot{M}_{\rm He-det} \sim 4 \times 10^{-8} M_\odot \ {\rm yr}^{-1}, \qquad (61)$$

for low metallicity stars (Nomoto 1982; Nomoto & Kondo 1991) instead of equation (52). Our estimated mass accretion rate of $\dot{M}_{\rm acc} = 1.2 \times 10^{-7} M_\odot$ yr^{-1} meets the above condition. Thus, we may conclude that RS Oph is an immediate progenitor of an SN Ia even if the donor is a metal-poor star.

6.5. *Absence of Secondary Maximum*

Among the four recurrent novae with a red giant companion, only T CrB shows a secondary maximum of $\Delta V \sim 2$ mag brighter than the quiescent level 120—190 days after the optical maximum. We discuss in more detail on the difference between T CrB and the others. The essential difference exists in the fact that the red giant component in T CrB fills its inner critical Roche lobe but the others do not (see the following sections for V745 Sco and V3890 Sgr).

In the T CrB system, the mass transfer continues from the red giant component to the white dwarf even in the outburst (hot) wind phase. Moreover, the strong irradiation increases the mass transfer rate from the red giant component; thus increasing the radius of the optically thick region of the accretion disk. The unstable warping grows shortly after the hot wind stops because the mass transfer rate satisfies the warping condition (49).

On the other hand, the RS Oph system cannot maintain the mass transfer because the cool red giant wind has once been evacuated by the outburst (hot) wind/ejecta from the white dwarf. During the day 0—80 (hot wind phase), the growth of warping was suppressed by the hot wind because the hot wind (matter) momentum is much larger than the photon momentum as shown by Kato & Hachisu (1994). During the day 80—120 (steady burning phase), the warping instability may grow to some extent. However, the disk cannot contribute much to the V light, since the optically thick region of the accretion disk has become as small as or smaller than $\sim 1 R_\odot$.

The mass transfer to the white dwarf resumes ~ 400 days after the optical maximum, that is, after the hot wind stops (~ 80 days) and then the cool red giant wind fills again the binary system ($\Delta t = a/v \sim 300 \ R_\odot/10$ km s^{-1} $= 300$ days) as already discussed earlier. At that time, the luminosity of the white dwarf has once decreased as low as ~ 100—$200 \ L_\odot$ and too low (two orders of magnitude lower) to excite the warping instability as easily understood from the condition for RS Oph (Southwell et al. 1997), i.e.,

$$\frac{\dot{M}_{\rm acc}}{3 \times 10^{-8} \ M_\odot \ {\rm yr}^{-1}} \lesssim \left(\frac{R_{\rm disk}}{R_\odot} \right)^{1/2} \left(\frac{L_{\rm bol}}{2 \times 10^{38} \ {\rm ergs \ s^{-1}}} \right) \times \left(\frac{R_{\rm WD}}{0.003 \ R_\odot} \right)^{1/2} \left(\frac{M_{\rm WD}}{1.377 \ M_\odot} \right)^{-1/2} \qquad (62)$$

In the cool wind accretion phase, our estimated accretion rate of the WD in RS Oph is $\dot{M}_{\rm acc} \sim 1.2 \times 10^{-7} M_\odot$ yr^{-1} (therefore, $L_{\rm bol} \sim 5 \times 10^{36}$ ergs s^{-1} for the accretion luminosity), which also does not meet the above condition even if $R_{\rm disk} = 10 \ R_\odot$, so that the radiation-induced instability does not occur in RS Oph. This is the reason why RS Oph does not show a second peak.

The other two, V745 Sco and V3890 Sgr, are similar systems to RS Oph, so that a secondary maximum was not observed, as will be shown in the following sections.

6.6. *Summary of RS Oph Outburst*

The main features of the RS Oph outbursts can be well understood with a thermonuclear runaway model on a very massive white dwarf close to the Chandrasekhar mass limit. We have summarized the following important points:
(1) It has been suggested that the M-giant in RS Oph is metal-poor. Assuming an upper limit of white dwarf mass, i.e., $M_{\rm WD} = 1.377\ M_\odot$, we have obtain a lower limit of metallicity, i.e., $Z \geq 0.004$ from the light curve fitting of the early phase ($\sim$ 0—4 days). In other words, the early visual light curve can be well reproduced only by a bloated white dwarf photosphere of $M_{\rm WD} = 1.377 \pm 0.01\ M_\odot$ for a low metallicity of $Z = 0.004$. On the other hand, $M_{\rm WD} = 1.35 \pm 0.01\ M_\odot$ is obtained for the solar metallicity of $Z = 0.02$.
(2) The ensuing phase ($\sim$ 5—80 days) visual light curve cannot be reproduced only by a white dwarf photosphere. It requires an irradiation effect of the accretion disk, the size of which is gradually decreasing from $\sim 10\ R_\odot$ to $\sim 1\ R_\odot$.
(3) The UV light curve can also be well reproduced with the same model as that of the visual luminosity. The early phase UV flux mainly comes from the bloated white dwarf photosphere while the late phase UV flux comes from the irradiated disk surface because the main emitting region of the white dwarf photosphere has shift from UV to soft X-ray in the late stage.
(4) The optically thick wind stops on the day $\sim$80. The WD photosphere quickly shrinks. The sharp drop in the UV flux around the day 80 can be understood from this quick shrink of the WD photosphere.
(5) The distance to RS Oph is estimated to be 0.6 kpc from the fitting with the dereddened UV flux. This distance is consistent with the V light curve fitting.
(6) The envelope mass of the bloated white dwarf is $2.2 \times 10^{-6} M_\odot$, suggesting the mass accretion rate of $1.2 \times 10^{-7} M_\odot$ yr^{-1}.
(7) The wind carries away about 90% of the envelope mass, so that the residual 10% can be accumulated to the helium layer of the white dwarf. As a result, the white dwarf grows at a rate of $1.2 \times 10^{-8} M_\odot$ yr^{-1}.
(8) RS Oph will certainly explode as a Type Ia supernova in quite a near future if the white dwarf consists of carbon and oxygen.

7. V745 SCORPII

V745 Scorpii underwent the second recorded outburst in 1989 (the first recorded outburst in 1937), and has been recognized as a member of recurrent novae (e.g., Sekiguchi et al. 1990, and references therein). Its light curve is characterized by a very rapid rise (in about half a day) and decline ($t_3 \sim 9$ days, t_3 is the time taken to drop 3 mag from maximum). The general spectral evolution closely resembles that of RS Oph (e.g., Sekiguchi et al. 1990). Although its orbital period, the most important system parameter, is still not known, the secondary cool component has been classified as M6—8 III (from optical spectra, Sekiguchi et al. 1990; Duerbeck & Seitter 1990; Williams et al. 1991), M4 III (from the infrared spectra and colors, Harrison et al. 1993), or M4—6 III (from the absorption line indices, Anupama & Mikołajewska 1999). Therefore, V745 Sco is a twin system to RS Oph, a member of the recurrent novae with a red giant secondary.

7.1. *The Model of the 1989 Outburst*

We have calculated V light curves for five cases of the WD mass ($M_{\rm WD} = 1.3$, 1.35, 1.36, 1.37, and $1.377 M_\odot$) by assuming the hydrogen content $X = 0.70$, 0.50, or 0.35 with the solar metallicity ($Z = 0.02$). By fitting light curves in the first 25 days of the 1989 outburst, we have determined the WD mass of $M_{\rm WD} = 1.35 \pm 0.01 M_\odot$ as shown in Figure 13. Here, we have shifted the visual magnitude obtained with orange filter or 2415 films (Liller 1989a,b) by $\sim$ 0.8 mag down (crosses, $\times$) because they are systematically about 0.8 mag brighter than the V-magnitude obtained by Sekiguchi et al. (1990). The decline rate of the V light in the early phase depends very sensitively on the WD mass, but depends hardly on the hydrogen content X, the companion (its mass and radius), or the size of the accretion disk, so that we can safely determine the WD mass from the early light curve (see also Kato 1999).

Our fitting indicates an apparent distance modulus of $(m - M)_V = 17.0$. Thus, the distance to V745 Sco is derived to be $d = 5.0$ kpc if we adopt the absorption of $A_V = 3.1 \times E(B-V) = 3.5$, where $E(B-V) = 1.1$ (Harrison et al. 1993; Williams 1994).

From our solutions, the envelope mass at the maximum V light is estimated to be $\Delta M = 4.6 \times 10^{-6} M_\odot$, indicating a mass accretion rate of $\dot{M}_{\rm acc} = 0.9 \times 10^{-7} M_\odot$ yr^{-1} between the 1937 and 1989 outbursts. About 95% of the envelope mass has been blown off by the wind and the residual 5% ($2.3 \times 10^{-7} M_\odot$) has been left and added to the helium layer of the WD. Therefore, we obtain the net mass increasing rate of the WD as $\dot{M}_{\rm He} = 0.45 \times 10^{-8} M_\odot$ yr^{-1}.

7.2. *Irradiation Effect of Companion M-giant*

In the late phase ($t \sim$ 25—200 days after the optical maximum), contributions of the irradiated red giant (RG) and accretion disk (ACDK) to the V light may become dominant like as in T CrB and RS Oph. First, in this subsection, we examine the irradiation effect of the M-giant, and then, in the next subsection, we also study the irradiation of the ACDK.

In order to examine companion's irradiation effect, we need to know the separation, mass ratio, inclination angle, and the radius of the red giant, but none of them is known. The lack of both the orbital information and the visual luminosity observation in the late phase clouds the accurate determination of the outburst model because of ample ambiguity in the system parameters.

The orbit is assumed to be circular. It is observationally suggested that orbital periods of S-type symbiotic stars are related to their spectral type by

$$P \sim (1.31)^S \times 190 \text{ days}, \tag{63}$$

where the power of S means the sub-spectral type of M-giants ($S = 4$ for M4 III, see, e.g., Mürset & Schmid 1999; Harries & Howarth 2000). From this relation, we assume $P = 560$ days for V745 Sco (M4 III, e.g., Harrison et al. 1993) and the ephemeris for inferior conjunction of the M-giant in front, $\phi_{\rm min} = {\rm HJD}\ 2,448,700.0 + 560E$. In what follows, we refer this ephemeris simply as $\phi_{\rm min} = 700$ day.

It has also been suggested that M-giants in S-type symbiotic stars lies well within the inner critical Roche lobe,

that is, $\gamma \sim 0.3 - 0.6$ (e.g., Mürset & Schmid 1999). Therefore, we assume roughly the ratio of

$$\frac{R_{\rm RG}}{R_2^*} \equiv \gamma \sim \frac{1}{2}. \quad (64)$$

In addition, we also assume 50% efficiency of the irradiation ($\eta_{\rm RG} = 0.5$). For the companion M-giant, Sekiguchi et al. (1990) suggested $m_V = 17$ in quiescence from the V magnitude just after the outburst. Anupama & Mikołajewska (1999) obtained $m_{5500} = 17.7$ in March 1998. We adopt here $m_V = 17.7$ in quiescence.

The light curves are calculated for six cases of the companion mass, i.e., $M_{\rm RG} = 0.5$, 0.6, 0.7, 0.8, 1.0, and $1.2 M_\odot$. Since we have obtained similar light curves for all of these six masses, we show here only the results for $M_{\rm RG} = 1.0 M_\odot$. For this case, the separation is $a = 380.1 R_\odot$, the effective radii of the inner critical Roche lobes are $R_1^* = 154.0 R_\odot$ for the WD component, and $R_2^* = 134.3 R_\odot$ for the RG component. If $\gamma = 0.5$, then we have $R_2 = R_{\rm RG} = 0.5 R_2^* \sim 67 R_\odot$. Then, the nonirradiated photospheric temperature of the RG is estimated to be $T_{\rm ph,RG} = 2700$ K from the light curve fitting in quiescence.

We have finally adopted the best fit set of the inclination angle $i = 80°$ for the ephemeris of $\phi_{\rm min} = 700$ day as shown in Figure 13. Dash-dotted curves in Figure 14 show V light curves for various inclination angles ($i = 30°$, $60°$, $80°$) of the orbit for the ephemeris of $\phi_{\rm min} = 700$ day. Their light curves depends hardly on the inclination angle because the non-irradiated hemisphere of the M-giant faces towards the Earth. On the other hand, V light is much brighter (dotted curves) if the ephemeris of $\phi_{\rm min} = 500$ day is adopted because the irradiated hemisphere of the M-giant faces towards the Earth, which is not compatible with the observation.

Figure 15 shows the dependency of the hydrogen content, X. The early-phase V light curve depends hardly on the hydrogen content, while the late-phase V light curve is weakly identified by the hydrogen content of the WD envelope. The optically thick, outburst wind stops 59, 69, 82 days after maximum, and the steady hydrogen shell burning ends 71, 90, 123 days after maximum, for $X = 0.35$, 0.50, and 0.70, respectively. The V light curve indicates that the hydrogen content is somewhere between $X = 0.5$ and $X = 0.7$ (dash-dotted curves).

We have also calculated light curves for a much longer orbital period ($P = 1000$ days, for M6 III, e.g., Anupama & Mikołajewska 1999), and have obtained similar results to those for $P = 560$ days. In this case, the binary parameters are $a = 559.4 R_\odot$, $R_1^* = 226.7 R_\odot$, $R_2^* = 197.6 R_\odot$, $R_2 = 99 R_\odot$. We have estimated $T_{\rm RG} = 2500$ K for the best fit model in the late phase.

7.3. *Small Irradiation Effect of Accretion Disk*

In this subsection, we show that the ACDK should not contribute so much to the V light. Since the visual light curve is well reproduced by M-giant's irradiation with no accretion disk, one may imagine that the accretion disk does not contribute much. Here, we determine the upper limit of the ACDK size in relation to the reason why a secondary maximum does not occur in V745 Sco.

We here again assume 50% efficiency of the ACDK irradiation ($\eta_{\rm DK} = 0.5$). The temperature of the unheated surface of the ACDK including the rim is assumed to be $T_{\rm disk} = 1000$ K. We have examined another case of $T_{\rm disk} = 0$ K, but found no significant differences in the V light curves. The power of ν is assumed to be $\nu = 9/8$ from the standard disk model.

We have finally obtain allowable sets of the disk parameters of $\alpha \lesssim 0.01$ and $\beta \lesssim 0.01$ for the orbital inclination angle of $i \sim 80°$ as shown in Figure 13. Here, the thin solid line denotes the case of $\alpha = 0.01$ and $\beta = 0.01$, while the dash-dotted line corresponds to $\alpha = 0$ (no accretion disk). Both can reproduce the V light curve of the 1989 outburst.

We have examined six cases of the inclination angle of the orbit, $i = 80°$, $70°$, $60°$, $50°$, $40°$, and $30°$ and shown three of them in Figure 14. The V light curves are more luminous for a lower inclination angle of the orbit, since a larger area of the ACDK can be seen from the Earth. This means that lower inclinations of the orbit contradicts the existence of a large ACDK. To summarize, for any case, the ACDK should not contribute so much to the V light.

Figure 15 shows the dependency of the hydrogen content for the case with an accretion disk. The V light curves suggest that the hydrogen content is not clearly identified by the observation but it may be somewhere between $X = 0.5$ and 0.7 (solid curves).

Thus, a very small size of the optically thick ACDK, i.e., $R_{\rm disk} \lesssim 1\ R_\odot$, in the late phase indicates no secondary maximum of the light curve as discussed in RS Oph even if the warping instability sets in.

7.4. *The Distance, Envelope Mass of the White Dwarf, and Possibility of SN Ia Explosion*

The distance to V745 Sco is estimated to be $d = 5.0$ kpc with the absorption of $A_V = 3.5$. This is roughly consistent with Harrison et al.'s (1993) estimation of $d = 4.6$ kpc. Harrison et al. attributed M4 III to the cool component from the infrared CO lines. Assuming the absolute magnitude of $M_K = -5.5$ (M4 III), they obtain the distance modulus of $(m - M)_0 = m_K - M_K - A_K = 8.2 - (-5.5) - 0.4 = 13.3$, where they adopted $m_K = 8.2$ from Sekiguchi et al. (1990) and used a relation between the absorptions of A_K and A_V given by Rieke & Lebofsky (1985), i.e., $A_K/A_V = 0.112$.

Sekiguchi et al.'s (1990) K-band luminosity $m_K = 8.21$ (87 days after maximum) is about 0.2 mag brighter than Harrison et al.'s (1993) K-band luminosity $m_K = 8.41$ (two years after the 1989 outburst). This is consistent with our models as seen in Figure 13, because the cool component had been strongly irradiated by the WD photosphere always during Sekiguchi et al.'s observations. Using $m_K = 8.41$, we obtain a distance modulus of $(m - M)_0 = m_K - M_K - A_K = 8.41 - (-5.5) - 0.4 = 13.5$, i.e., $d = 5.0$ kpc, being coincided with our distance estimation.

At the end of this section, we discuss the possibility of SN Ia explosion. We have already obtained the average mass accretion rate of $\dot{M}_{\rm acc} = 0.9 \times 10^{-7} M_\odot$ yr^{-1} between the 1937 and 1989 outbursts from the envelope mass of $\Delta M = 4.6 \times 10^{-6} M_\odot$. This meets condition (52) for SN Ia explosions (Nomoto & Kondo 1991), For all the three cases of $X = 0.70$, 0.50, and 0.35, about 95% of the envelope mass has been blown off in the outburst wind and the residual 5% ($2.3 \times 10^{-7} M_\odot$) has been left and added to the

helium layer of the WD. Therefore, we obtain the net mass increasing rate of the WD of $\dot{M}_{\rm He} = 0.45 \times 10^{-8} M_\odot$ yr^{-1}. Thus, we may conclude that V745 Sco is also an immediate progenitor of Type Ia supernova if the hot component is a carbon-oxygen white dwarf.

8. V3890 SAGITTARII

V3890 Sagittarii underwent the second recorded outburst in 1990 (since the 1962 first recorded outburst), and has been recognized as a member of the recurrent novae (Jones 1990a; Liller 1990). Its light curve is characterized by a very rapid rise (within two days) and fast decline ($t_3 \sim 17$ days; see, e.g., Fig. 1 in González-Riestra 1992). The general spectral evolution closely resembles that of RS Oph (e.g., Sekiguchi 1990). The cool component has been classified from optical spectra as M4 III (Sekiguchi 1990), M8 III (Williams et al. 1991), or M5 III (Anupama & Mikołajewska 1999). The infrared spectra and colors indicate a spectral type M5 III (Harrison et al. 1993). Thus, V3890 Sgr is a similar system to RS Oph and V745 Sco, a member of the recurrent novae with an M-giant secondary.

8.1. *The Model of the 1990 Outburst*

We have calculated the total V light of the WD photosphere and the non-irradiated RG photosphere for the WD mass of $M_{\rm WD} = 1.2$, 1.3, 1.34, 1.35, 1.36, 1.37, and $1.377 M_\odot$ by assuming the hydrogen content $X = 0.70$ and the solar metallicity of $Z = 0.02$. Four of them (1.2, 1.3, 1.35, and 1.37 $M_\odot$) are plotted in Figure 16 (solid curves). Here, we assume that the optical maximum was reached on HJD 2,2448,009. This is because the irradiation of the M-giant cannot contribute to the early phase V light.

The observed V light curve in the first 20 days can be roughly reproduced by the model of $1.3 M_\odot$ WD, but it deviates greatly in the ensuing phase (20—40 days after maximum). The envelope mass of the $1.3 M_\odot$ WD at the optical maximum is too large to be compatible with the TNR model. The envelope mass of $\Delta M \sim 5 \times 10^{-6} M_\odot$ suggests $\dot{M}_{\rm acc} \sim 2 \times 10^{-7} M_\odot$ yr^{-1}, which is just below the lower limit of steady hydrogen shell burning for $X = 0.7$, i.e., $\dot{M}_{\rm std}$ in equation (7) and also in Figure 2.

Only a bloated WD photosphere cannot reproduce the V light curve even in the early phase of outburst. Moreover, our simple picture of the WD photosphere never shows a sharp spike on the light curve as seen in Figure 16. These features strongly suggest that the irradiation of the accretion disk is important even in the early phase: if the optically thick region of the accretion disk is as large as or larger than $\sim 10\ R_\odot$, the decay of the V light becomes much slower as seen in RS Ohp (see, e.g., Fig. 11). Therefore, we seek a reasonable set of system parameters based on the assumption that the V3890 Sgr system consists of the WD photosphere, the irradiated M-giant, and the irradiated accretion disk.

8.2. *Large Size of Accretion Disk in Early Phase*

In order to obtain a consistent set of system parameters, we have to adopt the WD mass more massive than $M_{\rm WD} \gtrsim 1.35 M_\odot$, and a size of the irradiated ACDK larger than $R_{\rm disk} \gtrsim 10\ R_\odot$ at the initial phase of outburst. The condition of $M_{\rm WD} \gtrsim 1.35 M_\odot$ is required from the consistencies with the TNR model, i.e., the mass accretion rate is smaller than $\dot{M}_{\rm acc} \lesssim 1 \times 10^{-7} M_\odot$ yr^{-1}, and the rapid decline of the V light curve 20—40 days after maximum as shown in Figure 16. The V light curve of a $1.34 M_\odot$ WD model lies above the observational points on the day 26 and the upper limits on the day 33 and 37, being not consistent with the observation. On the other hand, V light curve of a $1.35 M_\odot$ or $1.37 M_\odot$ WD is less bright during the day 3—40. The lack of the luminosity during these days can be supplied by the irradiation of a large size accretion disk.

Figure 17 shows V light curves of fixed-size disk models for the WD masses of 1.35 $M_\odot$ (solid curves) and 1.37 $M_\odot$ (dashed curves). The disk size parameters are $\alpha = 0.7$, 0.1, and 0.01. It is clear that the fixed-size disk model cannot reproduce the V light curve in the later stage. This is simply because the large disk contributes too much in the later phase.

Here, we summarize our parameters: the orbital period of $P = 730$ days from equation (63) and the spectral type of M5 III (Anupama & Mikołajewska 1999) for the cool component, the ephemeris for the M-giant in front is $\phi_{\rm min}$ = HJD 2,448,050.0 $+730 \times E$, $\gamma = 0.5$ from equation (64), 50% efficiency of the irradiation ($\eta_{\rm RG} = 0.5$), the M-giant mass of $M_{\rm RG} = 1.0\ M_\odot$. In this case, the separation is $a = 453.5 R_\odot$, the effective radii of the inner critical Roche lobes are $R_1^* = 183.8 R_\odot$ for the WD component and $R_2^* = 160.2 R_\odot$ for the RG component. Then, we have $R_{\rm RG} = 0.5 R_2^* \sim 80 R_\odot$. The nonirradiated photospheric temperature of the RG is estimated to be $T_{\rm ph,RG} = 2600$ K from fitting with the quiescent V magnitude of $m_V \sim 16$ (Anupama & Mikołajewska 1999). For the accretion disk, we assume 50% efficiency of the irradiation ($\eta_{\rm DK} = 0.5$), the unheated surface temperature of $T_{\rm disk} = 1000$ K.

8.3. *Evaporating Accretion Disk*

The optically thick strong wind blows during the outburst so that the disk surface is certainly blown off in the wind due to drag and ablation. Moreover, the mass transfer from the M-giant is certainly inhibited during the strong wind phase because the cool red giant wind has been evacuated by the hot wind from the WD as discussed in RS Oph. In such a situation, it is very likely that the edge of the disk is gradually dissipating with time. We here simulate such an effect by shrinking the disk size exponentially, i.e.,

$$\alpha = \alpha_0 \left(\frac{\alpha_1}{\alpha_0} \right)^{(t-t_0)/30}, \tag{65}$$

where we adopt $\alpha_0 = 0.7$ and $\alpha_1 = 0.01$, t_0 is the time of the optical maximum, and the time t is in units of day. We set the minimum size of the ACDK at $\alpha = 0.001$ in our calculations.

Thus, we have obtained the best fit model for the WD mass of $M_{\rm WD} = 1.35 \pm 0.01\ M_\odot$ as shown in Figures 17 and 18. The envelope mass at the maximum V light is estimated to be $\Delta M = 3.1 \times 10^{-6} M_\odot$, indicating a mass transfer rate of $\dot{M}_{\rm acc} = 1.1 \times 10^{-7} M_\odot$ yr^{-1} between the 1962 and 1990 outbursts. The efficiency of the ACDK irradiation has been examined for other two cases of $\eta_{\rm DK} = 1.0$ (dot-dashed line) and 0.25 (dotted line) only for $X = 0.70$ and $M_{\rm WD} = 1.35\ M_\odot$ as shown in Figure 18.

We have examined the dependency of the V light curve on the orbital inclination angle. The luminosity of the ACDK depends largely on the the orbital inclination angle mainly because a larger area of the ACDK can be seen from the Earth for a smaller inclination angle. Therefore, the inclination angle should be as low as $i \lesssim 30^\circ$ to reproduce the V light curve during $t \sim 5$—20 days after maximum.

We have also calculated V-light curves for other four cases of the companion mass, i.e., $M_{\rm RG}$ =0.6, 0.7, 0.8, and 1.2 $M_\odot$, but obtained similar light curves to $M_{\rm RG} = 1.0\ M_\odot$. We have checked the other case of $T_{\rm disk} = 0$ K, but found no significant differences in the light curves. The power of ν is fixed to be $\nu = 9/8$, but we cannot find any significant differences in the light curves even if we adopt $\nu = 2$. Finally, we have study the effect of hydrogen content. Either the early- or late-phase V light curve depends hardly on the hydrogen content X as shown in Figure 18. The optically thick, outburst wind stops 56, 68, and 80 days after maximum, and the steady hydrogen shell burning ends 68, 89, and 122 days after maximum, for $X = 0.35$, 0.50, and 0.70, respectively.

Anupama & Sethi (1994) obtained optical spectra 18—20 days after maximum. They pointed out that these line features closely resembles the spectrum of RS Oph 60 days after maximum. Anupama & Sethi derived the Zanstra temperature $T_* = 300,000$ K of the ionizing central source from the helium and hydrogen line (Hβ and He II 4686 Å) ratios and its radius $R_* = 0.06 R_\odot$ from Hβ line flux. For RS Oph, our model gives us $T_{\rm ph} = 300,000$ K and $R_{\rm ph} = 0.08\ R_\odot$ about 70 days after maximum (see the previous section), being roughly consistent with the Zanstra temperature derived by Anupama & Sethi. For V3890 Sgr, however, our model suggests $T_{\rm ph} = 83,000$ K and $R_{\rm ph} = 1.0\ R_\odot$ on the day 18, being not consistent. This may indicate the importance of the contribution from the shocked layer photons.

Mukai et al. (1990) obtained optical spectrum on May 14 (17 days after maximum). Comparing them with the earlier spectra observed by Wagner, Bertram, & Starrfield (1990) and Buckley et al. (1990), Mukai et al. pointed out that V3890 Sgr had progressed to a higher ionization state on that day. In our modeling of the light curve, the accretion disk plays a key role in these days. It is very likely that the conspicuous change in the spectrum ~ 20 days after maximum is caused by the evaporation of the accretion disk. As seen in Figure 17, the disk size decreases to $\lesssim 1\ R_\odot$ on the day ~ 20. Then, the mean temperature of the disk surface increases to $\gtrsim 50,000$ K. The same thing happens in RS Oph around the day $\sim$60—70.

We thus suggest a very small size of the optically thick ACDK or no disk, that is, $R_{\rm disk} \lesssim 0.1\ R_\odot$, in the late phase (after HJD 2,448,036, indicated by "disk vanishes" in Figure 17). Therefore, no secondary maximum of the light curve is expected as well as in RS Oph and V745 Sco.

8.4. *The Distance, Envelope Mass of the White Dwarf, and Possibility of SN Ia Explosion*

Fitting indicates an apparent distance modulus of $(m - M)_V = 14.7$. Thus, the distance to V3890 Sgr is derived to be $d = 4.2$ kpc if we adopt the absorption of $A_V = 3.1 \times E(B-V) = 1.6$, where $E(B-V) = 0.5$ (Harrison et al. 1993), because the distance modulus is $(m - M)_0 = (m - M)_V - A_V = 14.7 - 1.6 = 13.1$. This is roughly consistent with Harrison et al.'s (1993) estimation of $d = 5.2$ kpc. Harrison et al. determined the infrared spectral type of the cool companion as M5 III. Assuming $M_K = -5.5$ (M5 III), they obtained the distance modulus of $(m - M)_0 = m_K - M_K - A_K = 8.24 - (-5.5) - 0.17 = 13.6$ by using Rieke & Lebofsky (1985) relation of $A_K/A_V = 0.112$. It should be noted here that there are a large divergence in the observed color excesses: González-Riestra (1992) determined $E(B-V) = 1.1$ from UV lines; Williams (1994) obtained $E(B-V) = 0.76$ from H I and He II line ratios; Anupama & Sethi (1994) obtained $E(B-V) = 1.1$ from the He I line ratios, and $E(B-V) = 1.2$ from the Hα/Hβ ratio.

Finally, we examine the possibility of Type Ia supernova explosion. The envelope mass at the maximum V light is estimated to be $\Delta M = 3.1 \times 10^{-6} M_\odot$ from our solutions, indicating a mass transfer rate of $\dot{M}_{\rm acc} = 1.1 \times 10^{-7} M_\odot$ yr^{-1} between the 1962 and 1990 outbursts. Moreover, about 90% of the envelope mass has been blown off in the outburst wind and the residual 10% ($3 \times 10^{-7} M_\odot$) has been left and added to the helium layer of the WD. Therefore, we obtain the net mass increasing rate of $\dot{M}_{\rm He} = 1.1 \times 10^{-8} M_\odot$ yr^{-1}. This meets condition (52) of SN Ia explosion (e.g., Nomoto & Kondo 1991), if the WD consists of carbon and oxygen. Thus, we may conclude that V3890 Sgr is an immediate progenitor of Type Ia supernova if the hot component is a carbon-oxygen white dwarf. The white dwarf can grow to $1.378 M_\odot$ even if mild helium shell flashes repeatedly occur after the helium layer grows to the critical mass at which helium ignites (see, e.g., Kato & Hachisu 1999).

9. CONCLUSIONS

We have developed a numerical method for calculating light curves of recurrent nova outbursts. Our basic model consists of a white dwarf with an accretion disk and a red giant companion. The calculated light curves includes contributions from the white dwarf photosphere, the irradiated accretion disk, and the irradiated red giant. We summarize our main results on the light curve analysis of the four recurrent novae with a red giant companion, T CrB, RS Oph, V745 Sco, and V3890 Sgr.

9.1. *Relevance to Type Ia Supernova Progenitors*

1. The mass of white dwarf (WD) has been estimated, from the decline of early-phase light curve, to be $M_{\rm WD} = 1.37 \pm 0.01\ M_\odot$ for T CrB, $1.35 \pm 0.01\ M_\odot$ with solar metallicity ($Z = 0.02$) or $1.377 \pm 0.01\ M_\odot$ with low metallicity ($Z = 0.004$) for RS Oph, $1.35 \pm 0.01\ M_\odot$ for V745 Sco, and $1.35 \pm 0.01\ M_\odot$ for V3890 Sgr.

2. The apparent distance moduli are obtained, with the light curve fitting, to be $(m - M)_V = 10.2$ for T CrB, $(m - M)_V = 11.2$ for RS Oph, $(m - M)_V = 17.0$ for V745 Sco, and $(m - M)_V = 14.7$ for V3890 Sgr. Therefore, the distances are estimated to be $d = 0.94$ kpc with $A_V = 0.35$ for T CrB, $d = 0.57$ kpc with $A_V = 2.3$ for RS Oph, $d = 5.0$ kpc with $A_V = 3.5$ for V745 Sco, and $d = 4.2$ kpc with $A_V = 1.6$ for V3890 Sgr.

3. Each envelope mass at the optical maximum is also calculated to be $\Delta M \sim 3 \times 10^{-6} M_\odot$ (T CrB), $2 \times 10^{-6} M_\odot$ (RS Oph), $5 \times 10^{-6} M_\odot$ (V745 Sco), $3 \times 10^{-6} M_\odot$ (V3890 Sgr), which indicates an average mass accretion rate of $\dot{M}_{\rm acc} \sim 0.4 \times 10^{-7} M_\odot$ yr^{-1} (80 yrs, T CrB), $1.2 \times 10^{-7} M_\odot$ yr^{-1} (18 yrs, RS Oph), $0.9 \times 10^{-7} M_\odot$ yr^{-1} (52 yrs, V745 Sco), $1.1 \times 10^{-7} M_\odot$ yr^{-1} (28 yrs, V3890 Sgr) during quiescent phase.
4. Although a large part of the envelope mass is blown in the wind, each white dwarf can retain a substantial part of the envelope mass after hydrogen burning. Thus, we have obtained net mass-increasing rates of the WDs, $\dot{M}_{\rm He} \sim 0.10 \times 10^{-7} M_\odot$ yr^{-1} (T CrB), $0.12 \times 10^{-7} M_\odot$ yr^{-1} (RS Oph), $0.05 \times 10^{-7} M_\odot$ yr^{-1} (V745 Sco), $0.11 \times 10^{-7} M_\odot$ yr^{-1} (V3890 Sgr).
5. These results strongly indicate that the white dwarfs in recurrent novae have now grown up to near the Chandrasekhar mass limit and will soon explode as a Type Ia supernova if the white dwarf consists of carbon and oxygen.

9.2. *Appearance/Absence of Secondary Maximum*

6. Among the four recurrent novae with a red giant companion, only T CrB shows a secondary maximum 120—190 days after the optical maximum. This secondary maximum can be well reproduced if an irradiated accretion disk of $R_{\rm disk} \sim 6\ R_\odot$ around the white dwarf tilts due to a radiation-induced warping instability. If we neglect the accretion disk, we cannot fully reproduce the secondary peak by an irradiated M-giant model.
7. The difference between T CrB and the others is in the companion: it fills its inner critical Roche lobe only in T CrB but in the others does not. Therefore, in T CrB the mass transfer is mainly driven by the Roche lobe overflow while in the other systems matter is fed by cool red giant winds. In T CrB, the mass transfer continues even in the outburst wind phase, which maintains an optically thick accretion disk large enough to show a secondary maximum after a tilting instability grows up.
8. The other three systems, RS Oph, V745 Sco, and V3890 Sgr, cannot maintain the mass transfer during the outburst because the cool red giant wind has once been evacuated by the ejecta of the outburst. The light curves of RS Oph and V3890 Sgr require a relatively large size accretion disk of $R_{\rm disk} \sim 10\ R_\odot$ in the mid-phase but a small size of $R_{\rm disk} \lesssim 1\ R_\odot$ in the late-phase. The late-phase UV data of RS Oph can be well reproduced with a small accretion disk of $R_{\rm disk} \sim 0.5 R_\odot$. No or a very small accretion disk is also derived in V745 Sco. These accretion disks are quickly dissipating to become as small as $R_{\rm disk} \lesssim 1\ R_\odot$, at least, in the late phase of the outbursts, because no mass is fed. Such a small disk cannot contribute much to the V light. Even if the tilting instability begins to grow after the wind stops, it is therefore very unlikely that secondary maxima like in T CrB are observed in these three systems.
9. The post-outburst minima of RS Oph outbursts, which is 1 mag (in V) below the quiescent level and continues for $\sim$ 300 days from 100 to 400 days after the optical maximum, is understood from the evacuation of the cool red giant wind by the ejecta of nova. After the hot WD wind stops 80 days after the optical maximum, the cool red giant wind expands to recover again in $\sim$ 300 days. Then, $\sim$ 400 days after maximum, mass accretion from the red giant wind to the white dwarf resumes. Supersoft X-rays from the white dwarf, which were observed about 250 days after maximum, are very consistent with the end of hot WD wind and the evacuation of the cool red giant wind.

This research has been supported in part by the Grant-in-Aid for Scientific Research (08640321, 09640325, 11640226) of the Japanese Ministry of Education, Science, Culture, and Sports.

REFERENCES

Albinson, J. S., Bode, M. F., Evans, A., & Goldsmith, M. J. 1985, IAU Circ. No. 4091
Alcock, G. E. D. 1985, IAU Circ. No. 4031
Allen, C. W. 1973, Astrophysical Quantities (London: The Athlone Press), chap. 10
Anupama, G. C., & Mikołajewska, J. 1999, A&A, 344, 177
Anupama, G. C., & Sethi, S. 1994, MNRAS, 269, 105
Ashbrook, J. 1946, Harvard Bull., 918, 7
Bailey, J. 1975, JBAS, 85, 217
Bailey, J. 1981, MNRAS, 197, 31
Belczyński, K., & Mikołajewska, J. 1998, MNRAS, 296, 77
Bessell, M. S. 1990, PASP, 102, 1181
Bessell, M. S., & Brett, J. M. 1988, PASP, 100, 1134
Boattini, A. 1990, IAU Circ., No. 5007
Bode, M. F. 1987, RS Ophiuchi (1985) and the Recurrent Novae Phenomenon (VNU Science Press, Utrecht)
Bode, M. F., & Kahn, F. D., 1985, MNRAS, 217, 205
Bohigas, J., Echevarría, J., Diego, F., & Sarmiento, J. A. 1989, MNRAS, 238, 1395
Bortle, J. 1985a, IAU Circ. No. 4048
Bortle, J. 1985b, IAU Circ. No. 4049
Bortle, J. 1985c, IAU Circ. No. 4074
Buckley, D. A., Wargau, W. F., & Soltynski, M. G. 1990, IAU Circ., No. 5019
Cannizzo, J. K., & Kenyon, S. J. 1992, ApJ, 386, L17
Contini, M., Orio, M., & Prialnik, D. 1995, MNRAS, 275, 195
Cook, L. 1985a, IAU Circ. No. 4036
Cook, L. 1985b, IAU Circ. No. 4048
Cook, L. 1985c, IAU Circ. No. 4066
Cordova, F. A., Mason, K. O., & Nelson, J. E. 1981, ApJ, 245, 609
Danskin, K. 1985, IAU Circ. No. 4031
Della Valle, M., Livio, M. 1996, ApJ, 473, 240
Deutsch, A. J. 1948, PASP, 60, 120
Dobrzycka, D., & Kenyon, S. J. 1994, AJ, 108, 2259
Dobrzycka, D., Kenyon, S. J., Proga, D., Mikołajewska, J., Wade, R. A. 1996, AJ, 111, 2090
Ducoty, R. 1985a, IAU Circ. No. 4031
Ducoty, R. 1985b, IAU Circ. No. 4036
Ducoty, R. 1985c, IAU Circ. No. 4066
Duerbeck, H. W., & Schwarz, H. E. 1989, IAU Circ., No. 4825
Duerbeck, H. W., Schwarz, H. E., & Augusteijn, T. 1989, IAU Circ., No. 4844
Duerbeck, H. W., Seitter, W. C. 1990, in IAU Colloquium 122, The Physics of Classical Novae, eds. A. Cassatella & R. Viotti (Berlin: Springer), 425
Dufay, J., Bloch, M., Bertaud, Ch., & Dufay, M. 1964, Annales d'Astrophysique, 27, 555
Eggleton, P. P. 1983, ApJ, 268, 368
Ellerbe, J. 1985, IAU Circ. No. 4066
Evans, A., Callus, C. M., Albinson, J. S., Whitelock, P. A., Glass, I. S., Carter, B., & Roberts, G. 1988, MNRAS, 234, 755
Fekel, F. C., Joyce, R. R., Hinkle, K. H., & Skrutskie, M. 2000, AJ, 119, 1375
González-Riestra, R. 1992, A&A, 265, 71
Gorbatskii, V. G. 1972, Soviet Astr., 16, 32
Hachisu, I., & Kato, M. 1999, ApJ, 517, L47
Hachisu, I., & Kato, M. 2000a, ApJ, 536, L93
Hachisu, I., & Kato, M. 2000b, ApJ, 540, 447
Hachisu, I., Kato, M., Kato, T., & Matsumoto, K. 2000a, ApJ, 528, L97

Hachisu, I., Kato, M., Kato, T., Matsumoto, K., & Nomoto, K. 2000b, ApJ, 534, L189
Hachisu, I., Kato, M., & Nomoto, K. 1996, ApJ, 470, L97
Hachisu, I., Kato, M., & Nomoto, K. 1999a, ApJ, 522, 487
Hachisu, I., Kato, M., Nomoto, K., & Umeda, H. 1999b, ApJ, 519, 314
Harries, T. J., & Howarth, I. D. 2000, A&A, 361, 139
Harrison, T. E., Johnson, J. J., & Spyromilio, J. 1993, AJ, 105, 320
Herbig, G. H., & Neubauer, F. J. 1946, PASP, 58, 196
Hjellming, R. M. 1989, IAU Circ., No. 4853
Hjellming, R. M., van Gorkom, J. H., Taylor, A. R., Seaquist, E. R., Padin, S., Davis, R. J., & Bode, M. F. 1986, ApJ, 305, L71
Honda, M. 1989, IAU Circ., No. 4829
Hric, L., Petrik, K., Urban, Z., Niarchos, P., & Anupama, C. G. 1998, A&A, 339, 449
Hurst, G. M. 1985a, IAU Circ. No. 4031
Hurst, G. M. 1985b, IAU Circ. No. 4048
Ianna, P. A. 1964, ApJ, 139, 780
Iben, I. Jr., & Tutukov, A. V. 1984, ApJS, 54, 335
Iglesias, C. A., & Rogers, F. 1996, ApJ, 464, 943
Itoh, H., & Hachisu, I. 1990, ApJ, 358, 551
Jones, A. F. 1990a, IAU Circ., No. 5002
Jones, A. F. 1990b, IAU Circ., No. 5004
Jones, A. F. 1990c, IAU Circ., No. 5007
Kahabka, P., Hartmann, H. W., Parmar, A. N., & Negueruela, I. 1999, A&A, 374, L43
Kahabka, P., & van den Heuvel, E. P. J. 1997, ARA&A, 35, 69
Kato, M. 1983, PASJ, 35, 507
Kato, M. 1990, ApJ, 355, 277
Kato, M. 1991, ApJ, 369, 471
Kato, M. 1994, A&A, 281, L49
Kato, M. 1995, in Cataclysmic Variables, eds. A. Bianchini, M. Della Valle, & M. Orio (Dordrecht: Kluwer), 243
Kato, M. 1999, PASJ, 51, 525
Kato, M., & Hachisu, I., 1994, ApJ, 437, 802
Kato, M., Hachisu, I., 1999, ApJ, 513, L41
Kenyon, S. J., Fernandez-Castro, T., & Stencel, R. E. 1988, AJ, 95, 1817
Kenyon, S. J., & Garcia, M. R. 1986, AJ, 91, 125
Kenyon, S., & Webbink, R. 1984, ApJ, 279, 252
King, R. 1985, IAU Circ. No. 4036
Kovetz, A., Prialnik, D. 1994, ApJ, 424, 319
Kraft, R. P. 1958, ApJ, 127, 625
Li, X.-D., van den Heuvel, E. P. J. 1997, A&A, 322, L9
Liller, W. 1989a, IAU Circ., No. 4820
Liller, W. 1989b, IAU Circ., No. 4826
Liller, W. 1990, IAU Circ., No. 5010
Leibowitz, E. M., Ofek, E. O., & Mattei, J. A. 1997, MNRAS, 287, 634
Lines, H. C., Lines, R. D., & McFaul, T. G. 1988, AJ, 95, 1505
Livio, M. 2000, Type Ia Supernovae: Theory and Cosmology, (Cambridge: Cambridge Univ. Press), in press (astro-ph/9903264)
Livio, M., & Pringle, J. E. 1996, ApJ, 465, L55
Livio, M., & Truran, J. W. 1992, ApJ, 389, 695
Livio, M., Truran, J. W., & Webbink, R. F. 1986, ApJ, 308, 736
Lloyd, H. M., Bode, M. F., O'Brien, T. J., & Kahn, F. D. 1993, MNRAS, 265, 457
Lowder, W. 1985, IAU Circ. No. 4031
Lubbock, S. 1985a, IAU Circ. No. 4036
Lubbock, S. 1985b, IAU Circ. No. 4048
Makino, F. 1989, IAU Circ., No. 4285
Mason, K. O., Córdova, F. A., Bode, M. F., Barr, P. 1987, RS Ophiuchi (1985) and the Recurrent Novae Phenomenon, ed. M. F. Bode (VNU Science Press, Utrecht), 167
Maloney, P., Begelman, M. C., & Pringle, J. E. 1996, ApJ, 472, 582
Matsumoto, K., Kato, T., & Hachisu, I. 2000, PASJ, submitted
McLaughlin, D. B., 1946, PASP, 58, 159
McNaught, R. H. 1985a, IAU Circ. No. 4031
McNaught, R. H. 1985b, IAU Circ. No. 4036
McNaught, R. H. 1985c, IAU Circ. No. 4048
McNaught, R. H. 1985d, IAU Circ. No. 4066
Medway, K. 1985, IAU Circ. No. 4048
Mennickent, R. E.; Honeycutt, R. K. 1995, IBVS, No. 4232
Morgan, W. W., & Deutsch, A. J. 1947, ApJ, 106, 362
Mukai, K., Rosen, S. R., Supelli, K., & Allen, D. 1990, IAU Circ., No. 5015
Munari, U., Renzini, A. 1992, ApJ, 397, L87
Munari, U., Zwitter, T., Tomov, T., Bonifacio, P., Molaro, P., Selvelli, P., Tomasella, L., Niedzielski, A., & Pearce, A. 1999, A&A, 374, L39
Mürset, U., & Schmid, H. M. 1999, A&AS, 137, 473
Nomoto, K. 1982, ApJ, 253, 798
Nomoto, K., Nariai, K., & Sugimoto, D. 1979, PASJ, 31, 287
Nomoto, K., & Kondo, Y. 1991, ApJ, 367, L19
Nomoto, K., Thielemann, F., & Yokoi, K. 1984, ApJ, 286, 644
Nussbaumer, H., & Stencel, R. E. 1989, Exploring the Universe with the IUE Satellite, ed. Y. Kondo (Dordrecht: Kluwer), 203
O'Brien, T. J., Bode, M. F., & Kahn, F. D. 1992, MNRAS, 255, 683
O'Brien, T. J., & Kahn, F. D. 1987, MNRAS, 228, 277
Orio, M. 1993, A&A, 274, L41
Overbeek, D. 1989, IAU Circ., No. 4035
Paczynski, B. 1965, Acta Astronomica, 15, 197
Padin, S., Davis, R. J., & Bode, M. F. 1985, Nature, 315, 306
Patterson, J. et al. 1998, PASP, 110, 380
Payne-Gaposchkin, C., & Wright, F. W. 1946, ApJ, 104, 75
Pearce, A. 1990a, IAU Circ., No. 5002
Pearce, A. 1990b, IAU Circ., No. 5004
Pearce, A. 1990c, IAU Circ., No. 5007
Pearce, A. 1990d, IAU Circ., No. 5015
Pearce, A. 1990e, IAU Circ., No. 5021
Pearce, A. 1990f, IAU Circ., No. 5028
Pereira, A. 1990a, IAU Circ., No. 5007
Pereira, A. 1990b, IAU Circ., No. 5015
Perlmutter, S. et al. 1999, ApJ, 1999, 517, 565
Pettit, E. 1946a, PASP, 58, 153
Pettit, E. 1946b, PASP, 58, 213
Pettit, E. 1946c, PASP, 58, 255
Pettit, E. 1946d, PASP, 58, 359
Pottasch, S. R. 1967, Bull. Astr. Insts. Neth., 19, 227
Prialnik, D. 1986, ApJ, 310, 222
Pringle, J. E. 1996, MNRAS, 281, 357
Rieke, G. H., & Lebofsky, M. J. 1985, ApJ, 288, 618
Riess, A. G. et al. 1998, AJ, 116, 1009
Riggs, J. 1985, IAU Circ. No. 4036
Rosino, L. 1987, RS Ophiuchi (1985) and the Recurrent Novae Phenomenon, ed. M. F. Bode (VNU Science Press, Utrecht), 1
Rosino, L., & Iijima, T., 1987, RS Ophiuchi (1985) and the Recurrent Novae Phenomenon, ed. M. F. Bode (VNU Science Press, Utrecht), 27
Ruffert, M., Cannizzo, J. K., & Kenyon, S. J. 1993, ApJ, 419, 780
Sanford, R. F. 1946, PASP, 58, 156
Sanford, R. F. 1947, PASP, 59, 87
Sanford, R. F. 1949, ApJ, 109, 81
Schaefer, B. 1990, ApJ, 355, L39
Schaefer, B. E., Landold, A. U., Vogt, N., Buckley, D., Warner, B., Walker, A. R., & Bond, H. B. 1992, ApJS, 81, 321
Schaefer, B., & Ringwald, F. A. 1995, ApJ, 447, L45
Schandl, S., Meyer-Hofmeister, E., & Meyer, F. 1997, A&A, 318, 73
Schmeer, P. 1999, IAU Circ., No. 7113
Schmeer, P. 1990a, IAU Circ., No. 5015
Schmeer, P. 1990b, IAU Circ., No. 5021
Schmeer, P. 1990c, IAU Circ., No. 5028
Scovil, C. 1985, IAU Circ. No. 4031
Scott, A. D., Rawlings, J. M. C., Krautter, J., & Evans, A. 1994, MNRAS, 268, 749
Sekiguchi, K. 1990, IAU Circ., No. 5047
Sekiguchi, K., Whitelock, P. A., Feast, M. W., Barrett, P. E., Caldwell, J. A. R., Carter, B. S., Catchpole, R. M., Laing, J. D., Laney, C. D., Marang, F., & van Wyk, F. 1990, MNRAS, 246, 78
Sekiguchi, K. 1992, Variable Stars and Galaxies, ed. B. Warner (ASP Conference Series), Vol. 30, p. 345
Selvelli, P. L., Cassatella, A., & Gilmozzi, R. 1992, ApJ, 393, 289
Shahbaz, T., Somers, M., Yudin, B., & Naylor, T. 1997, MNRAS, 288, 1027
Shahbaz, T., Hauschildt, P. H., Naylor, T., & Ringwald, F. 1999, MNRAS, 306, 675
Shakura, N. I., & Sunyaev, R. A. 1973, A&A, 24, 337
Shore, S. N., Kenyon, S. J., Starrfield, S., & Sonneborn, G. 1996, ApJ, 456, 717
Shore, S., Sonneborn, G., & Starrfield, S. 1989, IAU Circ., No. 4826
Smith, V. V., Cunha, K., Jorissen, A., & Boffin, H. M. J. 1996, A&A, 315, 179
Snijders, M. A. J. 1987a, RS Ophiuchi (1985) and the Recurrent Novae Phenomenon, ed. M. F. Bode (VNU Science Press, Utrecht), p. 51
Snijders, M. A. J. 1987b, Ap&SS, 130, 243
Southwell, K. A., Livio, M., & Pringle, J. E. 1997, ApJ, 478, L29
Spoelstra, T. A. T., Taylor, A. R., Pooley, G. G., Evans, A., & Albinson, J. S. 1987, MNRAS, 224, 791
Starrfield, S., Sparks, W. M., & Shaviv, G. 1988, ApJ, 325, L35
Starrfield, S., Sparks, W. M., & Truran, J. W. 1985, ApJ, 291, 136
Sventek, P. 1985, IAU Circ. No. 4066
Taylor, A. R.; Davis, R. J.; Porcas, R. W.; Bode, M. F. 1989, MNRAS, 237, 81
Umeda, H., Nomoto, K., Kobayashi, C., Hachisu, I., & Kato, M. 1999a, ApJ, 522, L43
Umeda, H., Nomoto, K., Yamaoka, H., Wanajo, S. 1999b, ApJ, 513, 861
Verdenet, M. 1985, IAU Circ. No. 4066
Wallerstein, G. 1958, PASP, 70, 537
Wallerstein, G. 1961, PASP, 73, 153

Wallerstein, G., & Garnavich, P. M. 1985, PASP, 98, 875
Wagner, R. M., Bertram, R., & Starrfield, S. 1990, IAU Circ., No. 5006
Wagner, R. M., Bertram, R., Starrfield, S., & Shore, S. 1989, IAU Circ., No. 4822
Warner, B. 1995, Cataclysmic Variable Stars, (Cambridge: Cambridge University Press), chaps. 4 and 5
Webbink, R. F. 1976, Nature, 262, 271
Webbink, R. F. 1984, ApJ, 277, 355
Webbink, R. F., Livio, M., Truran, J. W., & Orio, M. 1987, ApJ, 314, 653
Weier, D. 1985, IAU Circ. No. 4036
Williams, R. E. 1992, AJ, 104, 725
Williams, R. E. 1994, ApJ, 426, 279
Williams, R. E., Hamuy, M., Phillips, M. M., Heathcote, S. R., Wells, L., & Navarrette, M. 1991, ApJ, 376, 721
Williams, R. E., Phillips, M. M., & Hamuy, M. 1994, ApJS, 90, 297
Williams, R. E., Sparks, W. M., Gallagher, J. S., Ney, E. P., Starrfield, S. G., & Truran, J. W. 1981, ApJ, 251, 221
Wright, F. W. 1946, Harvard Bull., 918, 9
Yudin, B, Munari, U. 1993, A&A, 270, 165
Zamanov, R. K., & Bruch, A. 1998, A&A, 338, 988

Table 1
Recurrent novae

Star	Subclass	$P_{\rm orb}$ (day)	Outburst Dates
RS Oph	RS Oph	457	1898,1933,1958,1967,1985
T CrB		227.6	1866,1946
V745 Sco		—	1937,1989
V3890 Sgr		—	1962,1990
U Sco	U Sco	1.23	1863,1906,1936,1979,1987,1999
V394 CrA		0.757	1949,1987
LMC RN		—	1968,1990
CI Aql		0.618	1917,2000
T Pyx	T Pyx	0.076	1890,1902,1920,1944,1966

Table 2
Physical properties of Recurrent novae outbursts

Star	$P_{\rm orb}$ (day)	$M_{\rm WD}$ ($M_\odot$)	X	$\Delta M_{\rm max}$ ($M_\odot$)	$\tau_{\rm rec}$ (yr)	$\dot{M}_{\rm acc}$ ($M_\odot$ yr^{-1})	$\eta_{\rm H}$	$\dot{M}_{\rm He}$ ($M_\odot$ yr^{-1})	$E(B-V)$	d (kpc)	Fate
T CrB	227.67	1.37	0.70	3×10^{-6}	80	4.1×10^{-8}	0.10	0.4×10^{-8}	0.11	0.9	SN Ia
RS Oph[a]	460	1.35	0.70	2×10^{-6}	18	1.2×10^{-7}	0.10	1.2×10^{-8}	0.73	0.6	SN Ia
RS Oph[b]	460	1.377	0.70	2×10^{-6}	18	1.2×10^{-7}	0.10	1.2×10^{-8}	0.73	0.6	SN Ia
V745 Sco	···	1.35	0.70	5×10^{-6}	52	9.0×10^{-8}	0.05	0.5×10^{-8}	1.1	5	SN Ia
V3890 Sgr	···	1.35	0.70	3×10^{-6}	28	1.1×10^{-7}	0.10	1.1×10^{-8}	0.5	4	SN Ia
U Sco[c]	1.23056	1.37	0.05	3×10^{-6}	12	2.5×10^{-7}	0.40	1.0×10^{-7}	0.20	6	SN Ia
V394 CrA[d]	0.7577	1.37	0.05	6×10^{-6}	39	1.5×10^{-7}	0.23	3.4×10^{-8}	0.26	4	SN Ia

[a]taken from Hachisu & Kato (2000a) of solar metallicity model for RS Oph

[b]the present low metallicity ($Z = 0.004$) model for RS Oph

[c]taken from Hachisu et al. (2000a)

[d]taken from Hachisu & Kato (2000b)

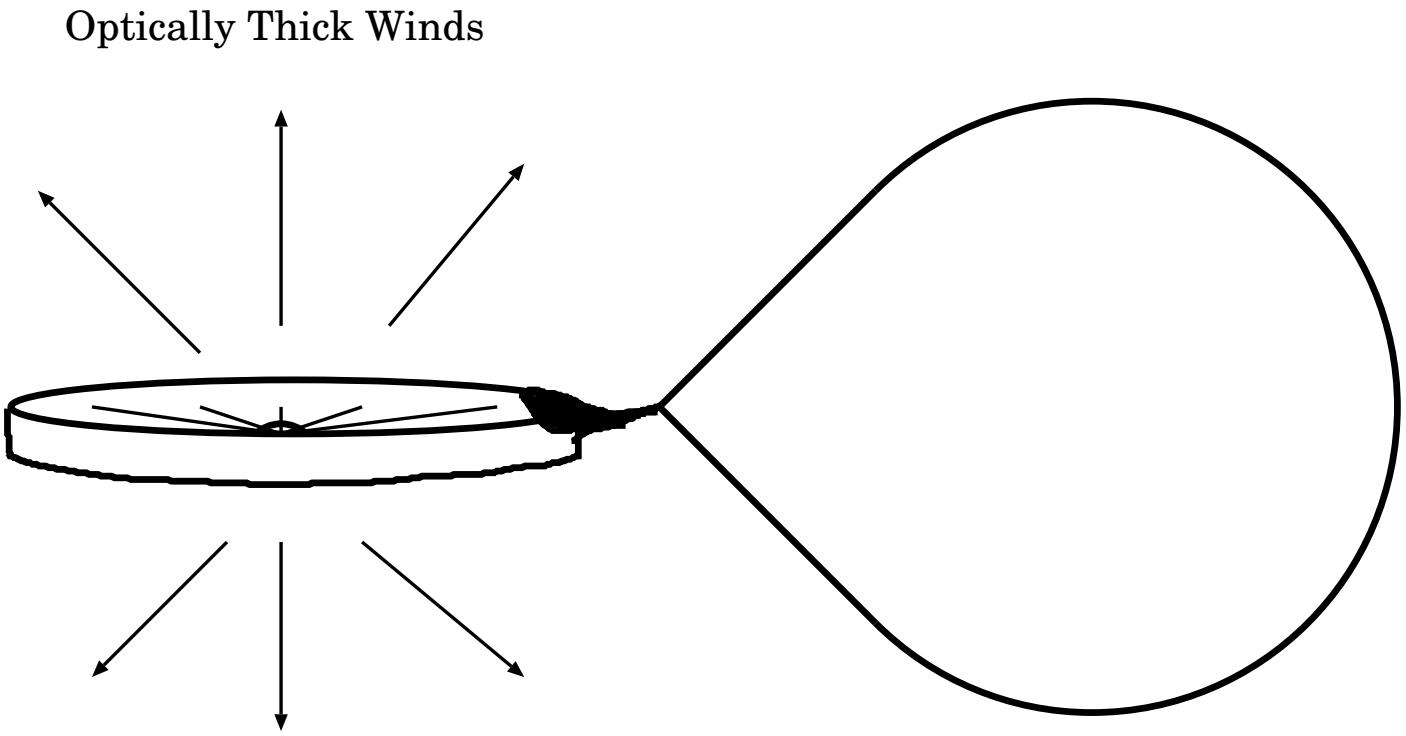

FIG. 1.— Optically thick winds blow from mass-accreting white dwarfs (*left figure*) when the mass transfer rate from a lobe-filling companion (*right figure*) exceeds a critical rate, i.e., $\dot{M}_{\rm acc} > \dot{M}_{\rm cr}$. Here, we assume that the white dwarf accretes mass from equatorial region and, at the same time, blows winds from polar regions as illustrated in the figure.

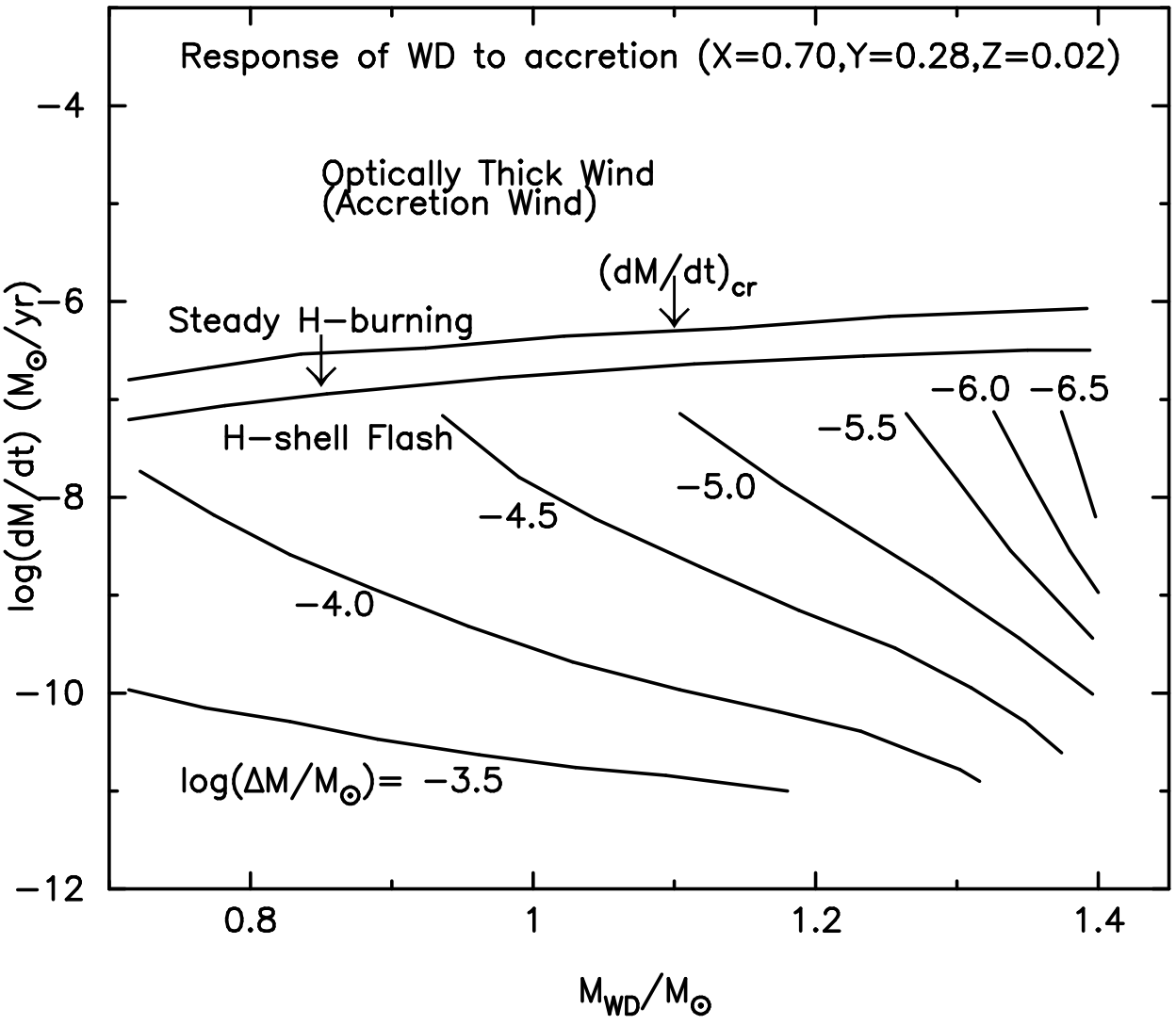

FIG. 2.— Response of white dwarfs to mass accretion is illustrated in the white dwarf mass and the mass accretion rate plane, i.e., in $M_{\rm WD}$-$\dot{M}_{\rm acc}$ plane. Strong optically thick winds blow above the line of $\dot{M}_{\rm acc} > \dot{M}_{\rm cr}$. The wind mass loss rate is $\dot{M}_{\rm wind} \approx \dot{M}_{\rm acc} - \dot{M}_{\rm cr}$. Steady hydrogen shell burning with no optically thick winds occur between $\dot{M}_{\rm std} \leq \dot{M}_{\rm acc} \leq \dot{M}_{\rm cr}$. There is no steady-state burning below $\dot{M}_{\rm acc} < \dot{M}_{\rm std}$. Instead, intermittent shell flashes occur. The envelope mass at which hydrogen shell flash occurs is also shown (taken from Fig. 9 of Nomoto 1982).

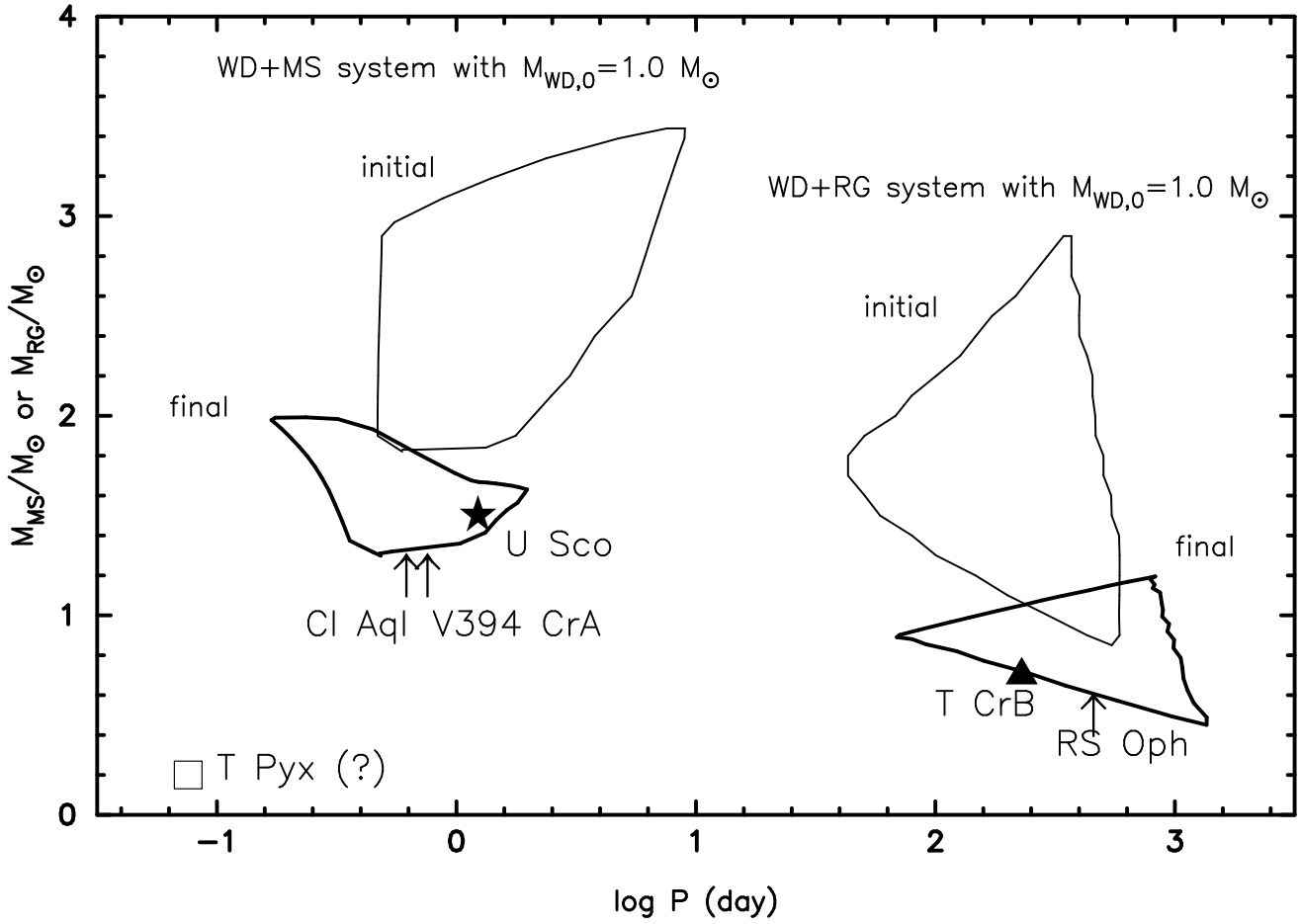

FIG. 3.— Regions producing SNe Ia are plotted in the $\log P - M_{\rm d}$ (orbital period — donor mass) plane for the WD+MS system (left in the figure) and the WD+RG system (right in the figure). Here we assume an initial white dwarf mass of $1.0 M_{\odot}$. The initial system inside the region encircled by a thin solid line (labelled by "initial") is increasing its white dwarf mass up to the critical mass ($M_{\rm Ia} = 1.378 M_{\odot}$) for Type Ia supernova explosion, the regions of which are encircled by a thick solid line (labelled by "final"). Currently known positions of each recurrent nova are indicated by a star mark ($\star$) for U Sco (e.g., Hachisu et al. 2000a), a filled triangle for T CrB (e.g., Belczyński & Mikołajewska 1998), an open rectangle for T Pyx (e.g., Patterson et al. 1998), but by arrows for the other three recurrent novae, V394 CrA, CI Aql, and RS Oph, because the mass of the companion is not yet available explicitly. Two subclasses of the recurrent novae, U Sco subclass and RS Oph (or T CrB) subclass correspond to the helium-rich supersoft X-ray source channel (Hachisu et al. 1999b) and the symbiotic channel (Hachisu et al. 1999a) of Type Ia supernovae, respectively.

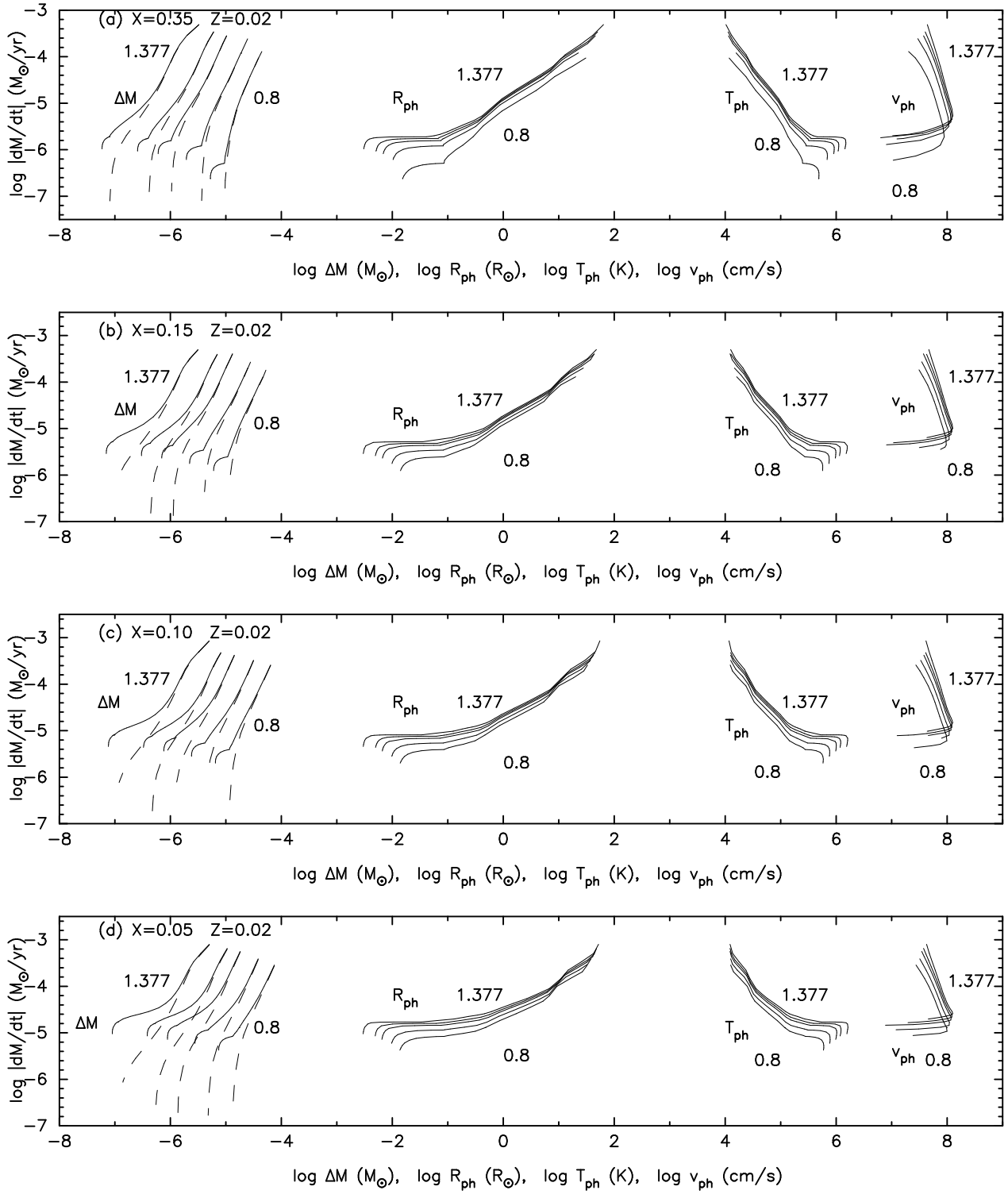

FIG. 4.— Wind mass loss rate (dashed lines) and total mass decreasing rate of the envelope (solid lines labeled by ΔM), i.e., wind mass loss rate plus nuclear burning rate, $\dot{M}_{\rm wind} + \dot{M}_{\rm nuc}$, are plotted against the envelope mass for WDs with masses of 0.8, 1.0, 1.2, 1.3 and $1.377 M_\odot$. There exist only wind solutions above the breaks on the solid lines while only static (no wind) solutions exist below the breaks. Thus, an optically thick wind stops at this break. The photospheric radius, $R_{\rm ph}$, the photospheric temperature, $T_{\rm ph}$, and the photospheric velocity, $v_{\rm ph}$, are also plotted against the total decreasing rate of the envelope mass in the figure. We have shown four different cases of hydrogen content of the envelope material, i.e., (a) $X = 0.35$, (b) 0.15, (c) 0.10, and (d) 0.05, from top to bottom panel, for the solar metallicity of $Z = 0.02$. Each sequence is plotted from the wind solution with $\log T_{\rm ph} = 4.0$ to the static solution with $\dot{M}_{\rm nuc} = \dot{M}_{\rm std}$, i.e., the lower limit for steady hydrogen burning.

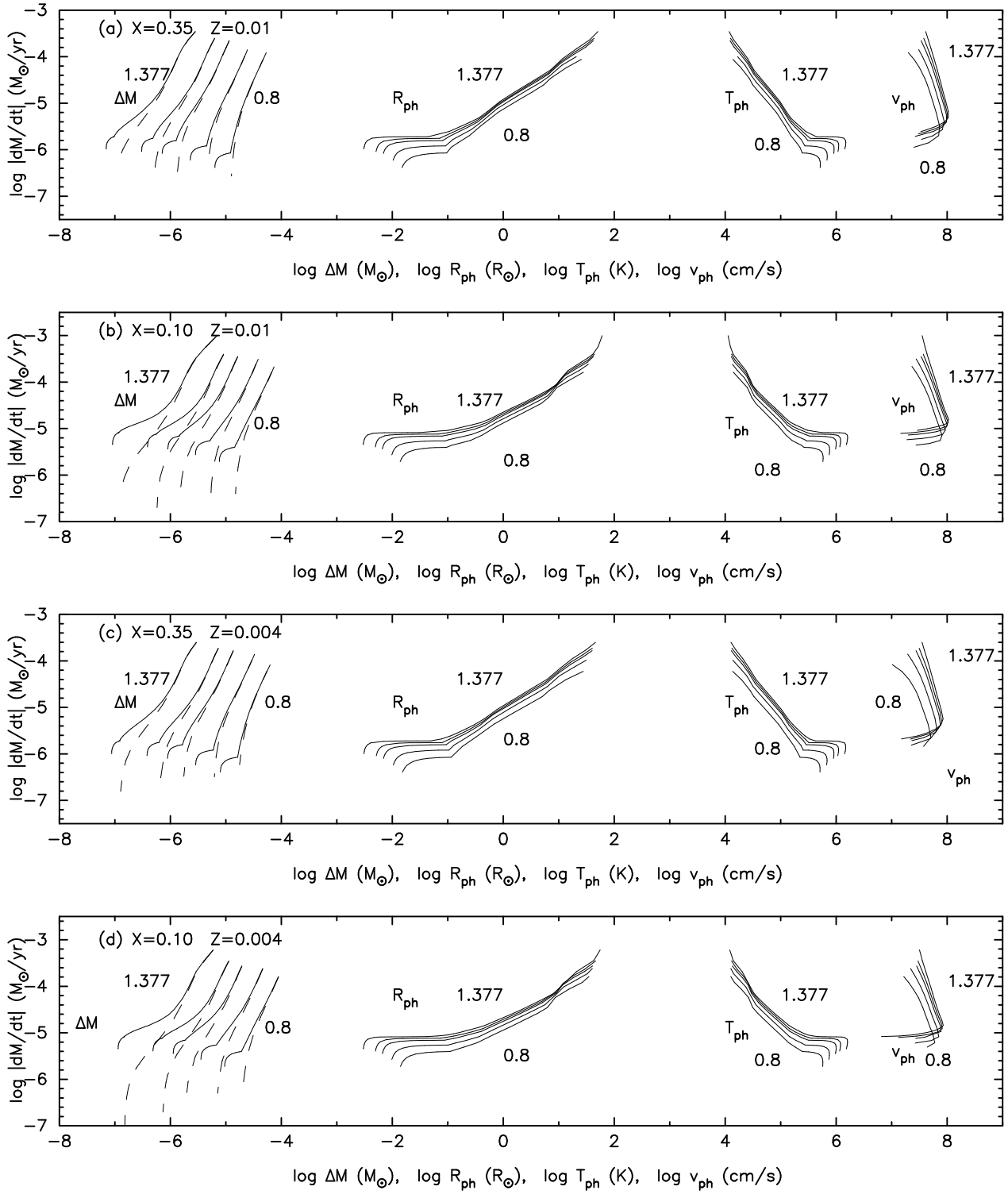

FIG. 5.— Same as Fig. 4, but for low metallicities of $Z = 0.01$ (upper two panels) and $Z = 0.004$ (lower two panels), i.e., (a) $X = 0.35$, $Z = 0.01$, (b) $X = 0.10$, $Z = 0.01$, (c) $X = 0.35$, $Z = 0.004$, and (d) $X = 0.10$, $Z = 0.004$.

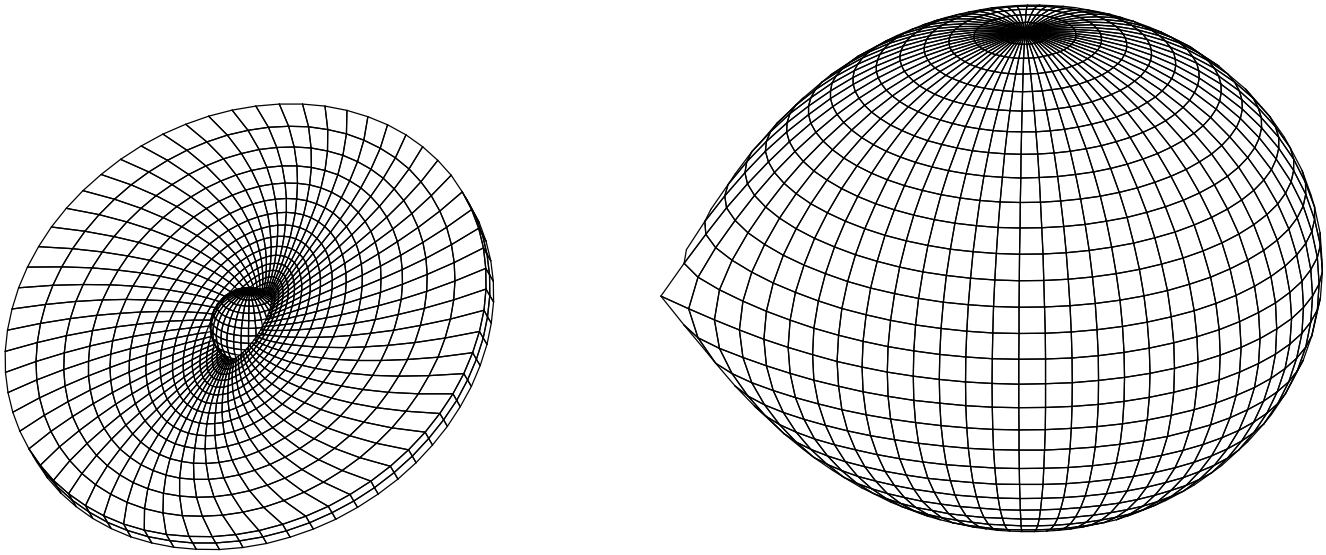

FIG. 6.— Model configuration near the second peak of the recurrent nova T CrB. The cool component (*right in the figure*) is a red giant filling up its inner critical Roche lobe. The hemisphere is heated up by the hot component (1.37 $M_\odot$ white dwarf, *left in the figure*). The photospheric radius of the hot component near the second peak is as small as $\sim 0.003\ R_\odot$, about ~ 0.00003 times the size of the cool component, but it is exaggerated in this figure to easily see it. We assume a warping accretion disk around the hot component, which is precessing at a period of about 140 days. The surface of the accretion disk is also heated up by the hot component. The radius of the accretion disk near the second peak is as small as $\sim 6\ R_\odot$, i.e., about ~ 0.07 times the inner critical Roche lobe size. The accretion disk is also exaggerated in this figure to easily see it.

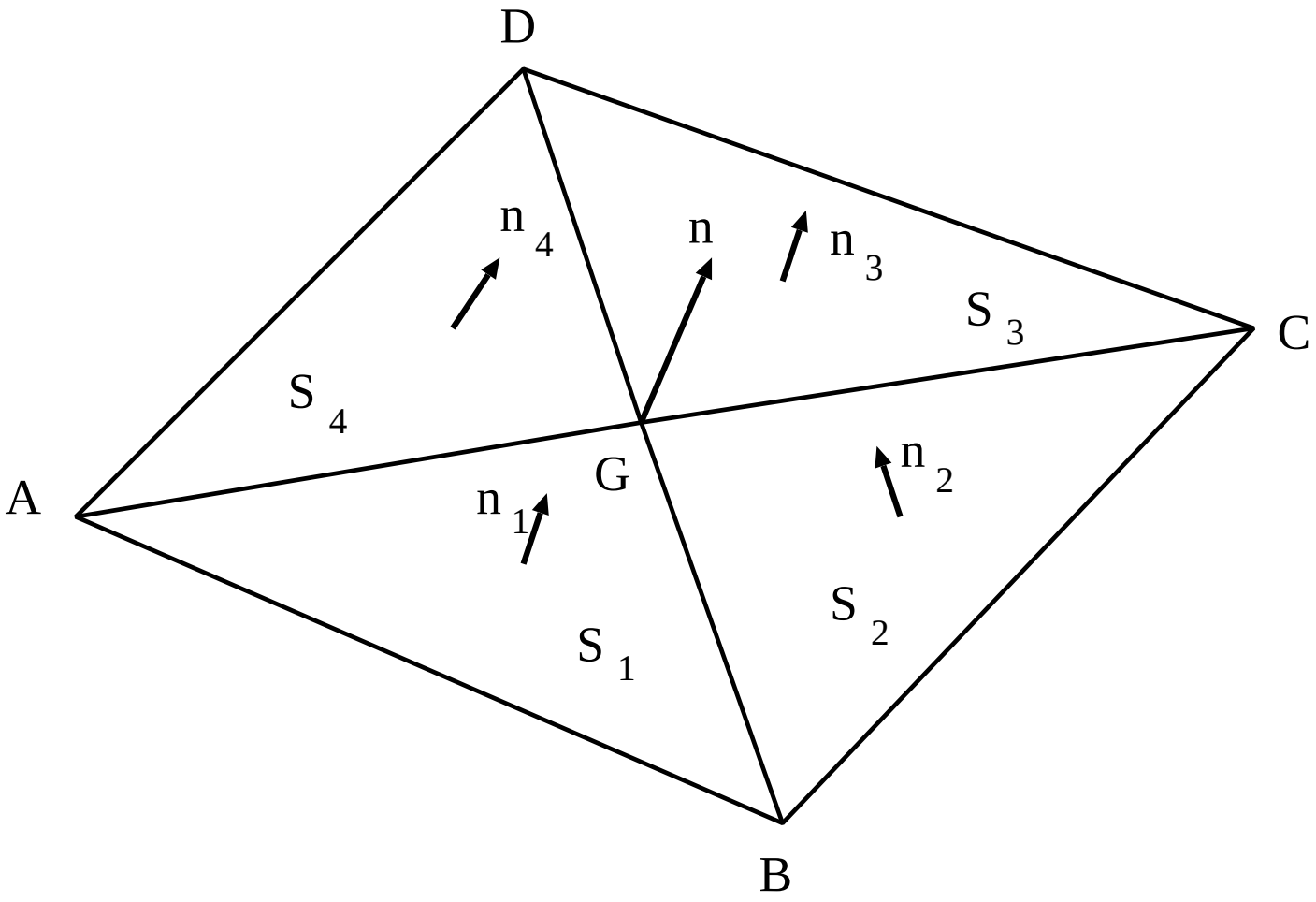

FIG. 7.— Each patch is divided into four triangle parts as shown in the figure, because each patch is almost a rectangular, but strictly speaking, not a rectangular for the Roche geometry of the companion star and for the warping disk surface. So that the normal unit vector to each patch, $\boldsymbol{n}$, is approximately calculated from the four triangle parts by equation (22).

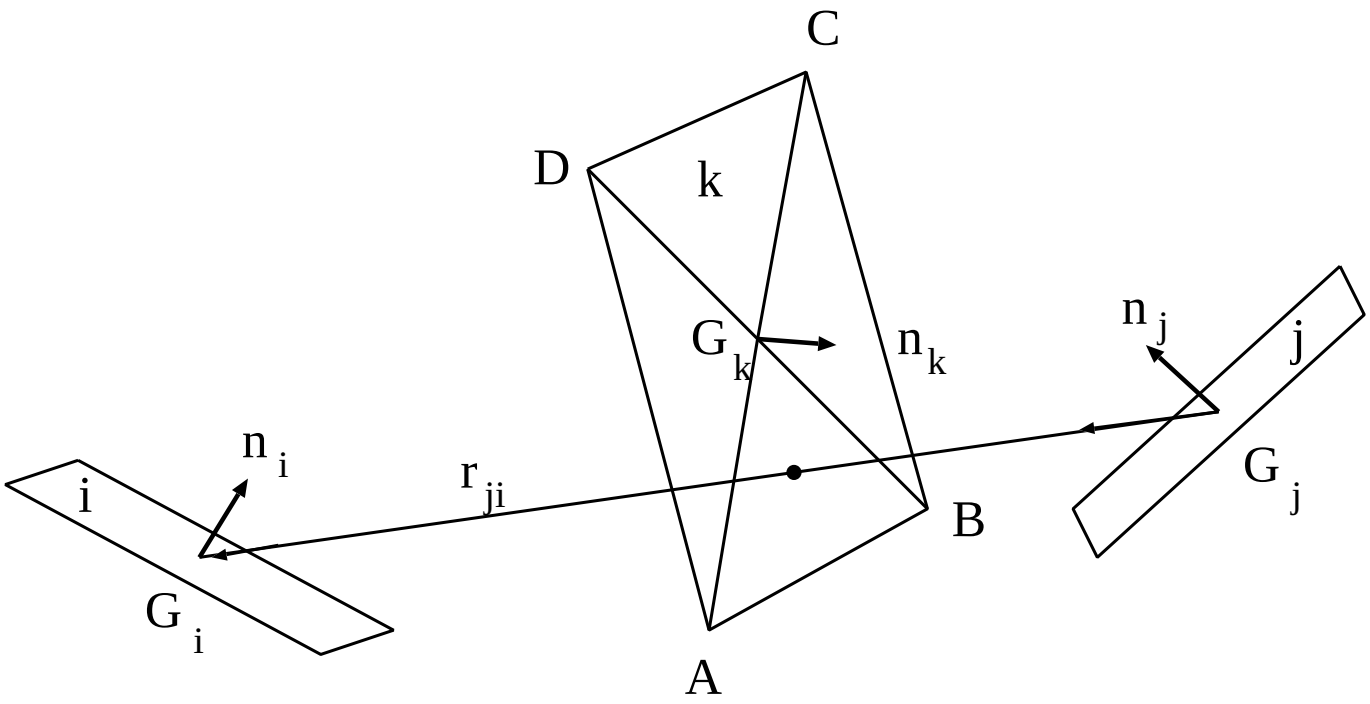

FIG. 8.— When patch k blocks the light from patch j to patch i, we do not sum up the contribution from j to i as shown in equations (29), (30), and (31).

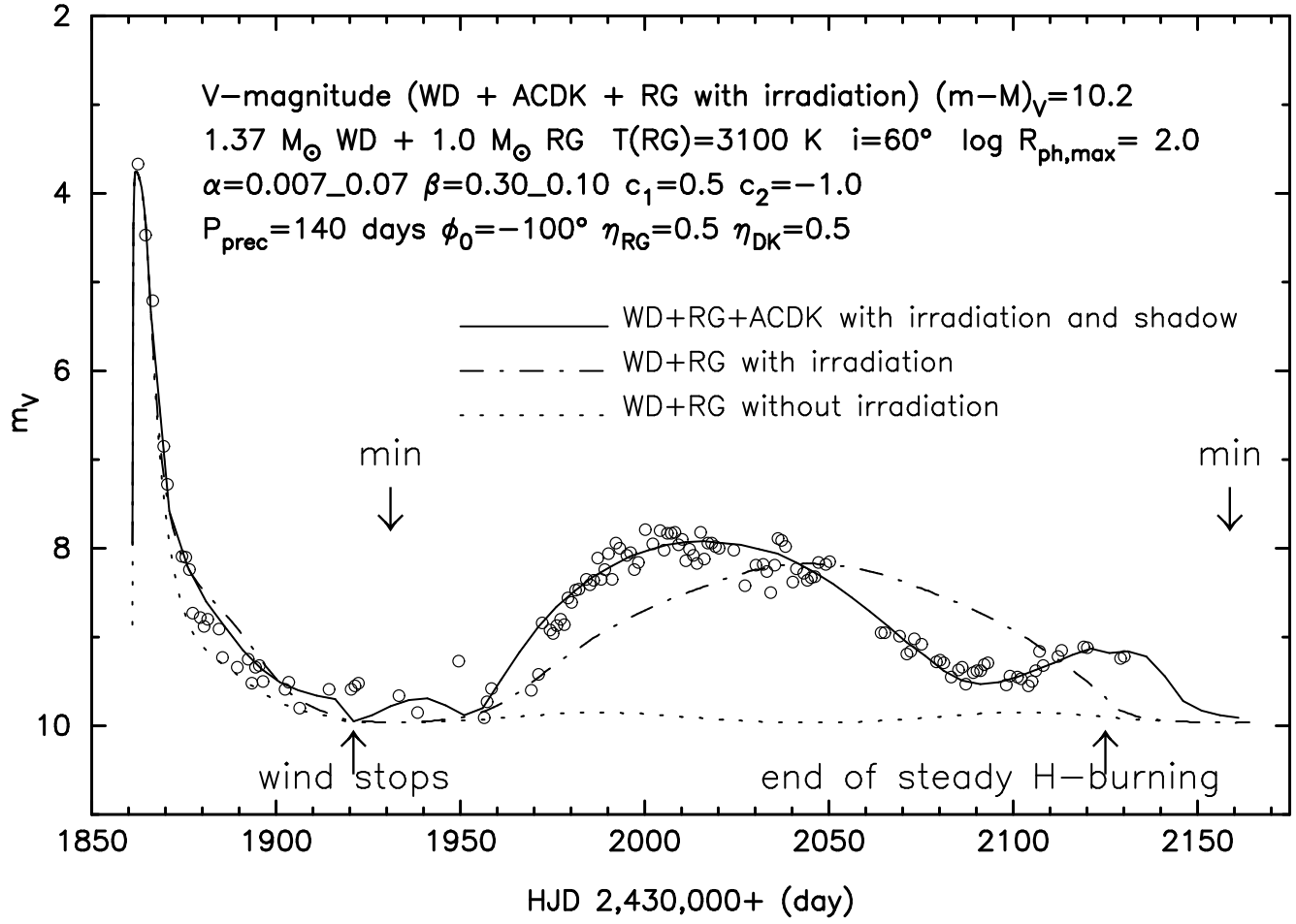

FIG. 9.— Model light curves are plotted against time (HJD 2,430,000+) together with the observational points (*open circles:* Pettit 1946a,b,c,d). *Dotted*: the total V light of the white dwarf (WD) photosphere and the red giant (RG) photosphere without irradiation. Large arrows attached by "min" indicate epochs at the spectroscopic conjunction with the M-giant in front. An ellipsoidal variation can be seen in the late phase. *Dash-dotted*: the total V light of the WD photosphere and the RG photosphere irradiated by the WD. The observed second peak cannot be reproduced only by the irradiation of the M-giant. *Solid*: the total V light of the WD photosphere, the RG photosphere with irradiation, and the accretion disk (ACDK) surface heated-up by the hot component. The parameters specifying the light curves are shown in the figure.

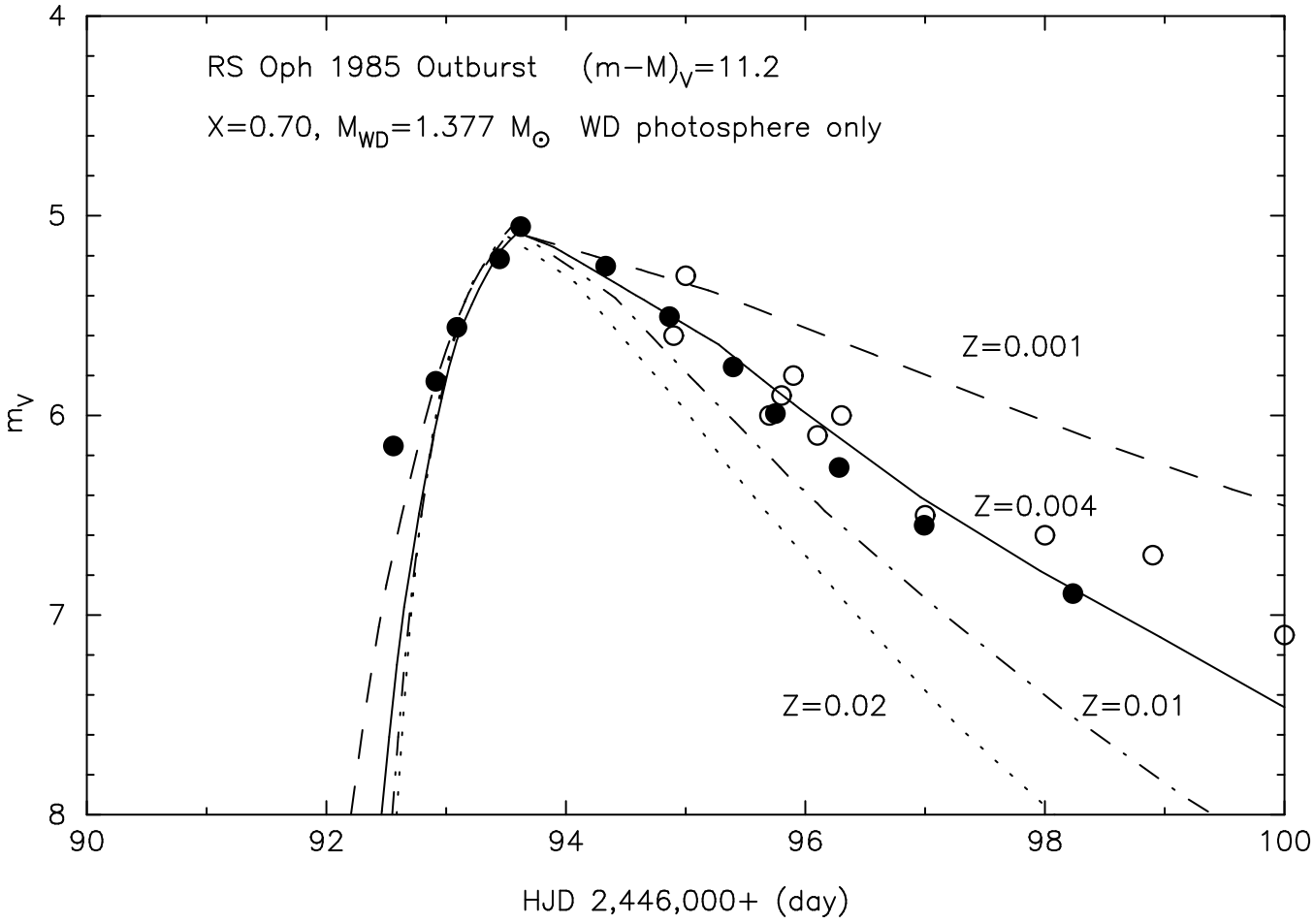

FIG. 10.— Model V light curves for various metallicities are plotted against time (HJD 2,446,000+) together with the observational points of RS Oph outbursts. Filled circles indicate observational points with the previous outbursts superposed (taken from Rosino 1987, see also Hachisu & Kato 2000a). Open circles correspond to the observational points of the 1985 outburst, which are taken from IAU Circulars (Scovil 1985; Lowder 1985; Alcock 1985; Hurst 1985a,b; Danskin 1985; Ducoty 1985a,b,c; McNaught 1985a,b,c,d; Lubbock 1985a,b; King 1985; Weier 1985; Riggs 1985; Cook 1985a,b,c; Medway 1985; Bortle 1985a,b,c; Ellerbe 1985; Verdenet 1985; Sventek 1985; Albinson et al. 1985), i.e., No.4031, 4036, 4048, 4049, 4066, 4074, and 4091. The WD mass is assumed to be the extreme case of $M_{\rm WD} = 1.377\ M_\odot$ just before the SN Ia explosion. The metallicity is attached to each line (for $Z = 0.001$, $Z = 0.004$, $Z = 0.01$, $Z = 0.02$). Each line denotes the V light of the WD photosphere only. The hydrogen content of the WD envelope is assumed to be $X = 0.70$ for all models. The apparent distance modulus is $(m - M)_V = 11.2$. The lowest metallicity case of $Z = 0.001$ cannot reproduce the rapid decline of the V light curve of RS Oph outburst. Since the hydrogen content, X, hardly affect the decline rate of the V light curve (e.g., Kato 1999), we may conclude that $Z \gtrsim 0.004$ in RS Oph outbursts.

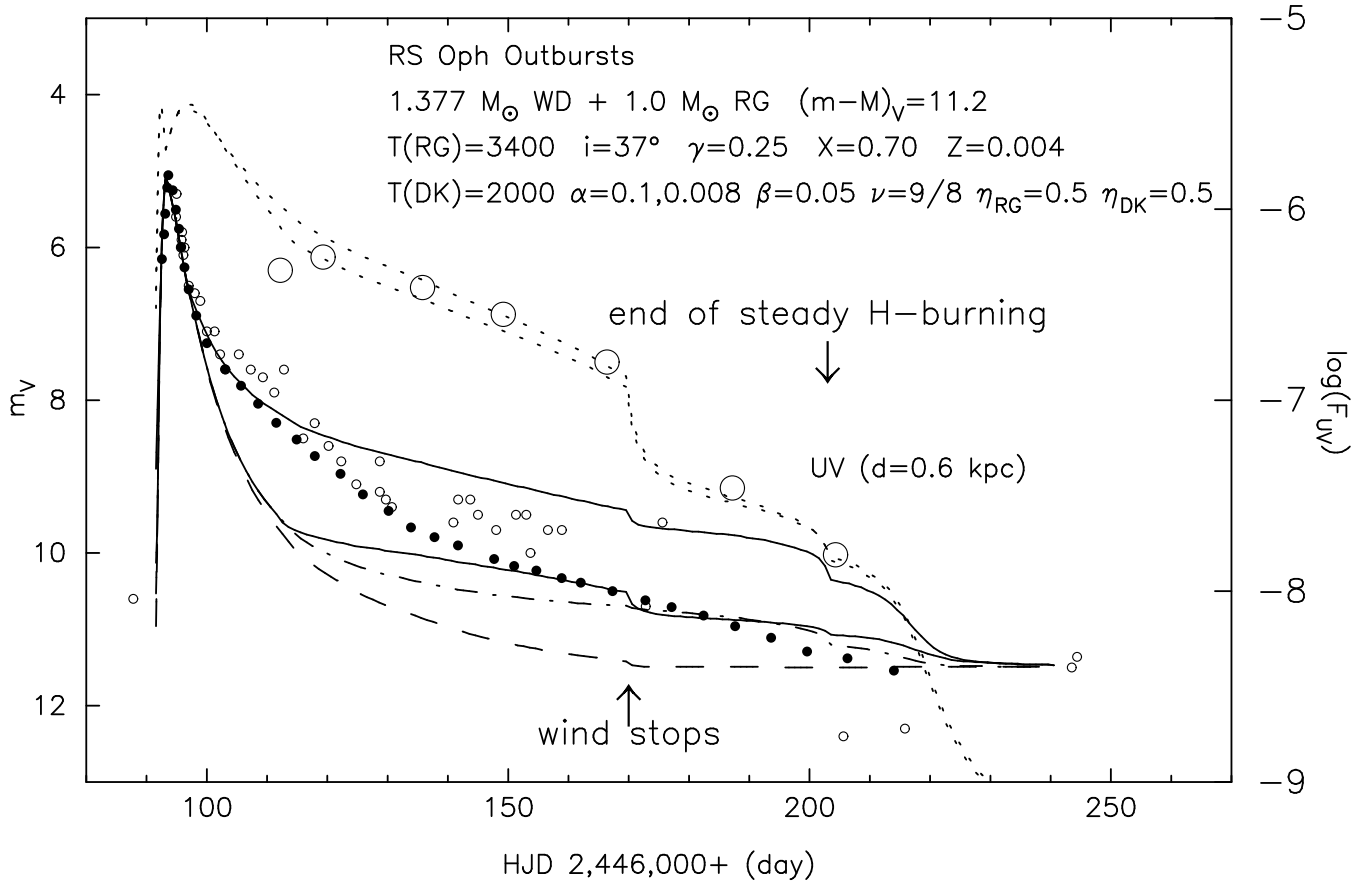

FIG. 11.— Same as Fig. 10 but for the entire outburst phase for $M_{\rm WD} = 1.377 M_\odot$, $X = 0.7$, and $Z = 0.004$. *Dashed line*: Sum of the contributions from the white dwarf (WD) photosphere and the non-irradiated red giant (RG) photosphere with the surface temperature of $T_{\rm ph} = 3400$ K. The RG lies well within the inner critical Roche lobe, i.e., its radius is 0.25 times the Roche lobe size ($\gamma = 0.25$). *Dashed-doted*: Sum of the WD photosphere and the irradiated RG photosphere. *Solid*: the total V light of the WD photosphere, the irradiated RG photosphere and the accretion disk (ACDK) surface. *Dotted*: ultra-violet (UV) radiation (911–3250 Å) from the WD photosphere, the irradiated RG photosphere, and the irradiated ACDK surface. The UV data (large open circles) are taken from Snijders (1987a). Here both the disk shape and size are assumed to be constant during the outburst, i.e., $\alpha = 0.01$ ($R_{\rm disk} \sim 14\ R_\odot$) and $\beta = 0.05$ for the upper solid (and upper dotted) line, and $\alpha = 0.008$ ($R_{\rm disk} \sim 1\ R_\odot$) and $\beta = 0.05$ for the lower solid (and lower dotted) line, respectively. Two epochs with "wind stops" and "end of steady H burning" are indicated by arrows. The optically thick wind blows during the period from the first phase of the outburst (HJD 2,446,092) to 79 days after maximum (HJD 2,446,170). The steady hydrogen shell burning ends at 112 days after maximum (HJD 2,446,203).

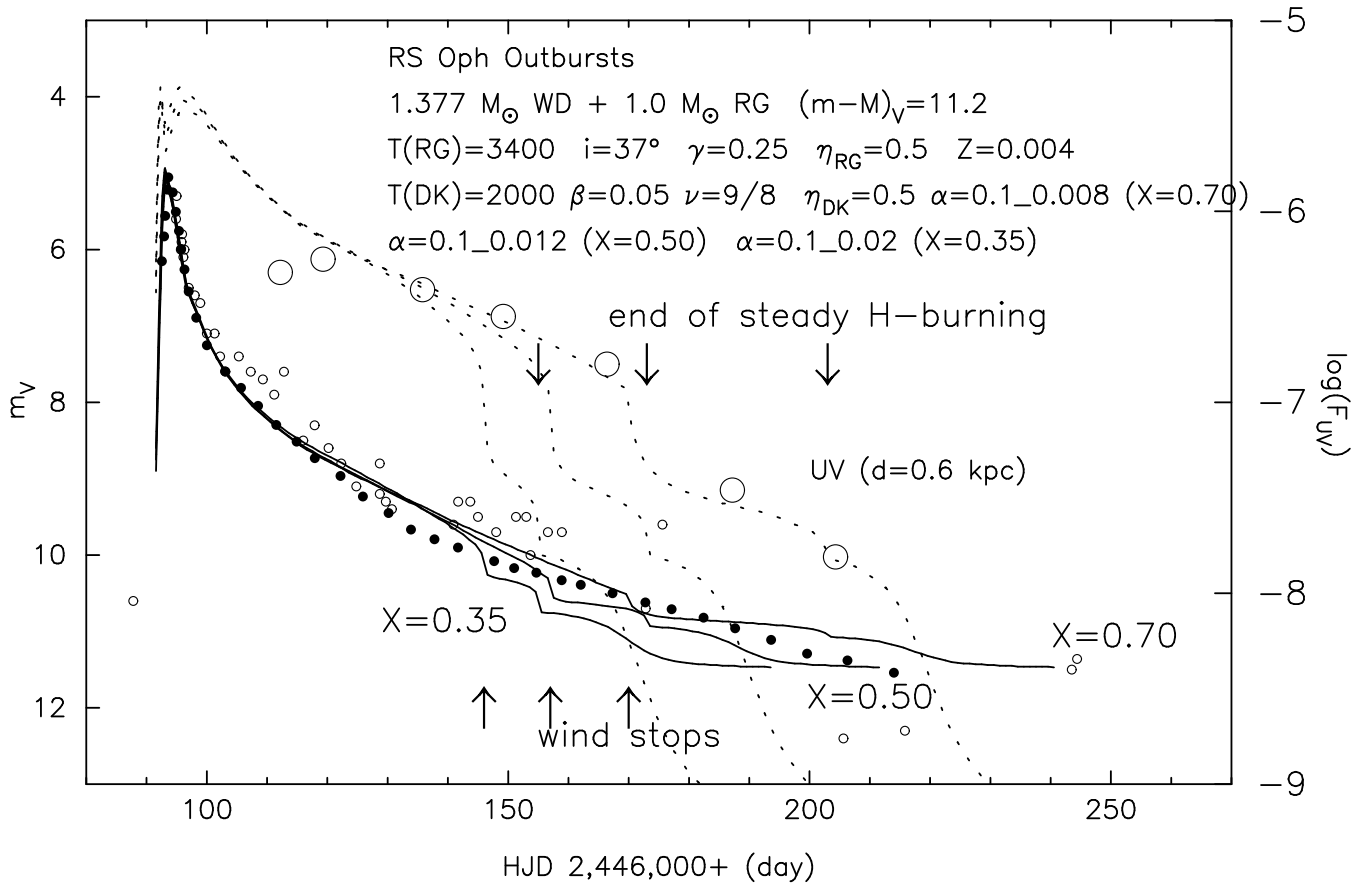

FIG. 12.— Same as Fig. 11 but for a case of gradually evaporating accretion disk. Here, we assume that the radius of the accretion disk is gradually shrinking from $\sim 14R_\odot$ ($\alpha = 0.1$) to $\sim 1R_\odot$ ($\alpha = 0.008$) for $X = 0.7$, to $\sim 2R_\odot$ ($\alpha = 0.012$) for $X = 0.5$, to $\sim 3R_\odot$ ($\alpha = 0.02$) for $X = 0.35$, during the wind phase. Its time variation is exponential as given by equation (56).

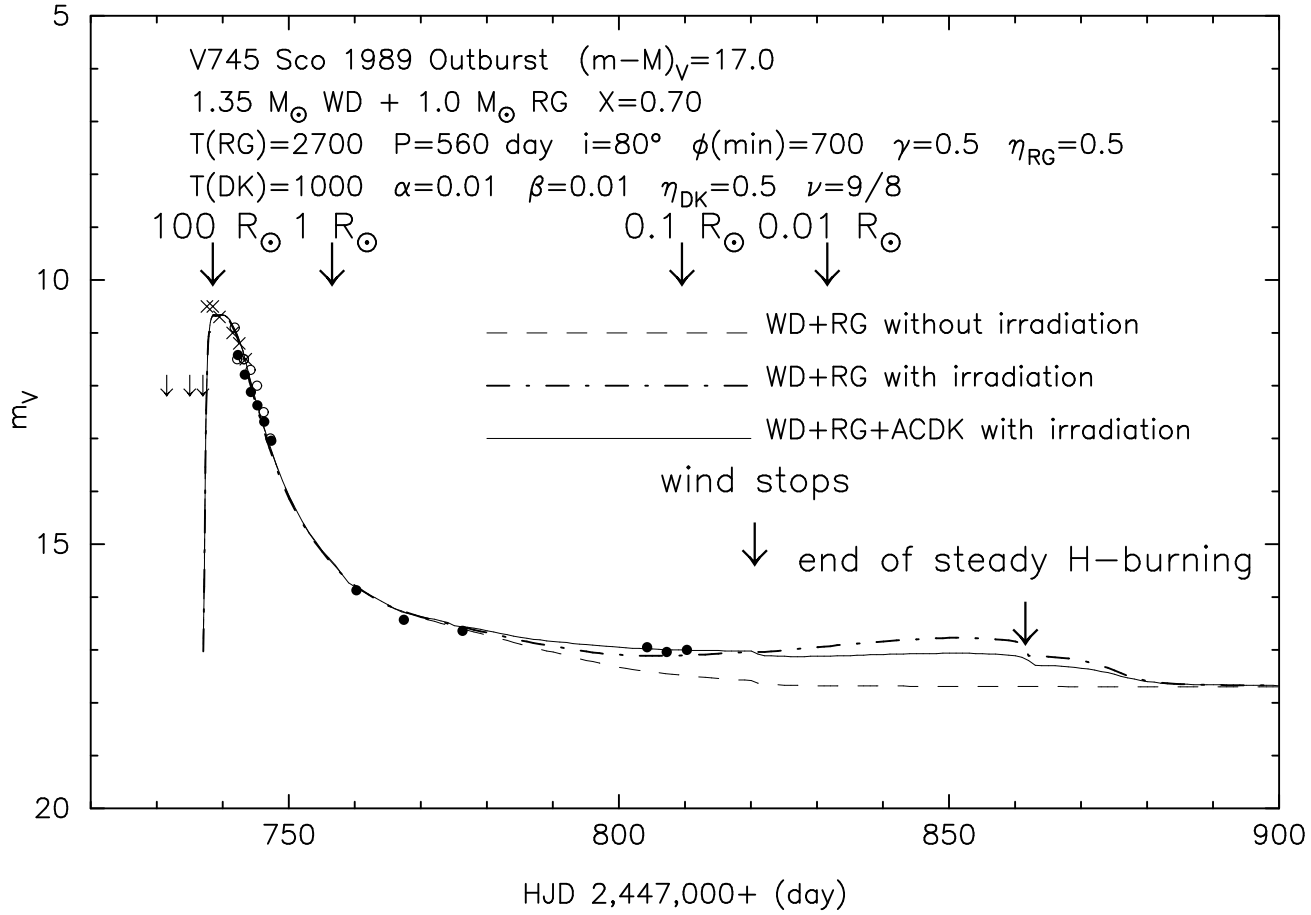

FIG. 13.— Model light curves are plotted against time (HJD 2,447,000+) together with the observational points of the V745 Sco 1989 outburst. Here, the inclination angle of $i = 80°$ is assumed. The other system parameters are shown in the figure. Filled circles indicate the observational points with V filter (taken from Sekiguchi et al. 1990). Crosses (taken from Liller 1989a,b) are shifted by 0.8 mag down because they are systematically 0.8 mag brighter than the V magnitude. Small allows (downwards) indicate an upper limit before the 1989 outburst (taken from Honda 1989). Open circles are visual magnitudes taken from Shore et al. (1989) and Overbeek (1989). Dashed line denotes the V light curve of the WD photosphere and the nonirradiated RG only. Dash-dotted line corresponds to the V light from the WD photosphere and the irradiated RG. Solid line represents the total V light of the WD photosphere, the irradiated RG, and the irradiated accretion disk. The photospheric radius of the WD is indicated above the V light curve. Two epochs are indicated by arrows with "wind stops" and "end of steady H-burning." The optically thick wind stops at HJD 2,447,819. The steady hydrogen shell burning ends at HJD 2,447,860. Fitting with the observations indicates an apparent distance modulus of $(m - M)_V = 17.0$.

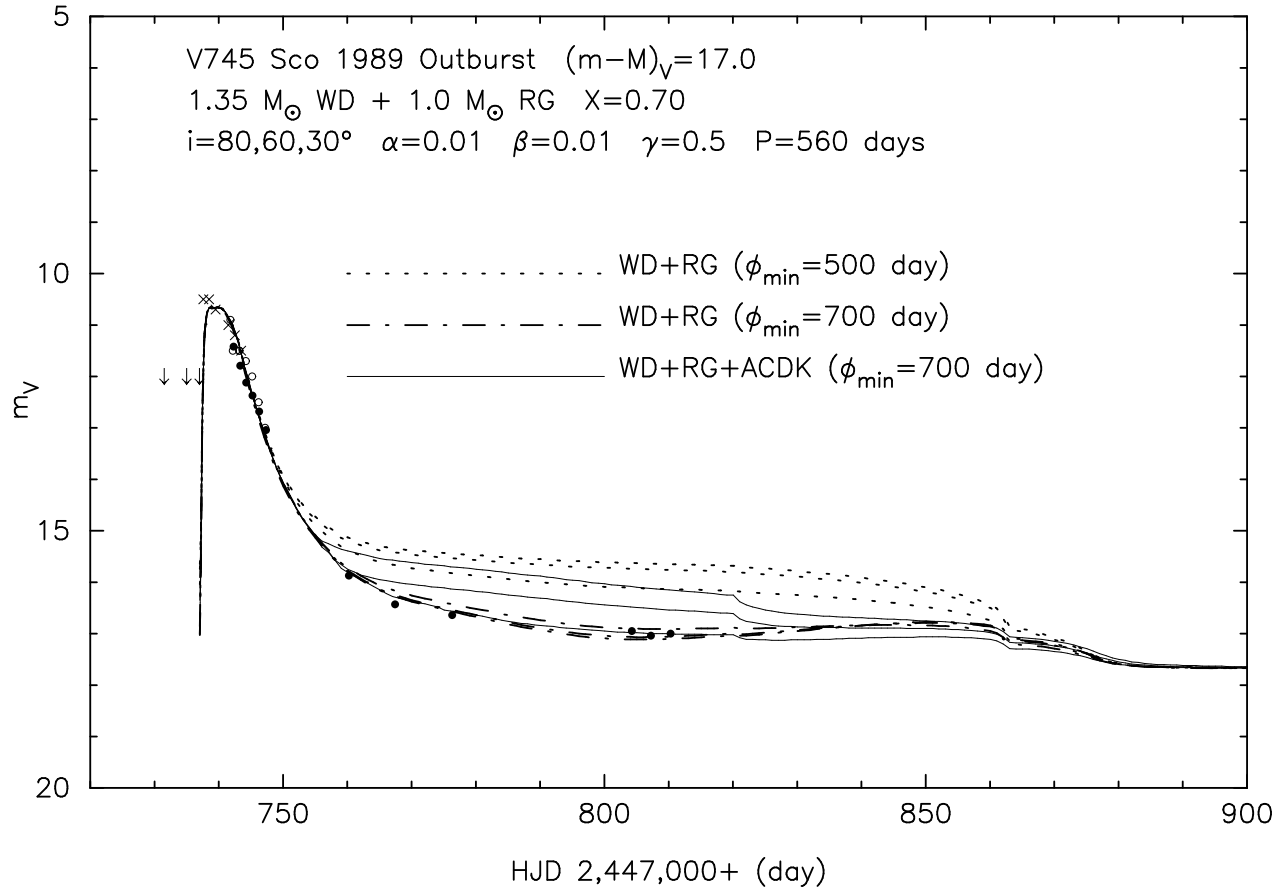

FIG. 14.— Same as Fig. 13 but for different inclination angles ($i = 30$, 60, 80° from top to bottom). Dot-dashed lines denote the model light curves for the cases of no accretion disk while solid lines denote the cases with an accretion disk. The model light curves with an accretion disk depend largely on the inclination angle, while we do not find any significant differences for the cases of no accretion disk. Dotted lines indicate a different ephemeris of $\phi_{\rm min} = 500$ day, which seems not to be compatible with the observation for all three inclination angles.

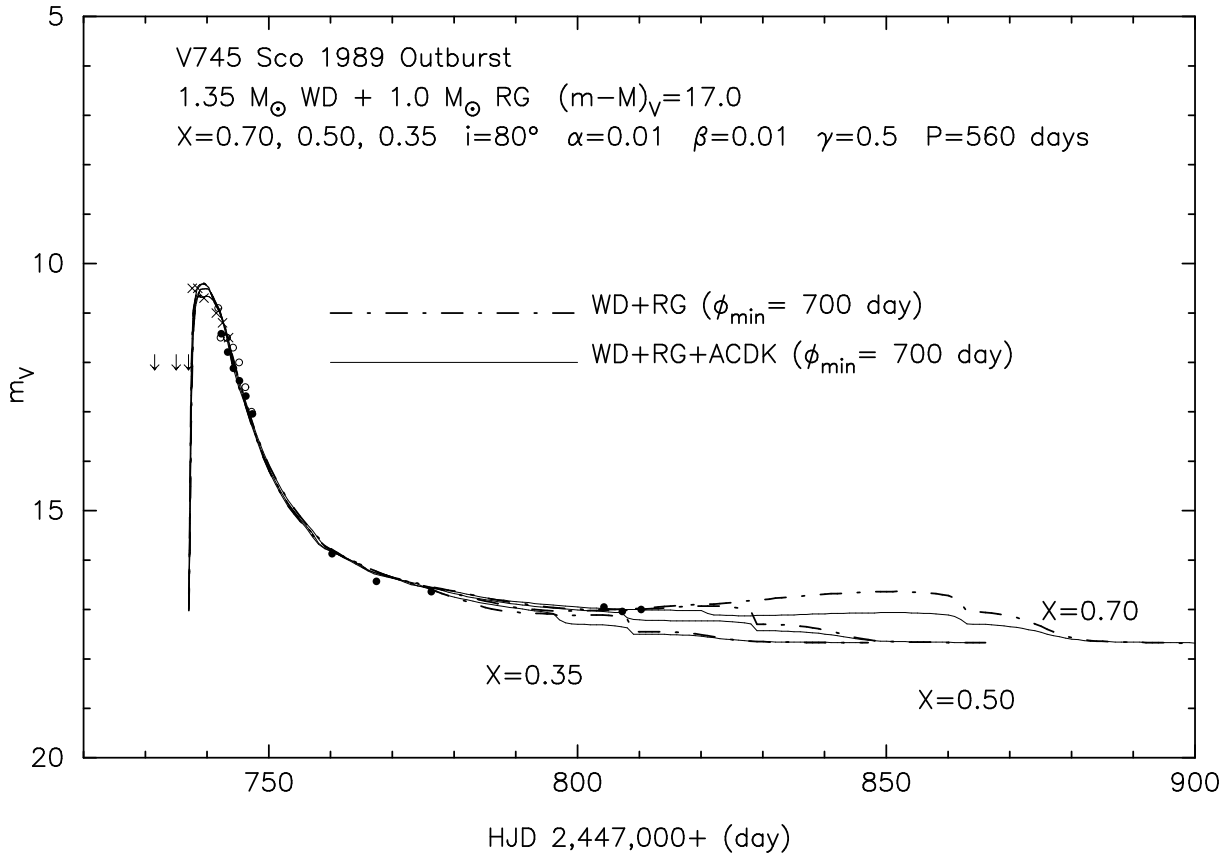

FIG. 15.— Same as Fig. 13 but for three different hydrogen content of $X = 0.35$, 0.50, and 0.70. We do not determine the hydrogen content from these observational points, but may conclude that it is somewhere between $X = 0.5$ and 0.7.

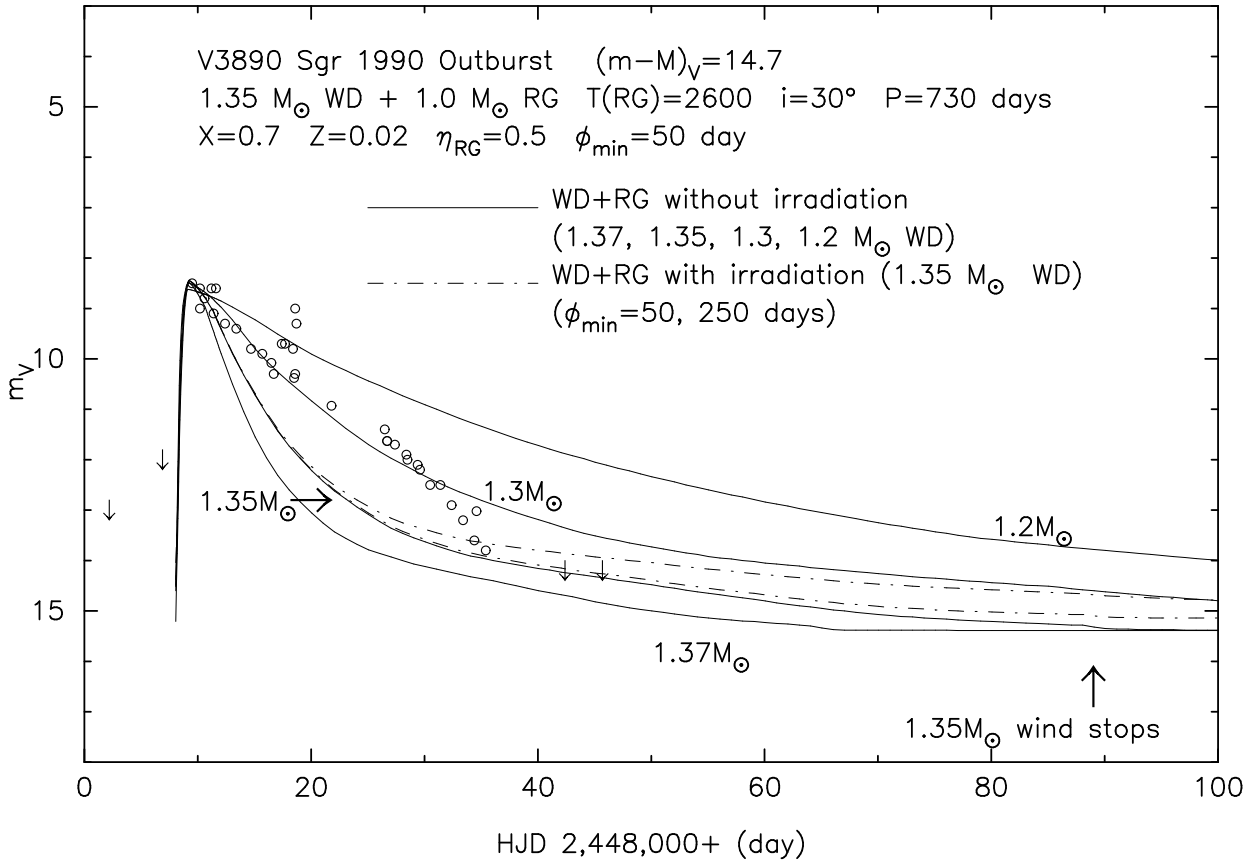

FIG. 16.— Model light curves are plotted against time (HJD 2,448,000+) together with the observational points of the V3890 Sgr 1990 outburst. Here, the inclination angle of $i = 30°$ is assumed. The other system parameters are shown in the figure. Open circles indicate the observational points taken from IAU Circulars (Jones 1990a,b,c; Pearce 1990a,b,c,d,e,f; Pereira 1990a,b; Boattini 1990; Liller 1990; Schmeer 1990a,b,c) and Figure 1 of González-Riestra (1992), while small downward arrows show an upper limit. Solid lines denote the total V light of the WD photosphere and the nonirradiated M-giant secondary. Dot-dashed lines depict the total V light of the WD photosphere and the irradiated M-giant secondary with two different $\phi_{\rm min}$, i.e., $\phi_{\rm min} = 50$ day (lower) and $\phi_{\rm min} = 250$ day (upper) only for $M_{\rm WD} = 1.35\ M_\odot$. Fitting with the observations suggests an apparent distance modulus of $(m-M)_V = 14.7$. Here, we assume that the WD photosphere reached its maximum expansion on HJD 2,448,009.

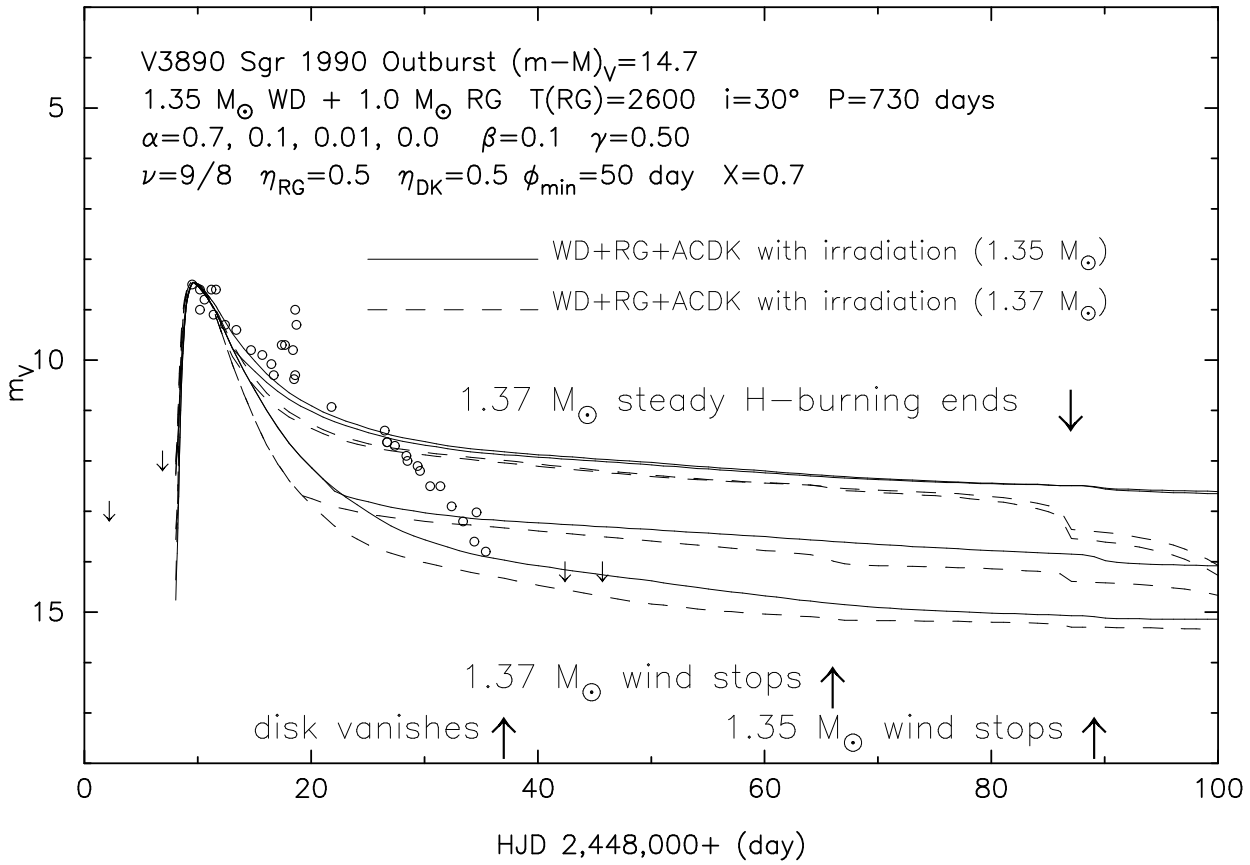

FIG. 17.— Same as Fig. 16 but for two white dwarf masses, i.e., 1.35 $M_\odot$ (solid lines) and 1.37 $M_\odot$ (dashed lines). Both solid and dashed lines represent the total V light of the WD photosphere, the irradiated M-giant, and the irradiated accretion disk, the size of which is fixed during the outburst as defined by equations (11) and (12). The optically thick wind blows during the outburst, from the beginning of the outburst (HJD 2,448,008) to 80 days after maximum (HJD 2,448,089), and then the steady hydrogen shell-burning ends at 122 days after maximum (HJD 2,448,131) for the 1.35 $M_\odot$ WD and the hydrogen content of $X = 0.7$, while 57 days and 78 days, respectively, for the 1.37 $M_\odot$ WD and the hydrogen content of $X = 0.7$. The slow decline just after the optical maximum can be reproduced by the relatively large disk size around the 1.35 $M_\odot$ WD but not by the 1.37 $M_\odot$ WD.

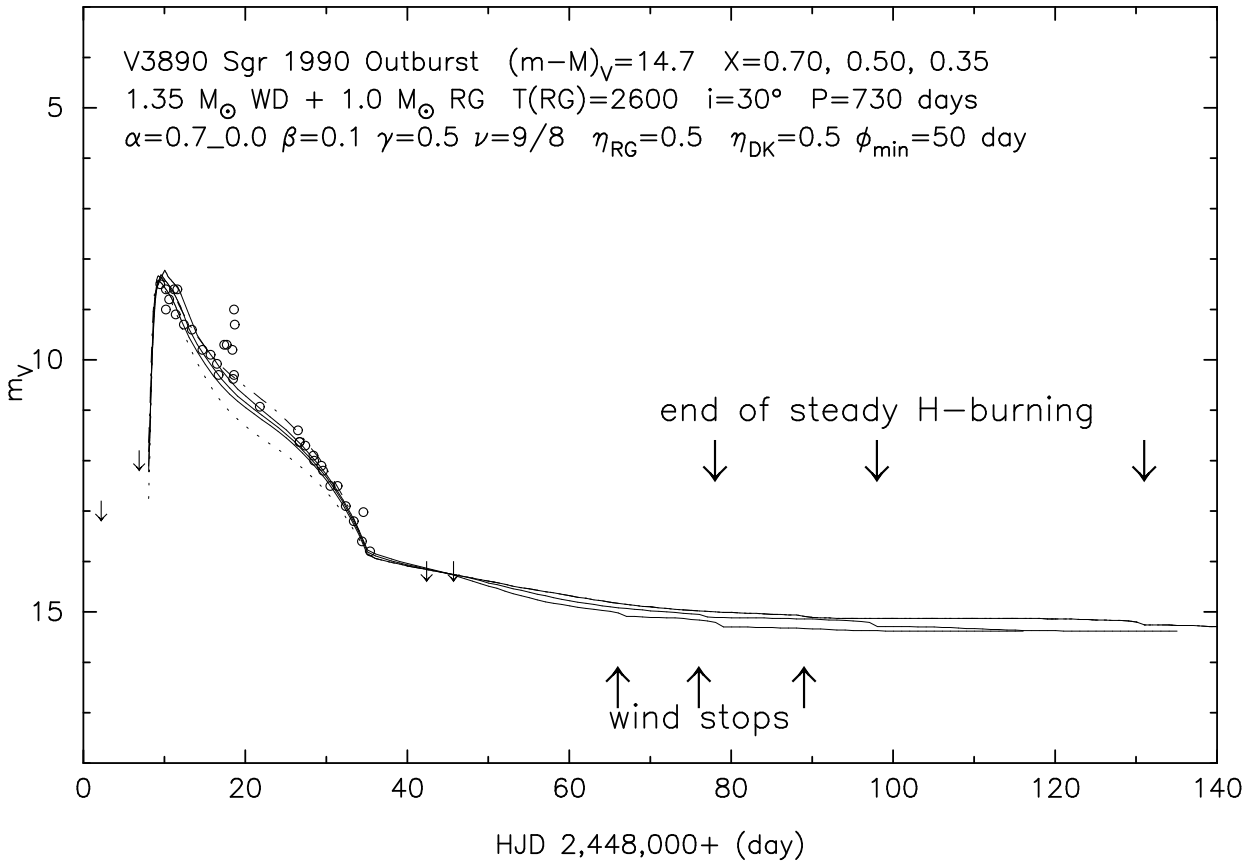

FIG. 18.— Same as Fig. 17 but for the case of evaporating accretion disk with three different hydrogen content of $X = 0.35$, 0.50, and 0.70 (*solid lines*). We do not pose any constraints on the hydrogen content from these observational points, because of a lack of data points in the later phase. For comparison, two other cases with different irradiation efficiencies, $\eta_{\rm DK} = 1.0$ (*dot-dashed*) and 0.25 (*dotted*), are added only for $X = 0.70$.